Acoustics in shear flows : geometrically complex boundary conditions, application to acoustic waves reflection and to viscous boundary layers

Gael Favraud

Université du Maine
Laboratoire d'Acoustique de l'Université du Maine

Thèse

Présentée pour obtenir obtenir le grade de Docteur, spécialité
« Acoustique »

par

Gael Favraud

Acoustique dans les écoulements cisaillés. Conditions limites de géométries complexes, application à l'acoustique et aux couches limites visqueuses.

Thèse soutenue le 8 Novembre 2012 devant le jury composé de :

M. Yves **Aurégan**	Directeur de recherche,	LAUM, Université du Maine	(Examinateur)
M^{me} Anne Sophie **Bonnet-Ben Dhia**	Directrice de recherche,	Equipe POEMS, UMA, ENSTA	(Rapporteur)
M. François **Coulouvrat**	Directeur de recherche,	Inst. J. Le Rond d'Alembert, UPMC	(Rapporteur)
M. Richard **Craster**	Professor,	Dpt. of Mathematics, Imperial College	(Examinateur)
M. Gwenael **Gabard**	Lecturer,	ISVR , University of Southampton.	(Examinateur)
M^{me} Agnès **Maurel**	Directrice de recherche,	Inst. Langevin, ESPCI	(Présidente du jury)
M. Vincent **Pagneux**	Directeur de recherche,	LAUM, Université du Maine	(Directeur de thèse)

Résumé

La première thématique abordée concerne les interactions entre acoustique et vorticité dans les écoulements cisaillés linéaires incompressibles, qui peuvent être décomposés en la somme d'une partie hyperbolique et d'une partie rotation solide. L'écoulement de Couette est un exemple de tels écoulements. En utilisant la démarche non-modale initiée par Kelvin, les équations d'évolution de perturbations compressibles se réduisent à une EDO de dimension trois en temps, qui dépend d'un paramètre adimensionné ε représentant le rapport entre le taux de cisaillement de l'écoulement et la fréquence des perturbations. Pour de faibles valeurs de ε, la méthode WKB permet d'exhiber naturellement trois modes : deux modes acoustiques et un mode de vorticité. La base constituée de ces trois modes permet de mettre en évidence des phénomènes de couplage entre ces modes qui ont lieux lorsque le nombre d'onde est minimal. Ces couplages sont d'un ordre de grandeur exponentiellement faible en $1/\varepsilon$, et ne peuvent être pris en compte par une méthode asymptotique. En effet, les approximations d'ordres supérieurs se rapprochent de la solution exacte mais sans jamais prendre en compte les couplages. Ces couplages semblent être liés à la partie hyperbolique de l'écoulement.

La seconde thématique traitée est la modélisation de conditions limites de géométries complexes. L'utilisation d'une transformation conforme permet de transformer une frontière complexe en une frontière plane, mais fait apparaître des coefficients non constants dans les équations en volume. Ces dernières sont résolues au moyen de la méthode de la matrice d'impédance multimodale qui ramène le problème à une équation de Riccati pour la matrice d'impédance. Cette méthode est d'abord appliquée à la réflexion d'une onde par une surface complexe. Une approche permettant de trouver des géométries admettant des modes quasi-piégés est proposée. Puis la méthode est appliquée à la modélisation de la couche limite visqueuse d'un fluide oscillant au contact d'une surface complexe périodique. Une solution perturbative est proposée pour un type de géométrie particulier. La présence de zones de recirculation est également étudiée.

Abstract

The first topic treated in this thesis is the interactions between acoustic and vorticity modes in incompressible linear shear flows, which can be decomposed as a sum of a hyperbolic part and of a rigid rotation part. The plane Couette flow is an example of such flows. Using the non-modal approach initiated by Kelvin, the equations of evolution of compressible perturbations reduce to an ODE of dimension 3 in time, which depends on a dimensionless parameter ε representing the ratio of the shear rate of the flow to the frequency of the perturbations. For small values of ε, the WKB methods naturally exhibits three modes : two acoustic modes and one vorticity mode. The basis made of these three modes highlights coupling phenomena between these modes, which occur at the moment where the wavenumber is minimal. These couplings are of an order exponentially small in $1/\varepsilon$, and cannot be taken into account by an asymptotic method. Indeed, higher order approximations get closer to the exact solution but never take into account these couplings. These couplings seem to be linked to the hyperbolic part of the flow.

The second topic treated is the modeling of geometrically complex boundary conditions. The use of a conformal mapping allows one to transform a complex boundary into a plane boundary, but makes appear varying coefficients in the bulk equations. These equations are solved with the multimodal impedance matrix method which reduce the problem to a Riccati equation for the impedance matrix. The method is first applied to the reflection of a wave by a complex surface. An approach allowing one to find geometries having quasi-trapped modes is proposed. Then, the method is applied to the modeling of the viscous boundary layer of an oscillating fluid near a periodic complex surface. A perturbative solution is proposed for a particular type of geometries. The existence of recirculation areas is also investigated.

Remerciements

Mes premiers remerciements vont tout naturellement à Vincent Pagneux, qui a accepté de diriger cette thèse. Je le remercie pour l'aide qu'il m'a apportée tout au long de ces trois années de thèses, pour la confiance qu'il m'a accordée, pour les nombreux enrichissements que m'ont procuré les discussions que j'ai pu avoir avec lui, ainsi que pour la patience dont il a su faire preuve.

Je remercie très chaleureusement Anne Sophie Bonnet-Ben Dhia et François Coulouvrat, rapporteurs de cette thèse, pour le travail qu'ils ont effectué. Je remercie de même Agnès Maurel, qui a présidé le jury de soutenance de thèse, et les autres membres du jury, Yves Aurégan, Richard Craster, et Gwenael Gabard.

Je souhaiterais remercier aussi Simon Félix qui, avec Agnès Maurel, a suivi ce travail en tant que membre du Comité de Suivi de Thèse.

Je tiens également à remercier l'ensemble de mes collègues du LAUM pour l'ambiance et l'atmosphère agréable et propice aux discussions, parfois très scientifiques, parfois moins, qui règnent au sein du laboratoire. Un grand merci à tous les enseignants et responsables de formations pour m'avoir fait confiance et m'avoir donné la chance de découvrir l'enseignement dans le cadre de ma "mission complémentaire". Merci en particulier à Sohbi Sarahoui qui a suivi mes premiers pas en tant qu'enseignant. Merci aussi aux étudiants qui ont bien voulu voir en moi leur enseignant, alors que six mois auparavant je n'étais qu'un étudiant insouciant comme eux.

J'aimerais exprimer une pensée amicale envers tous mes camarades de l'X avec qui je partage de nombreux et intenses souvenirs, et plus particulièrement envers ceux qui, parfois au péril de leur présence en PC, ont su sauver leurs camarades de la déshydratation, de l'ennui ou du silence ; et tous ceux avec qui j'ai profité de réhydratations, de divertissements et de ~~musique~~ bruit. Je porte une attention particulière à une douzaine d'entre eux au sein de chacune des promotions 2004 à 2010, qui ont su faire vivre un humour de très bon goût. Étant généreux, je remercie même celui qui, par antipathie ou par rancune, n'a pas souhaité assister à ma soutenance de thèse.

Ce travail de thèse vient clôturer un long parcours scolaire puis universitaire. Je souhaite remercier l'ensemble des professeurs qui m'ont instruit et plus particulièrement messieurs Coulhon, Delcourt, Derdouri, Rugh, et Truong de l'Université de Cergy-Pontoise pour le soutien qu'ils m'ont apporté lors de ma candidature à l'X. Je pense aussi aux personnes qui ont eu la gentillesse de m'accueillir en stage ou lors de projets, à savoir Cyril Touzé lors de mon projet en laboratoire à l'UME de l'ENSTA, François Gautier lors de mon stage de recherche au sein de l'OR PIM du LAUM, et enfin Thomas

Nodé-Langlois lors de mon stage de M2 à Airbus.

Ce long chemin n'aurait bien évidemment pas pu être fait sans l'aide et le soutien de toute ma famille. Je souhaite donc remercier mes parents, ma soeur ainsi que ma grand mère. Je pense aussi à toute ma famille au Paraguay, bien trop nombreuse pour que je puisse en citer les membres nominativement.

Soline est enfin la personne que je souhaite remercier tout particulièrement. Elle m'a apporté un soutien sans faille et de nombreux moments de bonheur.

Organisation du document

Ce manuscrit présente les travaux de recherche que j'ai menés au sein du LAUM sous la direction de Vincent Pagneux entre Septembre 2009 et Septembre 2012. Ces travaux portent sur deux thématiques différentes qui sont traitées dans chacune des deux parties que comporte ce document. Chaque partie est constituée de deux chapitres présentés sous la forme d'articles soumis ou prochainement soumis pour publication dans des revues scientifiques à comité de lecture.

La première partie traite de l'étude des interactions entre acoustique et vorticité dans les écoulements cisaillés linéaires incompressibles au moyen de la méthode asymptotique WKB. Le chapitre 1 propose une étude systématique des phénomènes en jeux en fonction des différentes classes d'écoulements. Le chapitre 2 se concentre sur les effets de l'utilisation d'approximations d'ordres supérieurs.

La seconde partie propose une méthode de résolution de problèmes impliquant des conditions limites de géométries complexes. Cette méthode consiste en l'utilisation d'une transformation conforme, puis d'une méthode multimodale. La méthode est d'abord appliquée au problème de la réflection d'une onde acoustique par une surface de géométrie complexe dans le chapitre 3. Puis, dans le chapitre 4, elle est employée pour la modélisation de la couche limite visqueuse d'un fluide oscillant à proximité d'une paroi de géométrie complexe (second problème de Stokes).

Table des matières

Première partie

Etude des couplages entre les modes acoustiques et le mode de vorticité au sein d'un écoulement cisaillé linéairement

1

Utilisation de l'approche WKB pour l'étude des couplages entre acoustique et vorticité dans un écoulement cisaillé linéairement

Ce premier chapitre, présenté sous la forme d'un article soumis au *Proceedings of the Royal Society A*, propose une étude des couplages entre le mode de vorticité et les modes acoustiques au sein des écoulements linéaires incompressibles.

L'une des particularités de ces écoulements est qu'ils peuvent être décrits comme la somme d'une partie hyperbolique et d'une partie rotation solide. L'ensemble de ces écoulements peut ainsi être paramétré au moyen d'un seul paramètre. Ceci permet de classer ces écoulements sur une droite qui décrit successivement l'écoulement hyperbolique potentiel, les écoulements hyperboliques non potentiels, l'écoulement de Couette plan, les écoulements elliptiques, et enfin l'écoulement de rotation solide. Les différentes formes d'écoulements sont étudiées de façon systématique.

Les équations d'évolutions des perturbations compressibles sont dérivées de façon classique par rapport à ce qui existe dans la littérature sur le sujet. La forme particulière de ces écoulements (linéarité) joue un rôle très important dans la simplification de ces équations. L'originalité du travail que nous proposons réside dans l'utilisation de la méthode asymptotique WKB. Elle repose sur l'existence d'un petit paramètre ε, qui est ici le rapport entre le taux de cisaillement de l'écoulement et la fréquence de la perturba-

tion. Il s'agit donc d'une approximation pour des écoulements faiblement cisaillés. Cette méthode permet de dégager naturellement trois modes : deux modes acoustiques et un mode de vorticité. Dès les premiers ordres, ces trois modes s'avèrent être très proches de solutions exactes. La base constituée de ces trois modes permet de constater des phénomènes de couplage en suivant l'évolution des amplitudes de ces trois modes.

Un des phénomènes des plus remarquables qui a lieu dans ces écoulements est la génération brusque des modes acoustiques par le mode de vorticité. D'un point de vue mathématique, ce phénomène est comparable aux transitions non-adiabatiques en mécanique quantique. Il s'agit d'un phénomène d'ordre exponentiellement faible qui ne peut être prédit de manière asymptotique. Le résultat le plus intéressant qui ressort de cette étude est que c'est la partie hyperbolique de l'écoulement qui est principalement responsable de ce couplage. Ainsi, c'est dans l'écoulement hyperbolique potentiel qu'une perturbation de vorticité génère le plus efficacement une perturbation acoustique.

Acoustic-vorticity coupling in linearly varying shear flows using the WKB method [1]

Abstract : The evolution of acoustic and vorticity perturbations in a 2D incompressible linear flow is investigated. A weighted decomposition of the flow into a hyperbolic part and a rotation part allows to continuously span all linear flows such as hyperbolic flow, plane Couette flow and rigid rotation for instance. Using the Kelvin non-modal approach, the equations governing the time evolution of plane wave perturbations are reduced into a system of three first order ODE. This system is analysed using a WKB method where the small parameter ε is the ratio of the shear rate of the flow over the typical frequency of the perturbations. With this method, a basis of three modes naturally appears : two acoustic modes and one vorticity mode. At finite but small ε, couplings between the modes appear when the length of the wavenumber is minimal. For hyperbolic flow, incident vorticity mode generates the two acoustic modes, and an incident acoustic mode generates the other acoustic mode. More generally, for all flows, the hyperbolic part of the flow is responsible of the coupling between acoustic and vorticity modes, but also of the coupling between the two acoustic modes. These phenomena are illustrated by displaying wavepacket evolutions.

1 Introduction

Propagation of acoustic waves in uniform flows is a well understood topic (Goldstein, 1976). In complex flows, this is a more complicated problem which is still investigated nowadays. For instance, efforts are still made to develop new robust numerical prediction methods for sound propagation in complex flows (Bonnet-BenDhia *et al.*, 2007, 2012, Gabard *et al.*, 2010). Indeed, most flows are not uniform, and shear flows are known to display subtle features as testified by the large range of literature devoted to the study of their stability in the incompressible limit (Craik & Criminale, 1986, Criminale & Drazin, 1990, Huerre & Monkewitz, 1990, Butler & Farrell, 1992, Reddy *et al.*, 1993, Trefethen *et al.*, 1993, Huerre & Rossi, 1998, Friedlander & Lipton-Lifschitz, 2003, Schmid, 2007, Schmid & Henningson, 2001). The classical modal analysis based on the study of the eigenvalues of the linearised equations used to be largely employed, but lead to predictions significantly different from experimental results due to the existence of transient growth (Butler & Farrell, 1992, Trefethen *et al.*, 1993, Reddy *et al.*, 1993). To overcome these discrepancies, non-modal methods, initiated by Kelvin (Thomson, 1887) has been developed (Craik & Criminale, 1986, Criminale & Drazin, 1990, Butler & Farrell, 1992, Trefethen *et al.*, 1993, Reddy *et al.*, 1993, Schmid, 2007, Schmid & Henningson, 2001). In the case of a linear flow, this method is greatly simplified by using a new system of

1. Submitted to *Proceedings of the Royal Society A*. Authors: Gael Favraud and Vincent Pagneux.

convected coordinates. One of its interests is to transform the governing equations into a three dimensional time ODE with constant coefficients with respect to space, what allows us analytic treatment of the equations.

Acoustic waves in the plane Couette flow have been studied by Chagelishvili *et al.* (1993) in the continuity of flow stability analysis. Using the non-modal approach, he derived an inhomogeneous equation governing the horizontal velocity disturbance evolution and defined acoustic waves as the solutions of the associated homogeneous equation, and vorticity waves as the particular solution of the complete equation. This frame permitted to show some coupling phenomena between what he defined as acoustic and vorticity effects (Chagelishvili *et al.*, 1997*a*,*b*, Rogava & Mahajan, 1997, Mahajan & Rogava, 1999, Rogava *et al.*, 2001, Chagelishvili, 2002, Gogoberidze *et al.*, 2004, Bakas, 2009). Among these effects one is the generation of acoustic waves by vortices, firstly attributed to a discontinuity by Chagelishvili *et al.* (1997*b*), and later to an interaction of the disturbance velocity field with mean shear by George & Sujith (2009). This approach has also been extended to arbitrary linear flow (Mahajan & Rogava, 1999, Rogava *et al.*, 2001) (including the Couette flow). The Wentzel Kramers Brillouin (WKB) method has been used since the earlier papers of Chagelishvili *et al.* (1994, 1997*a*) while not mentioned explicitly ("adiabatic evolution"). A more extensive use of it has been performed by Gogoberidze *et al.* (2004) to explain the couplings as resulting of "non-adiabatic transitions", firstly studied in quantum mechanics by Landau (Landau, 1932, Landau & Lifshitz, 1977) and Zener (1932).

In this paper, we propose a systematic study of compressible perturbations in general linear incompressible shear flows. We introduce a WKB method for which the two acoustic modes and the vorticity mode naturally come out from the equations as eigenvectors of an eigenvalue problem. An order 1 approximation is used instead of the classical order 0 WKB to improve the description and to take into account the well known inherent rotational part of the acoustic mode which is due to potential vorticity conservation (Mohring *et al.*, 1983). The plan of this paper is as follows. In the section 2 we derive the governing equations following the Kelvin non-modal approach (Chagelishvili *et al.*, 1993, Mahajan & Rogava, 1999). We display the variety of flows which can be described under the assumption of linear flow. We also briefly tackle two limit cases of the model : the no flow and the incompressible cases. The WKB method is presented in the section 3. The section 4 exhibits results obtained with the proposed approach. All flows are systematically investigated. Results are then applied to the evolution of wavepackets. Finally, we compare numerically the mode coupling efficiency depending on flow shape and intensity.

2 Model

We derive in this section the equations in the same way as Chagelishvili *et al.* (1994) and other papers (in particular Mahajan & Rogava (1999)). As mentioned in the introduction, the proposed method is inspired by the stability analysis which is itself closely linked to the rapid distortion theory (RDT) of homogeneous turbulence (e.g. Batchelor

& Proudman, 1954, Goldstein, 1978, Cambon & Scott, 1999). Indeed, as emphasised by Cambon *et al.* (1994) for example, the equations derived in these two approaches are similar. Hence the approach presented in this paper is also strongly related to the RDT. The aim of this work is the study of the local effect of the shearing of the steady flow on the coupling between acoustic and vorticity perturbations. We suppose that the variation length scales L_{ρ_0} and L_{s_0} of the density ρ_0 and of the entropy s_0 of the steady flow are large compared to the typical length scale l of the perturbations $L_{\rho_0} \gg l$, $L_{s_0} \gg l$. So we consider a bi-dimensional incompressible and homentropic steady flow $\boldsymbol{u_0}$ of ideal fluid on which we superimpose compressible unsteady perturbations. The steady flow satisfies the incompressible Euler equations. It is linearised by keeping the two first terms of its Taylor expansion

$$\boldsymbol{u_0}(\boldsymbol{x}) \simeq \boldsymbol{\mathcal{U}_0} + \mathsf{A}\boldsymbol{x} \ , \tag{1.1}$$

where $\boldsymbol{\mathcal{U}_0}$ is a constant vector, which is responsible for a simple convection, and A is the constant shear matrix, which is responsible for shearing. We also suppose that the mean flow has a small Mach number and a small shearing, namely $|\boldsymbol{\mathcal{U}_0}| \leqslant |\mathsf{A}| l \ll c_0$, where l is a length scale characteristic of the perturbations, and where $c_0 = \sqrt{\gamma \mathcal{P}_0/\rho_0}$ would be the adiabatic speed of sound at the origin ($\mathcal{P}_0$ being the pressure at the origin $\mathcal{P}_0 = p_0(\boldsymbol{x} = \boldsymbol{0})$). It is shown in Appendix A, that under these assumptions the variation of the steady flow pressure p_0 can also be neglected, as being a small quantity of order $|\mathsf{A}|^2$. Therefore c_0 is eventually the speed of sound which is supposed constant in space (within the frame of the local approximation of the general steady flow). It is also shown that the only effect of the constant component $\boldsymbol{\mathcal{U}_0}$ on the following development is to add an additional term to the phase of the perturbations. For this reason we consider in the following that $\boldsymbol{\mathcal{U}_0} = \boldsymbol{0}$ for the sake of clarity. The steady flow is then linear and is fully described by

$$\boldsymbol{u_0}(\boldsymbol{x}) = \mathsf{A}\boldsymbol{x} \ . \tag{1.2}$$

We now consider linear perturbations of velocity $\boldsymbol{u} = (u, v)^\mathsf{T}$, density ρ, and pressure p. Their evolution is governed by the linearised Euler equations

$$\rho_0 \left(\frac{\partial}{\partial t} + \boldsymbol{u_0} \cdot \boldsymbol{\nabla} \right) \boldsymbol{u} + \rho_0 \mathsf{A}\boldsymbol{u} = -\boldsymbol{\nabla} p \ , \tag{1.3a}$$

$$\left(\frac{\partial}{\partial t} + \boldsymbol{u_0} \cdot \boldsymbol{\nabla} \right) \rho = -\rho_0 \boldsymbol{\nabla} \cdot \boldsymbol{u} \ , \tag{1.3b}$$

in which we neglected the term $\rho(\boldsymbol{u_0} \cdot \boldsymbol{\nabla})\boldsymbol{u_0}$ which is of order $|\mathsf{A}|^2$. Assuming that the perturbations are also homentropic, the pressure and density are linked by the adiabatic law $p = c_0^2 \rho$. The Appendix A provide a more detailed derivation of equation (1.3) and a discussion on the order of magnitude of the neglected terms.

We introduce the convected coordinates coming from the solution of the trajectory equation $\dot{\boldsymbol{x}} = \mathsf{A}\boldsymbol{x}$ with $\boldsymbol{x}(0) = \boldsymbol{X}$:

$$\boldsymbol{X} = \exp(-\mathsf{A}t)\, \boldsymbol{x}, \qquad T = t \ , \tag{1.4}$$

where $\boldsymbol{X}$ corresponds to Lagrangian coordinates. Analytical expression of the exponential is obtained by use of Pauli matrices as is detailed in Appendix C (equation (1.98)). With these new coordinates $(\boldsymbol{X}, T)$, equations (1.3) become

$$\frac{\partial}{\partial T}\boldsymbol{u} + \mathsf{A}\boldsymbol{u} = -\frac{1}{\rho_0}\exp\left(-\mathsf{A}^{\mathsf{T}}T\right)\boldsymbol{\nabla}_{\boldsymbol{X}}p \ , \tag{1.5a}$$

$$\frac{\partial}{\partial T}p = -\rho_0 c_0^2\left[\exp\left(-\mathsf{A}^{\mathsf{T}}T\right)\boldsymbol{\nabla}_{\boldsymbol{X}}\right]\cdot\boldsymbol{u} \ , \tag{1.5b}$$

where the superscript $^{\mathsf{T}}$ stands for matrix transposition. The coefficients involved in (1.5) are constant with respect to space which will be of a particular interest to apply Fourier. Indeed, by writing $\boldsymbol{u}(\boldsymbol{X}, T) = \boldsymbol{U}(T)e^{i\boldsymbol{k_0}\cdot\boldsymbol{X}}$ and $p(\boldsymbol{X}, T) = P(T)e^{i\boldsymbol{k_0}\cdot\boldsymbol{X}}$ the equations become

$$\frac{\mathrm{d}}{\mathrm{d}\,T}\boldsymbol{U} + \mathsf{A}\boldsymbol{U} = -\frac{1}{\rho_0}i\boldsymbol{k}P \ , \tag{1.6a}$$

$$\frac{\mathrm{d}}{\mathrm{d}\,T}P = -\rho_0 c_0^2 \ \ i\boldsymbol{k}\cdot\boldsymbol{U} \ , \tag{1.6b}$$

where

$$\boldsymbol{k} \equiv \exp\left(-\mathsf{A}^{\mathsf{T}}T\right)\boldsymbol{k_0} \ . \tag{1.7}$$

Equations (1.6) constitute a system of three first order ordinary differential equations, which allows us to study the governing equations as an evolution problem of dimension three.

The equations are now turned into a dimensionless form. We define the dimensionless shear matrix

$$\mathsf{B} \equiv \frac{1}{\zeta}\mathsf{A} \ , \tag{1.8}$$

where the quantity ζ is defined in equation (1.16) of section 2a. We define $k_0 = \|\boldsymbol{k_0}\|$ and use $1/k_0$, $1/c_0k_0$, c_0, and $\rho_0 c_0^2$, as reference values to obtain dimensionless lengths, time, velocities and pressure (note that in the new dimensionless variables $k_0 = 1$). Equations (1.6) reduce to

$$\frac{\mathrm{d}}{\mathrm{d}\,T}\boldsymbol{U} + \varepsilon\mathsf{B}\boldsymbol{U} = -i\boldsymbol{k}P \ , \tag{1.9a}$$

$$\frac{\mathrm{d}}{\mathrm{d}\,T}P = -i\boldsymbol{k}\cdot\boldsymbol{U} \ , \tag{1.9b}$$

where appears the dimensionless parameter

$$\varepsilon \equiv \frac{\zeta}{c_0k_0} \ . \tag{1.10}$$

That ε is the ratio of the characteristic shear rate of the flow over the typical frequency of the perturbations. For instance, for the plane Couette flow, this is the ratio of the

vorticity of the mean flow over the typical frequency of perturbations. In the following we name the elements appearing in (1.9) as follows :

$$\boldsymbol{U}(T) = \begin{pmatrix} U(T) \\ V(T) \end{pmatrix} \quad , \qquad \boldsymbol{k}(T) = \begin{pmatrix} \alpha(T) \\ \beta(T) \end{pmatrix} \ , \tag{1.11}$$

$$\mathsf{B} = \begin{pmatrix} r & a \\ b & -r \end{pmatrix} \quad , \qquad \boldsymbol{k_0} = \begin{pmatrix} \alpha_0 \\ \beta_0 \end{pmatrix} \ . \tag{1.12}$$

A consequence of equations (1.7) and (1.9) is the conservation of potential vorticity

$$\mathcal{C} \equiv \beta U - \alpha V + i\varepsilon(a-b)P = \text{const.} \ . \tag{1.13}$$

This relation plays a very important role in the following developments, as it is responsible of cross dependences between acoustic and vorticity parts.

2.1 Linear flows parametrization

The incompressibility and linearity assumptions allows us to parametrize all flows with two parameters. As is developed in Appendix B we can, without loss of generality, write the shear matrix in the form

$$\mathsf{A} = \zeta(\ \delta\ \mathsf{B_h} + (1-\delta)\ \mathsf{B_r})\ , \tag{1.14}$$

$$\text{where } \mathsf{B_h} = \begin{pmatrix} 0 & 1 \\ 1 & 0 \end{pmatrix} \text{ and } \mathsf{B_r} = \begin{pmatrix} 0 & 1 \\ -1 & 0 \end{pmatrix} \ . \tag{1.15}$$

The dimensionless shape parameter $\delta \in [0;1]$, and the shear rate ζ (homogeneous to a frequency) are given by (see appendix B for derivation)

$$\zeta = \sqrt{A_{xx}^2 + \frac{(A_{xy}+A_{yx})^2}{4}} + \frac{|A_{xy}-A_{yx}|}{2}\ , \tag{1.16}$$

$$\delta = \frac{1}{\zeta}\sqrt{A_{xx}^2 + \frac{(A_{xy}+A_{yx})^2}{4}}\ . \tag{1.17}$$

The two matrices $\mathsf{B_h}$ and $\mathsf{B_r}$ correspond respectively to a hyperbolic flow and to a clockwise rigid rotation flow. Thus, any flow is decomposed as a weighted sum of a hyperbolic part and of a rotation part, and the whole set of flow shapes is parametrized by δ as shown on figure 1.1. It includes the rigid rotation ($\delta = 0$), elliptic flows ($0 < \delta < 1/2$), the plane Couette flow ($\delta = 1/2$) and the hyperbolic flow ($\delta = 1$). Note that with the present decomposition the parameters appearing in (1.11) are $r = 0$, $a = 1$ and $b = 2\delta - 1 \in [-1;1]$. The dimensionless shear matrix is then

$$\mathsf{B} = \delta\ \mathsf{B_h} + (1-\delta)\ \mathsf{B_r}\ . \tag{1.18}$$

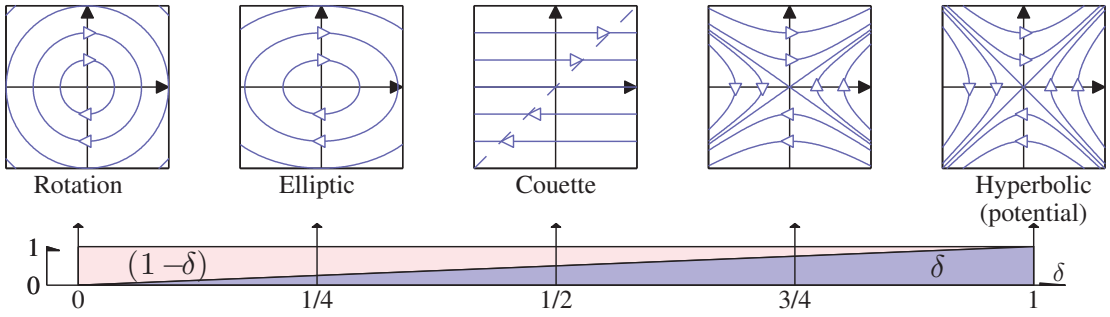

FIGURE 1.1 – Linear incompressible flow shapes depending on δ (streamlines).

2.2 Convected wavevector

We discuss here some points concerning the wavevector $\boldsymbol{k}$. Since it satisfies $\boldsymbol{k_0} \cdot \boldsymbol{X} = \boldsymbol{k} \cdot \boldsymbol{x}$, $\boldsymbol{k}$ is the wavevector in fixed coordinates $\boldsymbol{x}$. It is governed by

$$\frac{\mathrm{d}}{\mathrm{d}\,T}\,\boldsymbol{k} = -\varepsilon \mathsf{B}^{\mathsf{T}}\boldsymbol{k}\ , \tag{1.19}$$

which is the same equation as the one governing the wavenumber in geometrical acoustics approximation. It means that $\boldsymbol{k}$ is drifted by effect of the flow (Chagelishvili *et al.*, 1993), and the $\boldsymbol{k}$ vector follows the streamlines of the steady flow, up to a $-\pi/2$ rotation. Equation (1.7) gives an explicit formula to compute analytically $\boldsymbol{k}$. The derivation is based on Pauli matrices and is detailed in appendix C. It yields

$$\boldsymbol{k}(T) = \left[\cosh\left(\sqrt{2\delta-1}\ \varepsilon T\right)\mathsf{Id} - \frac{\sinh\left(\sqrt{2\delta-1}\ \varepsilon T\right)}{\sqrt{2\delta-1}}\mathsf{B}\right]\boldsymbol{k_0}\ , \tag{1.20}$$

where Id is the identity matrix.

Figure 1.2 illustrates for different flows the time evolution of the wavevector and of its norm that we name

$$k = \|\boldsymbol{k}\|\ . \tag{1.21}$$

In the case of the rigid rotation ($\delta = 0$), k is constant. When $\delta < 1/2$ (elliptic flows), $\boldsymbol{k}$ has a periodic behaviour with an amplitude and frequency which grow as $\delta \longrightarrow 1/2$. The Couette flow can be viewed as the limit when this frequency tends to zero. For this flow there is a minimum of k at $T_\star = \beta_0/\varepsilon\alpha_0$, which is 0 in figure 1.2 since $\beta_0 = 0$. Far from $T_\star$, k evolve as $\sim |\varepsilon T|$. When $\delta > 1/2$, the k curve is qualitatively the same but the behaviour of k becomes asymptotic to an exponential $\sim e^{\pm\sqrt{2\delta-1}\varepsilon T}$. The most important point for following developments is the presence of minima of k as time evolve, for all flows except rigid rotation ; this minima will correspond to couplings between acoustic and vorticity parts.

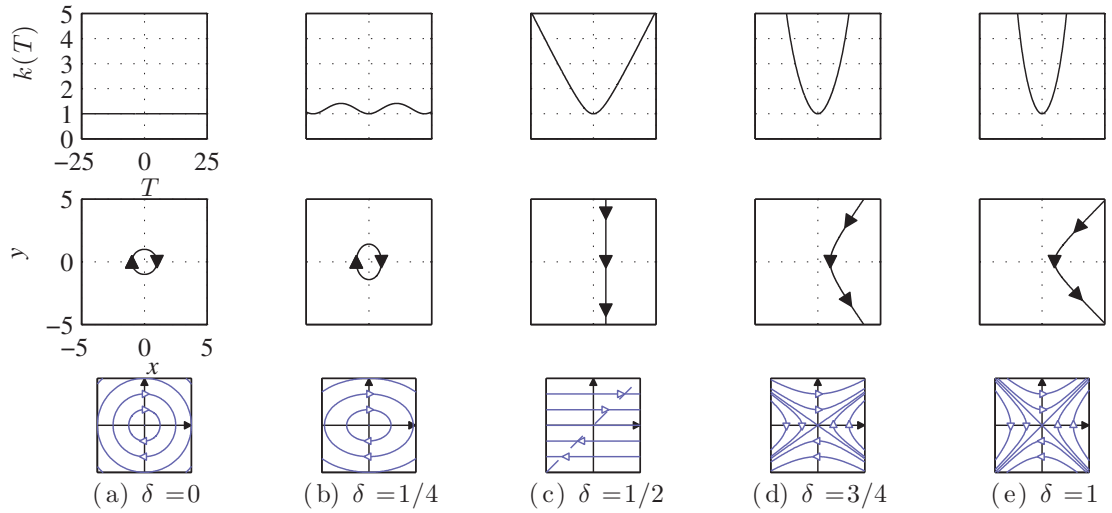

FIGURE 1.2 – Time evolution of k and $\boldsymbol{k}$ for $\varepsilon = .2$, $\alpha_0 = 1$, $\beta_0 = 0$, and $\delta = 0$ (a), 1/4 (b), 1/2 (c), 3/4 (d), and 1 (e). The graphs on the top line show the time evolution of k for these different flows. The graphs on the middle exhibit the time evolution of the vector $\boldsymbol{k}$ in space (fixed coordinates x and y). Flow shapes are shown on the graphs on the bottom line.

2.3 Acoustic waves : the no flow limit

We consider here, as an illustrative example, the no flow limit where $\boldsymbol{u_0} = \boldsymbol{0}$ ($\varepsilon = 0$ with finite speed of sound). In this case, the wavevector is constant with respect to time :

$$\boldsymbol{k} = \boldsymbol{k_0} = \text{const.} \; . \tag{1.22}$$

The equations (1.9), written as a vectorial ordinary differential equation, reduce to

$$\frac{\mathrm{d}}{\mathrm{d}\,T} \begin{pmatrix} \boldsymbol{U} \\ P \end{pmatrix} = \begin{pmatrix} 0 & 0 & -i\boldsymbol{k_0} \\ 0 & 0 & \\ -i\boldsymbol{k_0}^{\mathsf{T}} & & 0 \end{pmatrix} \begin{pmatrix} \boldsymbol{U} \\ P \end{pmatrix} \; , \tag{1.23}$$

which implies the scalar wave equation (more precisely an harmonic oscillator). The matrix in the right hand side of equation (1.23) has the three eigenvalues

$$\lambda_H = 0 \quad , \quad \lambda_\pm = \pm i k_0 = \pm i \; , \tag{1.24}$$

associated to the modes

$$\begin{pmatrix} \boldsymbol{U} \\ P \end{pmatrix}_H = \begin{pmatrix} \boldsymbol{k_0^\perp} \\ 0 \end{pmatrix} \qquad , \qquad \begin{pmatrix} \boldsymbol{U} \\ P \end{pmatrix}_\pm = \frac{e^{\pm iT}}{\sqrt{2}} \begin{pmatrix} \boldsymbol{k_0} \\ \mp 1 \end{pmatrix} \; , \tag{1.25}$$

where $\boldsymbol{k_0^\perp} = (\beta_0, -\alpha_0)^{\mathsf{T}}$. The first mode is a vorticity mode, and it has a divergence free velocity field, while the last ones, correspond to acoustic modes with curl-free velocity

fields. General solution of the system (1.23) is

$$\begin{pmatrix} \boldsymbol{U} \\ P \end{pmatrix} = C_H \begin{pmatrix} \boldsymbol{k_0^\perp} \\ 0 \end{pmatrix} + C_+ \frac{e^{+iT}}{\sqrt{2}} \begin{pmatrix} \boldsymbol{k_0} \\ -1 \end{pmatrix} + C_- \frac{e^{-iT}}{\sqrt{2}} \begin{pmatrix} \boldsymbol{k_0} \\ +1 \end{pmatrix} \ , \tag{1.26}$$

where C_H, C_+, C_- are constant. We recover here classical acoustics with two acoustic waves travelling towards opposite directions. The first term in (1.26) corresponds to trivial vorticity perturbations that are frozen in time.

2.4 Hydrodynamic waves : the incompressible limit

We now present as a second illustrative example the incompressible limit case (with infinite speed of sound and finite $\boldsymbol{u_0}$). The equations (1.9) become

$$\frac{\mathrm{d}}{\mathrm{d}\,T} \boldsymbol{U} = -\mathsf{B}\boldsymbol{U} - iP\boldsymbol{k} \ , \tag{1.27a}$$

$$\boldsymbol{k} \cdot \boldsymbol{U} = 0 \ . \tag{1.27b}$$

The dynamics of such systems has been the subject of many studies based on the work of Lord Kelvin (Thomson, 1887, Craik & Criminale, 1986, Criminale & Drazin, 1990, Huerre & Monkewitz, 1990, Butler & Farrell, 1992, Trefethen *et al.*, 1993, Reddy *et al.*, 1993, Huerre & Rossi, 1998, Schmid & Henningson, 2001, Friedlander & Lipton-Lifschitz, 2003, Schmid, 2007). For 3D linear flows, Craik & Criminale (1986) have given explicit solutions. Using the incompressibility condition (1.27b) the pressure is expressed in terms of the velocity

$$P = \frac{2i}{k^2} \mathsf{B}^\mathsf{T} \boldsymbol{k} \cdot \boldsymbol{U} \ , \tag{1.28}$$

and the velocity evolution is then governed by

$$\frac{\mathrm{d}}{\mathrm{d}\,T} \boldsymbol{U} = \Big(-\mathsf{B} + \frac{2}{k^2} \boldsymbol{k}\boldsymbol{k}^\mathsf{T} \mathsf{B} \Big) \boldsymbol{U} \ . \tag{1.29}$$

This equation has the two independent solutions

$$\boldsymbol{U_1} = \frac{1}{k^2}\boldsymbol{k} - 2(1-\delta)\frac{T}{k^2}\boldsymbol{k}^\perp \ , \tag{1.30}$$

$$\boldsymbol{U_2} = \frac{1}{k^2}\boldsymbol{k}^\perp \ . \tag{1.31}$$

Except for elliptic flows ($\delta < 1/2$), these solutions are bounded and tends to zero as $T \longrightarrow \pm\infty$. However, their components evolve as $1/k$, and the time dependence of k (see the minima in figure 1.2) allows the presence of a transient growth which can lead to high amplitudes at finite time (see for example Schmid & Henningson, 2001, Butler & Farrell, 1992, Trefethen *et al.*, 1993, Reddy *et al.*, 1993). The case of elliptic flows is different. One solution is bounded and periodic, and the other one grows as $\sim T$. Figure 1.3 gives an illustration of these two solutions for different flows. The solution $\boldsymbol{U_1}$ is unstable in the case of elliptic flows ($\delta < 1/2$) while $\boldsymbol{U_2}$ is stable. In the case of the Couette plane

flow ($\delta = 1/2$), the solution $\boldsymbol{U_1}$ becomes constant but the other solution $\boldsymbol{U_2}$ displays a transient growth. This solution tends to zero at infinite positive or negative times but has a strong maximum at $T = 0$ (here normalized to 1). Even if the solution finally tends to zero, it is possible to find an initial condition, say of norm 1, which leads to an arbitrary high amplitude depending on how far from $T = 0$ is imposed this initial condition. For elliptic and nearly elliptic flows ($\delta > 1/2$), the two solutions $\boldsymbol{U_1}$ and $\boldsymbol{U_2}$ are subject to a transient growth. They are even more efficient in the potential hyperbolic flow.

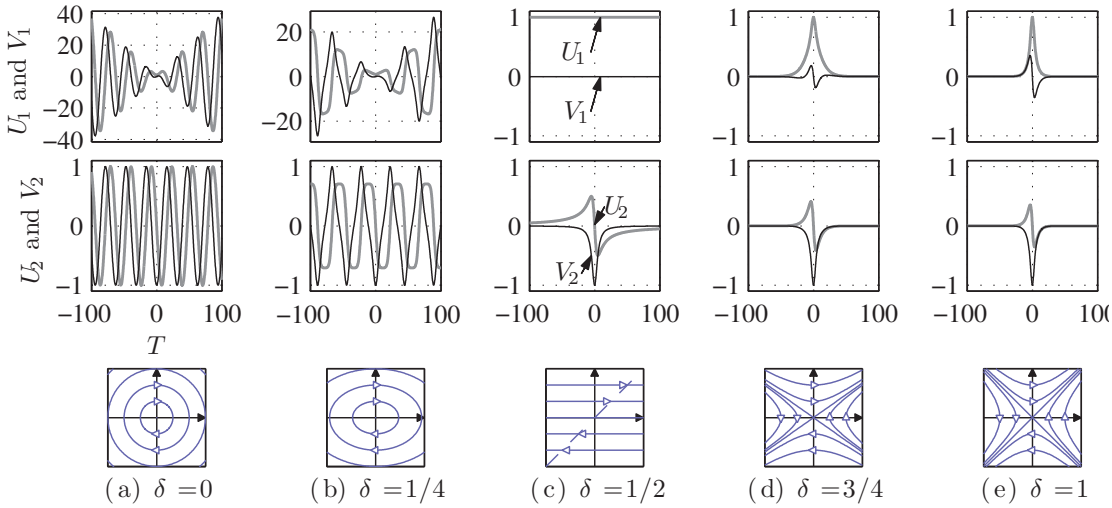

FIGURE 1.3 – Time evolution of incompressible perturbations $\boldsymbol{U_1}$ and $\boldsymbol{U_2}$ for $\alpha_0 = 1$, $\beta_0 = 0$, and $\delta = 0$ (a), 1/4 (b), 1/2 (c), 3/4 (d), and 1 (e). The graphs on the top and middle rows present the components along the x-axis (bold gray curve) and y-axis (thin black curve) of the velocity field of the two solutions $\boldsymbol{U_1}$ (top row) and $\boldsymbol{U_2}$ (middle row) of the incompressible model. Flow shapes are recalled on the graphs on the bottom line. See text for discussion.

In the next parts of this paper, we focus on situations where both acoustic and hydrodynamic modes coexist (finite $\varepsilon \ll 1$ and compressible perturbations).

3 WKB approach

In this section we use the WKB method (Hinch, 1991, Holmes, 1995) to construct the base of acoustic and vorticity modes in the presence of flow. For small values of ε, that means perturbations of frequency higher than the shear rate of the flow, we introduce the slow time $\tau = \varepsilon T$. From (1.9), it leads to

$$\varepsilon \frac{\mathrm{d}}{\mathrm{d}\,\tau} \boldsymbol{Y}(\tau) = \Big(\mathsf{H}_0(\tau) + \varepsilon \mathsf{H}_1\Big)\boldsymbol{Y}(\tau) \ , \tag{1.32}$$

where

$$\boldsymbol{Y}(\tau) \equiv \begin{pmatrix} U(\tau) \\ V(\tau) \\ iP(\tau) \end{pmatrix} , \tag{1.33}$$

$$\mathsf{H}_0(\tau) \equiv \begin{pmatrix} 0 & 0 & -\boldsymbol{k}(\tau) \\ 0 & 0 & \\ \boldsymbol{k}^{\mathsf{T}}(\tau) & & 0 \end{pmatrix} , \qquad \text{and} \qquad \mathsf{H}_1 \begin{pmatrix} -\mathsf{B} & & 0 \\ & & 0 \\ 0 & 0 & 0 \end{pmatrix} . \tag{1.34}$$

Here, H_0 is anti-symmetric, but the operator $\mathsf{H} \equiv \mathsf{H}_0 + \varepsilon \mathsf{H}_1$ has no particular symmetry in general ; it is anti-symmetric only in the case of the rigid rotation with antisymmetric B (which is also the only case where we know a simple analytic solution). This lack of symmetry implies the lack of the conservation of the canonical energy of the system defined by

$$E = \frac{1}{2}\|\boldsymbol{Y}\|^2 = \frac{1}{2}(|U|^2 + |V|^2 + |P|^2) . \tag{1.35}$$

Indeed, according to equation (1.32), its evolution is governed by

$$\frac{\mathrm{d}\, E}{\mathrm{d}\, T} = -\delta \boldsymbol{Y}^{\dagger} \begin{pmatrix} \mathsf{B}_{\mathsf{h}} & & 0 \\ & & 0 \\ 0 & 0 & 0 \end{pmatrix} \boldsymbol{Y} , \tag{1.36}$$

where the superscript † refers to the complex conjugation-transposition. Perturbations can therefore gain or lose energy over time, and this evolution is due to the hyperbolic part of the flow B_{h} defined in equation (1.15).

In previous works (*e.g.* Chagelishvili *et al.*, 1994, Gogoberidze *et al.*, 2004) the definition of acoustic and vorticity parts was based on whether the perturbation corresponds to the general homogeneous solution or to the particular non homogeneous solution of the second order non-homogeneous equation governing the horizontal component of the velocity perturbation. In our work, the WKB method will provide automatically three modes. Two of these modes will correspond to the acoustic part and the third mode will correspond to the vorticity part.

To apply the WKB method on (1.32), we assume the following *ansatz*

$$\boldsymbol{Y}(\tau) = e^{\frac{i}{\varepsilon}S(\tau)} \Big(\boldsymbol{\varphi_0}(\tau) + \ldots + \varepsilon^n \boldsymbol{\varphi_n}(\tau) + \ldots \Big) . \tag{1.37}$$

Injecting the equation (1.37) into (1.32), and identifying terms of same order in power of ε leads to the classical recursive WKB system to be solved

$$\Big(i\dot{S}(\tau)\mathsf{Id} - \mathsf{H}_0(\tau) \Big) \boldsymbol{\varphi_0}(\tau) = 0 , \tag{1.38a}$$

$$\Big(i\dot{S}(\tau)\mathsf{Id} - \mathsf{H}_0(\tau) \Big) \boldsymbol{\varphi_n}(\tau) = \mathsf{H}_1 \boldsymbol{\varphi_{n-1}}(\tau) - \dot{\boldsymbol{\varphi}}_{n-1}(\tau) \text{ , for } n \geq 1, \tag{1.38b}$$

where the overdot refers to differentiation with respect to the time τ.

3.1 Order 0 WKB modes

The order 0 equation (1.38a) is an eigenvalue problem. Therefore, $i\dot{S}$ is one the three eigenvalues of $\mathsf{H_0}$

$$\lambda_H = 0 \quad , \quad \lambda_\pm = \pm ik \ , \tag{1.39}$$

and $\boldsymbol{\varphi_0}$ is proportional to the associated eigenmode among

$$\boldsymbol{\varphi}_{\mathbf{0},\boldsymbol{H}} \propto \begin{pmatrix} \boldsymbol{k}^\perp \\ 0 \end{pmatrix} \qquad , \qquad \boldsymbol{\varphi}_{\mathbf{0},\pm} \propto \begin{pmatrix} \boldsymbol{k} \\ \mp ik \end{pmatrix} \ . \tag{1.40}$$

There remains to find the proportionality factors whose time dependence is imposed by the *compatibility condition* derived from the order 1 equation, as is usual in the WKB method (Folguera & Harris, 1999, Pagneux & Maurel, 2006). Taking the hermitian product of equation (1.38b) for $n = 1$ with $\boldsymbol{\varphi_0}$ shows that

$$0 = \boldsymbol{\varphi_0}(\tau) \cdot \Big(\mathsf{H_1} \boldsymbol{\varphi_0}(\tau) - \dot{\boldsymbol{\varphi}}_\mathbf{0}(\tau) \Big) \ , \tag{1.41}$$

which allows us to obtain the sought proportionality factors. Eventually, we have

$$\boldsymbol{\varphi}_{\mathbf{0},\boldsymbol{H}} = \frac{1}{k^2} \begin{pmatrix} \boldsymbol{k}^\perp \\ 0 \end{pmatrix} \qquad , \qquad \boldsymbol{\varphi}_{\mathbf{0},\pm} = \frac{1}{\sqrt{k}} \begin{pmatrix} \boldsymbol{k} \\ \mp ik \end{pmatrix} \ , \tag{1.42}$$

and the order 0 WKB modes in (1.37) are :

$$\boldsymbol{Y}_{\mathbf{0},\boldsymbol{H}} = \frac{1}{k^2} \begin{pmatrix} \boldsymbol{k}^\perp \\ 0 \end{pmatrix} \qquad , \qquad \boldsymbol{Y}_{\mathbf{0},\pm} = \frac{e^{\pm \frac{i}{\varepsilon} \int k}}{\sqrt{k}} \begin{pmatrix} \boldsymbol{k} \\ \mp ik \end{pmatrix} \ . \tag{1.43}$$

In the same manner as in the case of the no flow limit (1.25), we identify one vorticity mode (under-script H) and two acoustic modes, one backward-going (under-script $+$) and one forward-going (under-script $-$). To get some insights on these modes we first focus on the eigenvalues.

The figure 1.4(a) represents the time evolution of the imaginary part of the eigenvalues, in the widely studied Couette flow ($\delta = 1/2$), with $\varepsilon = 0.2$, $\alpha_0 = 1$, and $\beta_0 = 0$. This is a typical case of avoided crossing of the eigenvalues with near coalescence near $\tau_\star = \beta_0/\alpha_0 = 0$. This is because $\tau_\star$ is the closest point on the real τ axis to the complex zero $\tau_c = \beta_0/\alpha_0 + i\alpha_0$ of k, where all three eigenvalues coalesce. In the two-state Landau-Zener model (Landau, 1932, Landau & Lifshitz, 1977, Zener, 1932) two modes with opposite eigenvalues exchange energy at such a point. This phenomenon, called non-adiabatic transition, is of order $\sim e^{-C/\varepsilon}$, and cannot be produced by WKB asymptotics. We expect that some couplings occur at such $\tau_\star$.

Concerning the WKB modes themselves, they have a varying wavevector, in opposition to the exact modes obtained in the no flow limit (section 2c), and their norms depend on time. The components of the acoustic modes evolve as $\sim \sqrt{k}$. For flows where $\delta \geq 1/2$, they have a minimum at $\tau_\star$ and grow indefinitely over time. That phenomenon has been interpreted as an energy transfer phenomenon between disturbances and the

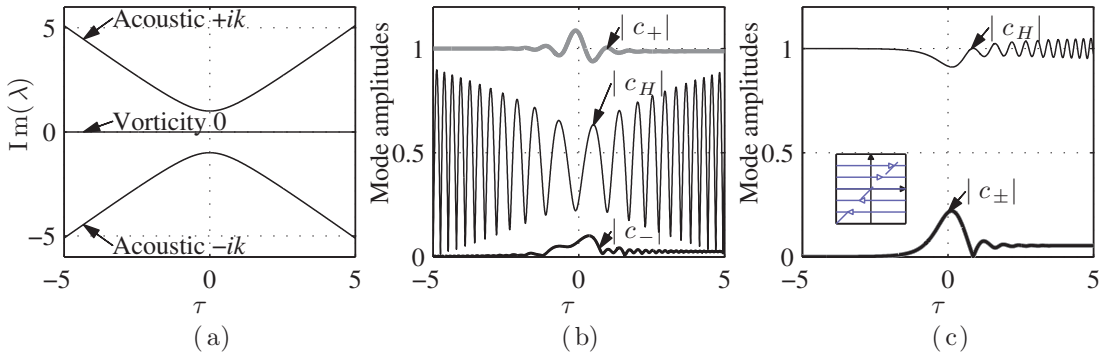

FIGURE 1.4 – Couette flow ($\delta = 1/2$, $\varepsilon = 0.2$, $\alpha_0 = 1$, $\beta_0 = 0$). Imaginary part of the eigenvalues 0, $\pm ik$ (a). Amplitudes of each order 0 WKB mode for an incident acoustic mode (b) and incident vorticity mode (c). Flow streamlines are presented on the graph (c).

mean flow for the plane Couette flow ($\delta = 1/2$) (Chagelishvili *et al.*, 1994). The vorticity mode evolves as $\sim 1/k$, it has a maximum at $\tau_\star$ and decay for positive and negative time. It is the compressible analogue of the incompressible solution $\boldsymbol{U_2}$ in equation (1.31) of section 2d, which displays one of the transient growths (see for example Schmid & Henningson, 2001, Butler & Farrell, 1992, Trefethen *et al.*, 1993, Reddy *et al.*, 1993). It is important to notice that at this order the acoustic modes are curl-free and the vorticity mode is divergence-free.

We now focus on the evolution of the solution in the base formed by these WKB modes. When $\varepsilon = 0$ with $\boldsymbol{u_0} = \boldsymbol{0}$, it has been already seen that these amplitudes are constant (see section 2c). When $\varepsilon \ll 1$, if the goal of providing analytic solutions is achieved, we would expect constant amplitudes for any solution expressed in this base. Let $\boldsymbol{c}(\tau) = (c_H(\tau), c_+(\tau), c_-(\tau))^\intercal$ be the vector representing the solution in this base :

$$\boldsymbol{Y} = c_H \boldsymbol{Y}_{\boldsymbol{0,H}} + c_+ \boldsymbol{Y}_{\boldsymbol{0,+}} + c_- \boldsymbol{Y}_{\boldsymbol{0,-}} \ , \tag{1.44}$$

where the coefficients c_m will be referred as the amplitude of the mode m ($m \in \{H, +, -\}$). In this base, the energy definition (1.35) becomes

$$E(\tau) = \frac{1}{2k^2}|c_H|^2 + k|c_+|^2 + k|c_-|^2 \ . \tag{1.45}$$

For constant amplitude c_m, acoustic modes see their energy evolving as k, and the vorticity mode as $1/2k^2$. This also means that for acoustic mode, the wave action (Bretherton & Garrett, 1968, Buhler, 2009)

$$\mathcal{A} = \frac{E}{k} \tag{1.46}$$

is conserved. Note that far from $\tau_\star$, the contribution of the vorticity mode to the wave action is very small ($\sim 1/k^3$) and that the total wave action is almost conserved.

Figure 1.4(b) displays the time evolution of mode amplitudes. At $\tau_i = -5$ the WKB acoustic mode is imposed as an initial condition $\boldsymbol{Y}(\tau_i) = \boldsymbol{Y}_{\mathbf{0},+}(\tau_i)$, or equivalently $c_+(\tau_i) = 1$, $c_H(\tau_i) = c_-(\tau_i) = 0$. It corresponds to an incident acoustic mode. Equation (1.32) is numerically integrated using a Magnus-Möbius scheme (Iserles *et al.*, 1999, Pagneux, 2010). As expected, the amplitude of the incident acoustic mode remains close to 1, but the vorticity mode amplitude immediately oscillates. These fluctuations may be understood from the potential vorticity conservation : using (1.13) and assuming $c_+ \simeq 1$, $c_- \simeq 0$ it comes that

$$|c_H| = \varepsilon \left| \sqrt{k(\tau_i)} - \sqrt{k(\tau)} e^{\int^\tau \frac{ik}{\varepsilon}} \right| \ . \tag{1.47}$$

So to ensure potential vorticity conservation the imposed purely acoustic perturbation (curl-free) acquire a rotational part by driving the vorticity mode ; we recover the well known fact that acoustic perturbation cannot be curl-free in shear flow (Mohring *et al.*, 1983). From a more technical point of view, it is in fact a non uniformity of the WKB method with an amplitude $\langle c_H \rangle \sim \varepsilon \tau_i$. More generally, for any flow, the potential vorticity conservation enforces

$$c_H = \mathcal{C} + 2i\varepsilon(1-\delta)\sqrt{k}\left(c_- e^{-\frac{i}{\varepsilon}\int k} - c_+ e^{+\frac{i}{\varepsilon}\int k} \right) \ . \tag{1.48}$$

The $(1-\delta)$ factor in (1.48) shows that the rotation part of the flow is responsible for this effect. This happens in all flows except the hyperbolic flow ($\delta = 1$), in which the vorticity mode has a constant amplitude. This comes with no surprise as the hyperbolic flow is potential and it is the only case where acoustic perturbations are curl-free (potential).

Another interesting effect is the emergence of the non-incident acoustic mode (of amplitude c_-) at the time $\tau_\star = 0$. This is a non-adiabatic transition due to the avoided crossing of the eigenvalues. As stated earlier, this is an exponentially small phenomenon of order $e^{-C/\varepsilon}$. This cannot be modelled by the standard WKB asymptotic expansion itself even if higher order approximation were used (all derivatives of the exponential are null at $\varepsilon = 0$). However a large number of authors have been investigating this kind of phenomena with extension of the WKB method. It is particularly popular to study non-adiabatic state transitions in quantum mechanics (e.g. Davis & Pechukas, 1976, Berry, 1990, Lim & Berry, 1991, Hagedorn & Joye, 2004).

Figure 1.4(c) displays the amplitudes of the three modes when vorticity mode is incident at $\tau_i = -5$. As in the preceding case, the incident mode amplitude stays close to 1. At $\tau_\star$ a non-adiabatic transition occurs, and the vorticity mode generates the two acoustic modes. After $\tau_\star$ we can notice that the vorticity mode amplitude starts to oscillate due to the presence of the acoustic modes and to the non-uniformity mentioned just above. The acoustics produced by the incident vorticity mode can be estimated analytically. The exact equations governing the evolution of $\boldsymbol{c}$ are derived from equations (1.32), (1.43), and (1.44) and yield

$$\begin{bmatrix} \dot{c}_H \\ \dot{c}_+ \\ \dot{c}_- \end{bmatrix} = \begin{bmatrix} 0 & -2(1-\delta)k^{3/2}e_+ & -2(1-\delta)k^{3/2}e_- \\ \frac{\mathcal{D}}{k^{7/2}}e_- & 0 & \frac{\dot{k}}{2k}e_-^2 \\ \frac{\mathcal{D}}{k^{7/2}}e_+ & \frac{\dot{k}}{2k}e_+^2 & 0 \end{bmatrix} \begin{bmatrix} c_H \\ c_+ \\ c_- \end{bmatrix} \ , \tag{1.49}$$

where $e_\pm$ stands for $e^{\frac{\pm i}{\varepsilon}\int k}$, and

$$\mathcal{D} = \boldsymbol{k} \times \dot{\boldsymbol{k}} \cdot \boldsymbol{e_Z} \ , \tag{1.50}$$

which is constant thanks to equation (1.19). We recover that for the hyperbolic flow ($\delta = 1$), c_H is constant. When the vorticity mode is incident, $c_H \sim 1$, c_+ is governed at first order by

$$\dot{c}_+ \approx \frac{\mathcal{D}}{k^{7/2}} e^{\int -\frac{ik}{\varepsilon}} \ , \tag{1.51}$$

and is obtained by quadrature. This estimation of the acoustic amplitude c_+ is similar to the Born approximation and it is displayed on figure 1.5. It provides a good approximation of the acoustic produced by vorticity.

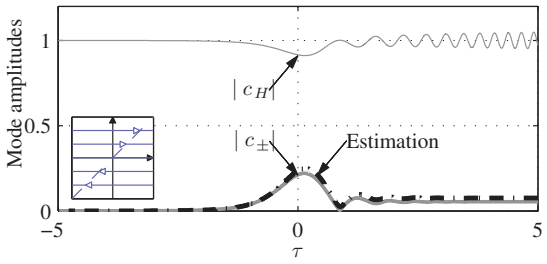

FIGURE 1.5 – Couette flow ($\delta = 1/2$ and $\varepsilon = 0.2$). Amplitudes of order 0 WKB mode (bold gray) for an incident vorticity mode, and approximation of acoustic amplitude transition (dash dotted).

In the following, in order to get rid of the non-uniformity, responsible for the fluctuations of c_H and due to the potential vorticity conservation, we propose a slight modification of the WKB base.

3.2 Order 1 WKB modes

To get the WKB modes at next order, we need to determine $\boldsymbol{\varphi_1}$. For this we use the equation (1.38b) with $n = 1$ and express $\boldsymbol{\varphi_1}$ in terms of the $\boldsymbol{\varphi_{0,m}}$ (the eigenmodes of $\mathsf{H_0}$). For the acoustic mode, it gives

$$\boldsymbol{\varphi}_{1,+} = -i\frac{\dot{k}}{4k^2}\boldsymbol{\varphi}_{0,-} + 2i\,(1-\delta)\,\sqrt{k}\,\boldsymbol{\varphi}_{0,H} + w_{++}\boldsymbol{\varphi}_{0,+} \ , \tag{1.52}$$

where w_{++}, the component of $\boldsymbol{\varphi}_{1,+}$ along $\boldsymbol{\varphi}_{0,+}$, is still undetermined because the kernel of $(i\dot{S}\mathsf{Id} - \mathsf{H_0})$ in equation (1.38b) is along $\boldsymbol{\varphi}_{0,+}$. To determine this last component w_{++}, the classical method would consist in taking the projection on $\boldsymbol{\varphi}_{0,+}$ of (1.38b) at order $n = 2$. In our case, this is the source of non-uniformities and secular terms. To avoid this problem, Smith proposed a method in which both phase and mode shape are expanded in ε power series (Smith, 1977, Gridin & Craster, 2003). As we only intend to remain at order 1, we propose a simpler method : we choose to determine the last component w_{++}

so as to minimize the variation of the invariant potential vorticity $\mathcal{C}$. This choice relies on the fact that the non-uniformity is imposed by the potential vorticity conservation. Combining (1.13), (1.43) and (1.52), we obtain

$$\mathcal{C} = 2i\varepsilon^2(1-\delta)\sqrt{k}\left(-i\frac{\dot{k}}{4k^2} - w_{+,+}\right)e^{\frac{i}{\varepsilon}\int k}\ . \tag{1.53}$$

To make $\mathcal{C}$ constant for the WKB mode, we impose

$$w_{+,+} = -i\frac{\dot{k}}{4k^2}\ . \tag{1.54}$$

Eventually, the order 1 acoustic WKB modes are

$$\boldsymbol{Y_{1,\pm}} = e^{\pm\frac{i}{\varepsilon}\int k}\Big(\boldsymbol{\varphi_{0,\pm}} \mp i\varepsilon\frac{\dot{k}}{4k^2}\left(\boldsymbol{\varphi_{0,+}} + \boldsymbol{\varphi_{0,-}}\right) \pm 2i\varepsilon\left(1-\delta\right)\sqrt{k}\,\boldsymbol{\varphi_{0,H}}\Big)\ . \tag{1.55}$$

The acoustic mode includes now the vorticity oscillations (non-uniformities) discussed in previous section. The factor $(1-\delta)$ shows that this correction is due to the rotation part of the flow, and, consequently, does not exist in the case of the hyperbolic flow. Applying the same method to determine the order 1 vorticity mode leads to

$$\mathcal{C} = 1 + \varepsilon k^2 w_{H,H} + 4\varepsilon^2\frac{(1-\delta)\mathcal{D}}{k^4}\ . \tag{1.56}$$

Here we can only make the invariant constant to order ε by setting $w_{H,H} = 0$. Therefore, the order 1 vorticity WKB mode is

$$\boldsymbol{Y}_{1,H} = \boldsymbol{\varphi}_{0,H} + i\varepsilon\frac{\mathcal{D}}{k^{9/2}}\left(\boldsymbol{\varphi}_{0,+} - \boldsymbol{\varphi}_{0,-}\right)\ . \tag{1.57}$$

Now that the order 1 base is obtained we define $\boldsymbol{d}$ the same manner as $\boldsymbol{c}$:

$$\boldsymbol{Y} = d_H\boldsymbol{Y_{1,H}} + d_+\boldsymbol{Y_{1,+}} + d_-\boldsymbol{Y_{1,-}}\ . \tag{1.58}$$

We will focus on the evolution of the exact solution in this order 1 base, which is free of non-uniformities and for which only non-adiabatic transitions at $\tau = \tau_\star$ may occur.

4 Main results

4.1 Plane Couette flow

The figure 1.6 shows the time evolution of order 1 WKB mode amplitudes in the plane Couette flow when order 1 WKB modes are incident. It is instructive to compare these results with those obtained with the order 0 WKB modes in figure 1.4(b-c). For an incident acoustic mode (figure 1.6(a)), the vorticity mode fluctuations discussed earlier in figure 1.4(b) no longer exist since the acoustic mode at order 1 contains the vorticity

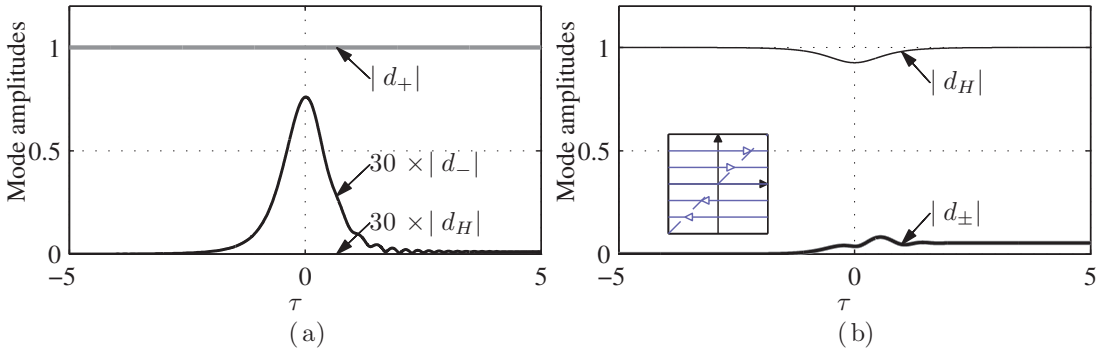

FIGURE 1.6 – Couette flow ($\delta = 1/2$ and $\varepsilon = 0.2$). Amplitudes of each order 1 WKB mode for an incident acoustic mode (a) and incident vorticity mode (b).

correction needed to ensure potential vorticity conservation. Indeed, this latter condition becomes

$$\mathcal{C} = d_H \left(1 + 4\varepsilon^2 \frac{(1-\delta)\mathcal{D}}{k^4}\right) . \tag{1.59}$$

From figure 1.6(a) and (b) we see that the order 1 WKB modes give results very near exact solutions except the presence of the non-adiabatic amplitude transitions at $\tau = \tau_\star$. The transition due to the order 1 acoustic mode is now very small on figure 1.6(a). The figure 1.6(b) shows a transition similar to the one with order 0 modes : the final amplitude is the same whereas the behaviour during transition is smoother. Note also that $|d_h|$ remains very close to one without the oscillations due to the non-uniformity observed in figure 1.4(c).

4.2 Hyperbolic flow

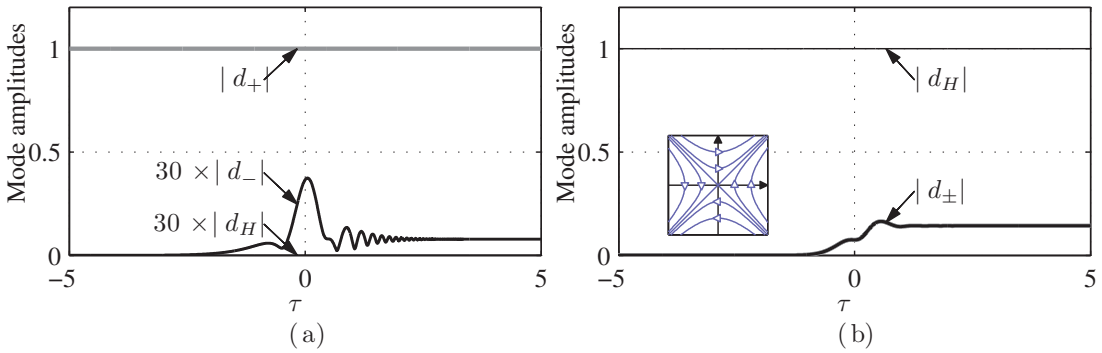

FIGURE 1.7 – Hyperbolic flow ($\delta = 1$ and $\varepsilon = 0.2$). Amplitudes of each order 1 WKB mode for an incident acoustic mode (a) and incident vorticity mode (b).

As the hyperbolic flow ($\delta = 1$) is the only one to be potential, we could guess

that no couplings would occur. Indeed the vorticity mode amplitude is constant since equation (1.59) reduces here to $d_H = \mathcal{C}$. However the two non-adiabatic transitions mentioned for the plane Couette flow also occur here, and the amplitude transitions are more important (see figure 1.7). Concerning intermediate flows between plane Couette and hyperbolic flows ($1/2 < \delta < 1$), mode amplitudes behave qualitatively as in the case of the Couette flow. As it could be expected, the closer the flow is to the hyperbolic flow (δ close to 1), the more the amplitude transition is important. Figure 1.8 corresponds to one of these intermediate flows, with $\delta = 0.6$.

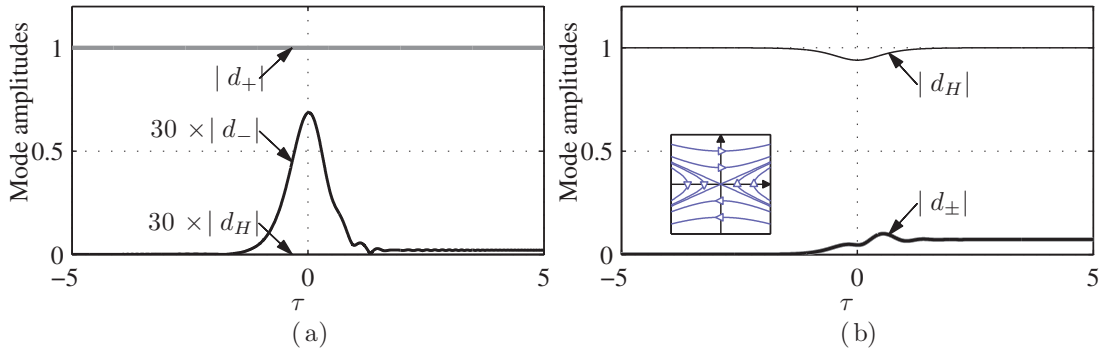

FIGURE 1.8 – Intermediate flow with dominant hyperbolic part ($\delta = 0.6$ and $\varepsilon = 0.2$). Amplitudes of each order 1 WKB mode for an incident acoustic mode (b) and incident vorticity mode (c).

4.3 Rigid rotation

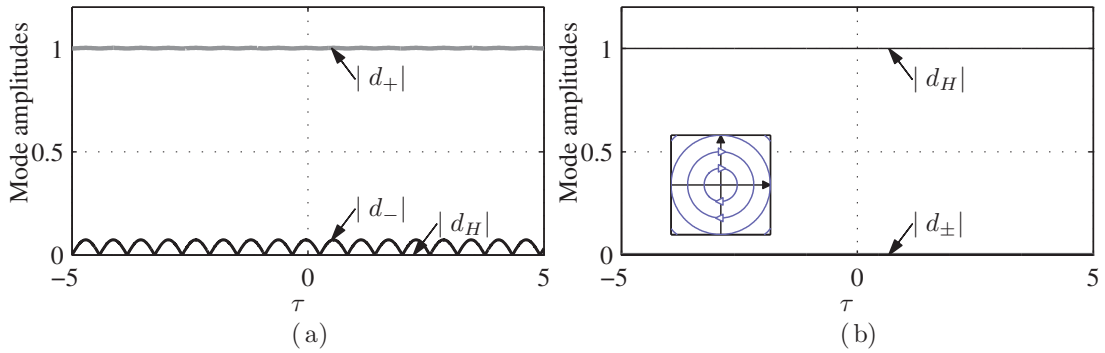

FIGURE 1.9 – Solid rotation flow ($\delta = 0$ and $\varepsilon = 0.2$). Amplitudes of each order 1 WKB mode for an incident acoustic mode (a) and incident vorticity mode (b).

The rigid rotation ($\delta = 0$) has two particularities : k is constant, and we analytically know the exact solution. This solution is the sum of the three following independent

solutions

$$\boldsymbol{\chi_H} = \begin{pmatrix} \beta \\ -\alpha \\ 2\varepsilon \end{pmatrix} , \tag{1.60}$$

$$\boldsymbol{\chi_\pm} = e^{\pm i \frac{\sqrt{k^2+4\varepsilon^2}\tau}{\varepsilon}} \begin{pmatrix} \sqrt{1+4\varepsilon^2/k^2}\alpha \pm \varepsilon\frac{2i}{k}\beta \\ \sqrt{1+4\varepsilon^2/k^2}\beta \mp \varepsilon\frac{2i}{k}\alpha \\ \mp ik \end{pmatrix} . \tag{1.61}$$

The order 1 WKB vorticity mode coincides with the exact solution $\boldsymbol{\chi_H}$. The WKB acoustic mode is composed of the first terms of the expansion in ε power series of the other solution $\boldsymbol{\chi_+}$. Figure 1.9 shows the evolution of the mode amplitudes for a rotation flow. There is no transition, but in the case of an incident acoustic mode the other acoustic mode has an amplitude which oscillates permanently. The difference between exact solution and WKB approximation can be obtained from equation (1.61) :

$$d_- = \frac{2i\varepsilon^2}{\sqrt{1+4\varepsilon^2/k^2}} \sin\left(\sqrt{k^2+4\varepsilon^2}(\tau-\tau_i)/\varepsilon\right) e^{\frac{-i}{\varepsilon}\int k} \tag{1.62}$$

so that

$$|d_-| \sim 2\varepsilon^2 \sin\left(\sqrt{k^2+4\varepsilon^2}(\tau-\tau_i)/\varepsilon\right) + \mathcal{O}(\varepsilon^4) . \tag{1.63}$$

The oscillations of the non incident acoustic mode are the result of an order ε^2 error.

Figure 1.10 shows an example concerning an elliptic flow ($0 < \delta < 1/2$). In such flows, $\boldsymbol{k}$ and its components become periodical. This leads to successive avoided crossings, and successive amplitude transitions occur. At each transition the same transition matrix is involved, but the mode amplitudes are each time different before the transitions explaining the apparent erratic transitions. The closer the flow is to the perfect rigid rotation (δ near to 0) the more important are the abrupt oscillations appearing during transitions, and the more the amplitude transitions become smaller.

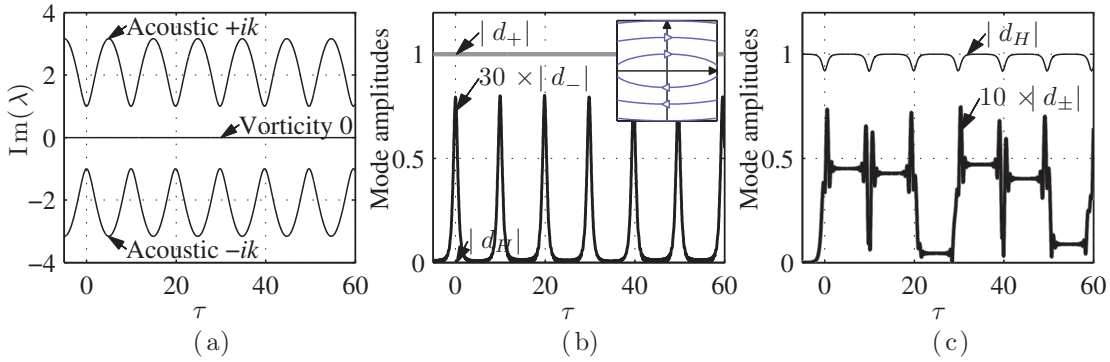

FIGURE 1.10 – Elliptic flow ($\delta = 0.45$ and $\varepsilon = 0.2$). Eigenvalues (a). Amplitudes of each order 1 WKB mode for an incident acoustic mode (b) and incident vorticity mode (c).

4.4 Wavepackets

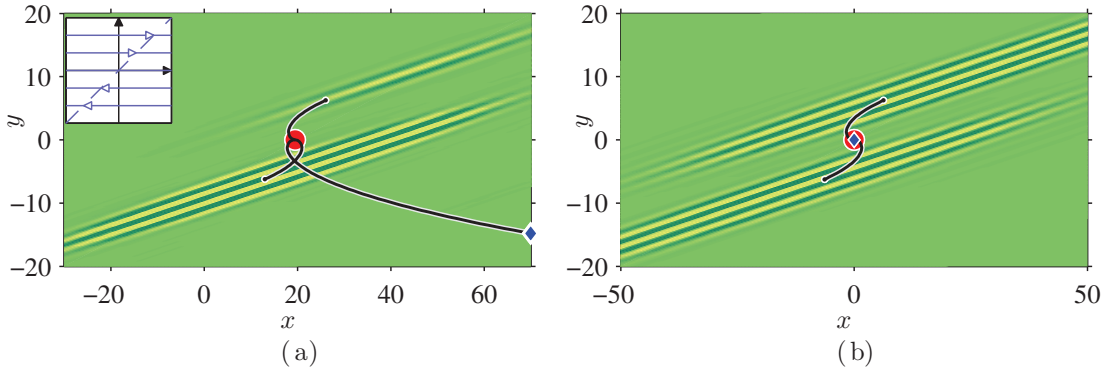

FIGURE 1.11 – Wavepackets in a Couette flow ($\delta = 1/2$) with $\alpha_0 = 1$, $\beta_0 = 0$. Pressure map at final time $\tau = 4$ in fixed coordinates (x, y) of an incident acoustic wavepacket with $\varepsilon = 0.6$ (a) and of an incident vorticity wavepacket with $\varepsilon = 0.2$ (b). At time $\tau = -4$, a packet of the corresponding order 1 WKB mode is imposed at the position of the diamond. The black lines represent the paths followed by the centres of each acoustic packet computed with the ray method. The diamonds mark the starting point of the incident packets and the big dots the position of the centres of the wavepackets at transition time. See text for detailed explanation. Note that figure (a) must be taken as an illustrative example more than quantitative result as the Mach $M \ll 1$ area is a very thin horizontal band around $y = 0$.

Hereafter are presented computations based on wavepackets and on the ray method. Narrow band wavepackets have to behave in a way very close to that of spatial Fourier harmonics studied in preceding sections. The figure 1.11(a) shows the time evolution of an acoustic wavepacket in a Couette flow ($\delta = 1/2$) with $\varepsilon = 0.6$. The choice of such a "high" value of ε is made so that the acoustic wavepacket generated during the transition can be seen. Note that this simulation is rather qualitative than quantitative as once the Mach number is greater than one the linearity assumption used in the model breaks down. At initial time ($\tau = -4$), a packet of order 1 WKB acoustic mode is imposed at the position of the blue diamond at the right of the figure. The acoustic wave propagates and is refracted by the flow (due to both convection and to the drift of the wavevector). When it reaches the transition time, the centre of the packet is located at the central dot. Then, the acoustic wavepacket generates the other acoustic mode packet, and each acoustic packet goes in opposite direction. The figure 1.11(b) shows the evolution of a vorticity wavepacket, in an area where the hypothesis of the base equation are respected (for a more moderate value of $\varepsilon = 0.2$). As the mean flow is null at its starting point it stands still. At the transition time, it generates two acoustic wavepackets which then propagates in opposites directions. The figure 1.12 shows trajectories of wavepackets (using the ray method) for Couette and elliptic flows. The ray trajectories are augmented by transitions occurring at $\tau = \tau_\star$. The figures 1.12(a-b) correspond to figures 1.6(a-b),

and figures 1.12(c-d) to figures 1.10(b-c).

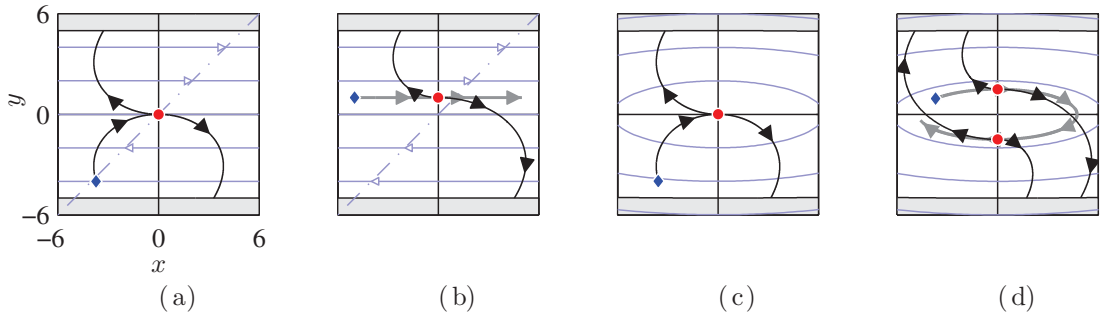

FIGURE 1.12 – Ray simulations for Couette flow $\delta = 1/2$ (a-b), and for an elliptic flow $\delta = 0.45$ (c-d), with $\varepsilon = 0.2$, $\alpha_0 = 1$, $\beta_0 = 0$. The figures (a) and (c) show the evolution of an incident acoustic mode ray, and figures (b) and (d) of an incident vorticity mode ray. The starting point of each incident ray is indicated by a diamond, and the position at a transition time by a dot. The path followed by acoustic and vorticity rays are respectively the thin black and bold gray curves. On figures (a) and (c), the incident acoustic mode generates the opposite acoustic mode, and on figures (b) and (d), the vorticity mode generates the two acoustic modes at each transition time. The flow streamlines are recalled in blue. The gray area represents the Mach $M \geq 1$ region near which the model of section 2 is no more valid (due to supposed non-linear effects).

4.5 Wave generation efficiency

We are now interested in the efficiency of different types of flows in transferring energy between two modes. Let be S the matrix composed of order 1 WKB modes as columns, which permits the transformation

$$\boldsymbol{Y}(\tau) = \mathsf{S}(\tau)\boldsymbol{d}(\tau) \ , \tag{1.64}$$

where $\boldsymbol{d}$ is the vector of amplitudes of acoustic and vorticity WKB modes (equation (1.58)). Let also be τ_1 and τ_2 two times respectively before and after a non-adiabatic transition at $\tau = \tau_\star$, and $\mathcal{R}_{\tau_1}(\tau)$ the resolvent associated to the evolution ODE (1.32)

$$\boldsymbol{Y}(\tau) = \mathcal{R}_{\tau_1}(\tau)\boldsymbol{Y}(\tau_1) \ . \tag{1.65}$$

We define the transmission matrix $\mathcal{T}$ such that

$$\boldsymbol{d}(\tau_2) = \mathcal{T}\boldsymbol{d}(\tau_1) \ . \tag{1.66}$$

We can compute this matrix using

$$\mathcal{T} = \mathsf{S}^{-1}(\tau_2)\mathcal{R}_{\tau_1}(\tau_2)\mathsf{S}(\tau_1) \ . \tag{1.67}$$

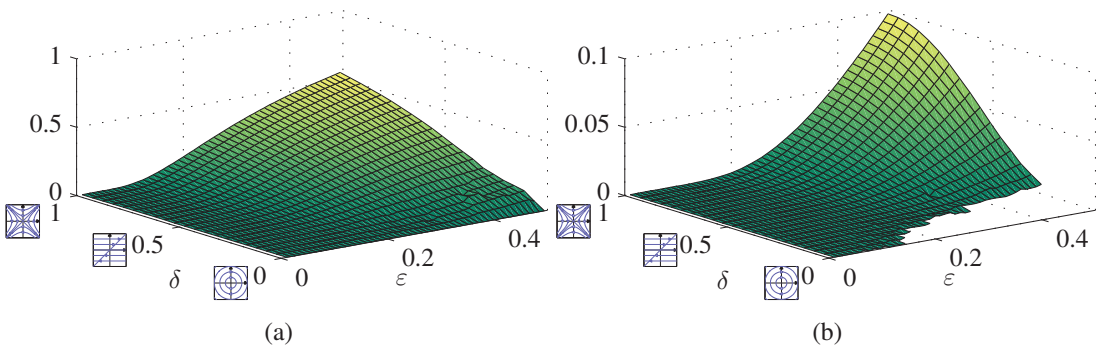

FIGURE 1.13 – Transmission coefficient between vorticity and acoustic order 1 WKB modes (a), and between two different acoustic order 1 WKB modes (b), depending on δ and ε. ($\alpha_0 = 1, \beta_0 = 0$).

Figures 1.13(a) and 1.13(b) show the transmission coefficients between, respectively, vorticity and acoustic order 1 WKB modes, and two different acoustic order 1 WKB modes, for flow of any shape (parametrised by δ) and for values of ε varying between 0 and 0.5. The hyperbolic flow once again appears as the most efficient flow in terms of coupling by non-adiabatic transitions. For any δ, the amount of coupling also shows an exponentially small behaviour $e^{-C/\varepsilon}$ when $\varepsilon \to 0$.

5 Concluding remarks

The proposed WKB method predicts good approximations of the evolution of compressible perturbations in all incompressible linear flows for small ε. It offers a relevant frame to analyse the involved physics. Moreover, WKB solutions provide a base where the coupling between acoustic and vorticity modes appear as non-adiabatic transitions. All the results obtained in this paper suggest that the hyperbolic part of a flow is responsible of the non-adiabatic transitions. This is a quite surprising result, since as the flow is potential, we could think that acoustic and hydrodynamic effects remain independent. Future developments will consist in deriving analytical asymptotic expressions of the transition amplitudes following the methods developed in quantum mechanics. The asymptotic smoothing phenomenon described by Berry (1990) and by Lim & Berry (1991) could be investigated. The intensively studied Couette flow finally appears as the middle step point being under the influence of the effects of the two reference flows : the rotation part induces a non-curl free velocity field of the acoustic waves, and the hyperbolic part induces couplings between the modes through non-adiabatic transitions. Meanwhile, for moderate flow shear rates, the major coupling effects remain (exponentially) small correction compared to solutions obtained with the WKB method. Another future work could consists in adapting the method developed in this paper to more general flows which are not linear. As an example we could consider flows which are locally linear, that is with a shear matrix which varies slowly in space. Provided the variation

scale of the shear matrix is sufficiently small compared to the length scale of the perturbations, we could consider the use of a multiple scales method involving these two length scale.

A Derivation of equations (1.3)

In this appendix we derive formally the equations governing the evolution of the unsteady perturbations. The starting point is to consider an incompressible steady flow and then to superimpose unsteady compressible perturbations on it. The study performed in this paper is focused on the local effect of the shearing of the flow on the perturbations. So this steady flow $\boldsymbol{u_0}$, which satisfies the incompressible Euler equations, is linearised. We also assume it has constant density and entropy. The linearisation of the steady flow yields

$$\boldsymbol{u_0} \simeq \boldsymbol{\mathcal{U}_0} + \mathsf{A}\boldsymbol{x} \ , \tag{1.68}$$

which corresponds to the sum of a convection part $\boldsymbol{\mathcal{U}_0}$ which is a constant vector, and of a shearing part with constant shear matrix A. It satisfies the incompressible Euler equations in steady regime :

$$\rho_0 \left(\boldsymbol{u_0} \cdot \boldsymbol{\nabla}\right) \boldsymbol{u_0} = -\boldsymbol{\nabla} p_0 \ , \qquad \text{div } \boldsymbol{u_0} = 0 \ . \tag{1.69}$$

The associated pressure is obtained by integration of (1.69) which gives

$$p_0 = \mathcal{P}_0 - \rho_0 \left(\mathsf{A}\boldsymbol{\mathcal{U}_0}\right) \cdot \boldsymbol{x} + \rho_0 \frac{\det(\mathsf{A})}{2} |\boldsymbol{x}|^2 \ . \tag{1.70}$$

This expression is in fact the Taylor expansion of p_0 at order 2, and represents the generic local description of the pressure of a linearised incompressible flow.

The equations governing the evolution of the compressible linear perturbations are

$$\rho_0 \mathrm{D}_t \, \boldsymbol{u} + \rho_0 \left(\boldsymbol{u} \cdot \boldsymbol{\nabla}\right) \boldsymbol{u_0} + \rho (\boldsymbol{u_0} \cdot \boldsymbol{\nabla}) \boldsymbol{u_0} = -\boldsymbol{\nabla} p \ , \tag{1.71a}$$

$$\mathrm{D}_t \, \rho = -\rho_0 \boldsymbol{\nabla} \cdot \boldsymbol{u} \ , \tag{1.71b}$$

where $\mathrm{D}_t = (\partial/\partial t + \boldsymbol{u_0} \cdot \boldsymbol{\nabla})$. We also consider the adiabatic ideal gas law which under the assumption of an homentropic flow reduces to

$$\mathrm{d}\, p = \left.\frac{\partial p_0}{\partial \rho_0}\right|_{s_0} \mathrm{d}\, \rho \ . \tag{1.72}$$

The equations are then turned into a dimensionless form by introducing $\tilde{x} = x/l$, $\tilde{t} = t c_0/l$, $\tilde{p} = p/\rho_0 c_0^2$, $\tilde{\boldsymbol{u}} = \boldsymbol{u}/c_0$, and $\tilde{\rho} = \rho/\rho_0$, where l is a characteristic length scale of the perturbations, and where $c_0^2 = \gamma \mathcal{P}_0/\rho_0$ is the adiabatic speed of sound at the origin. The dimensionless form of the components of the steady flow are $\widetilde{\boldsymbol{\mathcal{U}}}_{\boldsymbol{0}} = \boldsymbol{\mathcal{U}_0}/|\boldsymbol{\mathcal{U}_0}|$ and $\mathsf{B} = \mathsf{A}/\zeta$, where ζ is the characteristic order of magnitude of the shear matrix (defined precisely in Appendix B). Equations (1.71) then become

$$\mathrm{D}_{\tilde{t}} \, \tilde{\boldsymbol{u}} + \varepsilon \mathsf{B} \tilde{\boldsymbol{u}} + \left(\varepsilon \mathcal{M}_0 \widetilde{\boldsymbol{\mathcal{U}}}_{\boldsymbol{0}} - \varepsilon^2 \det(\mathsf{B}) \tilde{\boldsymbol{x}}\right) \tilde{\rho} = -\boldsymbol{\nabla} \tilde{p} \ , \tag{1.73a}$$

$$\mathrm{D}_{\tilde{t}} \, \tilde{\rho} = -\boldsymbol{\nabla} \cdot \tilde{\boldsymbol{u}} \ , \tag{1.73b}$$

where $\mathcal{M}_0 = |\boldsymbol{\mathcal{U}_0}|/c_0$ is the Mach number of the constant part of the steady flow, and $\varepsilon = \zeta l/c_0$ is defined the same way as in equation (1.10) if we consider l to be $1/k_0$. The work presented in this paper focuses on the local effect of the shearing of the steady flow by use of the asymptotic method WKB. For this reason, we consider the effects of the steady flow $\boldsymbol{u_0}$ to be small, meaning that both the convective and the shearing parts of the flow are small in the sense $|\boldsymbol{\mathcal{U}_0}| \leqslant \zeta l \ll c_0$. This is in fact a small Mach number and small shearing assumption which is equivalent to $\mathcal{M}_0 \leqslant \varepsilon \ll 1$. All quantities of order ε^2 are now neglected. Therefore the third term in the left hand side of (1.73a) is neglected. Note also that writing the steady flow pressure (equation (1.70)) in its dimensionless form yields

$$\tilde{p}_0 = \gamma^{-1} - \varepsilon \mathcal{M}_0 \left(\mathsf{B}\widetilde{\boldsymbol{\mathcal{U}}}_{\boldsymbol{0}} \right) \tilde{\boldsymbol{x}} + \varepsilon^2 \frac{\det(\mathsf{B})}{2} |\tilde{\boldsymbol{x}}|^2 \ . \tag{1.74}$$

The two last terms of the right hand side are also neglected as order ε^2 quantities, and the pressure is constant. Hence, c_0 is the relevant speed of sound and is constant in space. The equation (1.72) then reduces to $\tilde{p} = \tilde{\rho}$, and the evolution of the perturbations is finally governed by

$$\mathrm{D}_{\tilde{t}}\, \tilde{\boldsymbol{u}} + \varepsilon \mathsf{B} \tilde{\boldsymbol{u}} = -\boldsymbol{\nabla} \tilde{p} \ , \tag{1.75a}$$

$$\mathrm{D}_{\tilde{t}}\, \tilde{p} = -\boldsymbol{\nabla} \cdot \tilde{\boldsymbol{u}} \ . \tag{1.75b}$$

The transformations introduced in section 2 to derive the ODE (1.6), namely the convected coordinates (1.4) and the spatial Fourier harmonic form of the solution, can be reduced to the introduction of the following form for the solution

$$\begin{bmatrix} \tilde{\boldsymbol{u}} \\ \tilde{p} \end{bmatrix} (\tilde{\boldsymbol{x}}, \tilde{t}) = \begin{bmatrix} \hat{\boldsymbol{U}} \\ \hat{P} \end{bmatrix} (\tilde{t})\ e^{\,i\left(\boldsymbol{k}\cdot\tilde{\boldsymbol{x}} - \widetilde{\boldsymbol{\mathcal{U}}}_{\boldsymbol{0}} \cdot \int^{\tilde{t}} \boldsymbol{k} \right)} \ , \tag{1.76}$$

where $\boldsymbol{k}$ is the same as defined in equation (1.7). The injection of (1.76) into (1.75) gives

$$\hat{\boldsymbol{U}}' = -\varepsilon \mathsf{B} \hat{\boldsymbol{U}} - i \boldsymbol{k} \hat{P} \ , \tag{1.77a}$$

$$\hat{P}' = -i \boldsymbol{k} \cdot \hat{\boldsymbol{U}} \ . \tag{1.77b}$$

Therefore , $\hat{\boldsymbol{U}}$ and $\hat{P}$ satisfy the same equation as $\boldsymbol{U}$ and $\boldsymbol{P}$ (equations (1.6)). Eventually, the only effect due to the constant part $\widetilde{\boldsymbol{\mathcal{U}}}_{\boldsymbol{0}}$ of the steady flow on the work presented in this paper is to add the term $-\widetilde{\boldsymbol{\mathcal{U}}}_{\boldsymbol{0}} \cdot \int^{\tilde{t}} \boldsymbol{k}$ in the phase of the perturbation —(kind of) Doppler effect.

B Flow decomposition

We develop in this appendix how general linear incompressible flows are decomposed. The derivation relies on a decomposition of the shear matrix into symmetric and antisymmetric parts (using the same idea as Craik & Criminale, 1986). As any studied

flow is written in the form $\boldsymbol{u_0} = \mathsf{A}\boldsymbol{x}$, it is fully characterized by its shear matrix A. Because of the incompressibility assumption, the shear matrix is traceless :

$$\mathsf{A} = \begin{bmatrix} A_{xx} & A_{xy} \\ A_{yx} & -A_{xx} \end{bmatrix} . \tag{1.78}$$

The shear matrix is first decomposed into symmetric and antisymmetric parts

$$\mathsf{A} = \begin{bmatrix} A_{xx} & \frac{A_{xy}+A_{yx}}{2} \\ \frac{A_{xy}+A_{yx}}{2} & -A_{xx} \end{bmatrix} + \begin{bmatrix} 0 & \frac{A_{xy}-A_{yx}}{2} \\ -\frac{A_{xy}-A_{yx}}{2} & 0 \end{bmatrix} , \tag{1.79}$$

which can be written as

$$\mathsf{A} = \varrho_H \begin{bmatrix} \cos(\theta) & \sin(\theta) \\ \sin(\theta) & -\cos(\theta) \end{bmatrix} + s\varrho_R \begin{bmatrix} 0 & 1 \\ -1 & 0 \end{bmatrix} , \tag{1.80}$$

with

$$\varrho_H = \sqrt{A_{xx}^2 + \frac{(A_{xy}+A_{yx})^2}{4}} \quad , \quad \varrho_R = \frac{|A_{xy}-A_{yx}|}{2} \tag{1.81}$$

$$\theta = \arctan\left(\frac{2A_{xx}}{A_{xy}+A_{yx}}\right) \quad , \quad s = \operatorname{sign}(A_{xy}-A_{yx}) . \tag{1.82}$$

The first symmetric matrix in (1.80) describes a hyperbolic flow, which has two degrees of freedom, a scalar factor ϱ_H which determines its intensity and an angle θ. The second matrix corresponds to a solid rotation. It also has two degrees of freedom, the intensity ϱ_R and the parameter s defining if the rotation is clockwise ($s = +1$) or anticlockwise ($s = -1$). We will show that we can choose arbitrarily both $\theta = \pi/2$ and $s = 1$, without any loss of generality. This particular choice is explained below.

Let us first focus on the case $s = +1$. We introduce the change of basis $\tilde{\boldsymbol{x}} = \mathsf{R}_\phi \boldsymbol{x}$ where R_ϕ is the transformation matrix associated to a ϕ angle rotation :

$$\mathsf{R}_\phi = \begin{bmatrix} \cos\phi & -\sin\phi \\ \sin\phi & \cos\phi \end{bmatrix} . \tag{1.83}$$

Then A becomes in this new basis

$$\begin{aligned} \tilde{\mathsf{A}} &= \mathsf{R}_\phi \mathsf{A} \mathsf{R}_\phi^{-1} \\ &= \varrho_H \begin{bmatrix} \cos(\theta+2\phi) & \sin(\theta+2\phi) \\ \sin(\theta+2\phi) & -\cos(\theta+2\phi) \end{bmatrix} + \varrho_R \begin{bmatrix} 0 & 1 \\ -1 & 0 \end{bmatrix} \end{aligned} \tag{1.84}$$

and by choosing $\phi = -\theta/2 + \pi/4$ we obtain the desired form

$$\tilde{\mathsf{A}} = \varrho_H \begin{bmatrix} 0 & 1 \\ 1 & 0 \end{bmatrix} + \varrho_R \begin{bmatrix} 0 & 1 \\ -1 & 0 \end{bmatrix} . \tag{1.85}$$

In the case where $s = -1$, we introduce the change of basis $\tilde{\boldsymbol{x}} = \Delta_{\mathsf{y}} \mathsf{R}_\phi \boldsymbol{x}$ where Δ_{y} is the matrix associated to a symmetry with respect to the y-axis :

$$\Delta_{\mathsf{y}} = \begin{bmatrix} -1 & 0 \\ 0 & 1 \end{bmatrix} . \tag{1.86}$$

This time, the transformation becomes

$$\begin{aligned} \tilde{\mathsf{A}} &= \Delta_{\mathsf{y}} \mathsf{R}_\phi \mathsf{A} \mathsf{R}_\phi^{-1} {\Delta_{\mathsf{y}}}^{-1} \\ &= \varrho_H \begin{bmatrix} \cos(\theta+2\phi) & \sin(-\theta-2\phi) \\ \sin(-\theta-2\phi) & -\cos(\theta+2\phi) \end{bmatrix} + \varrho_R \begin{bmatrix} 0 & 1 \\ -1 & 0 \end{bmatrix} \end{aligned} \tag{1.87}$$

and, if we take $\phi = -\theta/2 - \pi/4$, we obtain the same decomposition as in equation (1.85).

Now, by defining $\zeta = \varrho_H + \varrho_R$ and $\delta = \varrho_H/\zeta$ we have the decomposition

$$\begin{aligned} \tilde{\mathsf{A}} &= \zeta \mathsf{B} \\ \mathsf{B} &= \delta \begin{bmatrix} 0 & 1 \\ 1 & 0 \end{bmatrix} + (1-\delta) \begin{bmatrix} 0 & 1 \\ -1 & 0 \end{bmatrix} . \end{aligned} \tag{1.88}$$

Eventually, we showed that for any flow matrix A we can find a basis in which this matrix has the form we wanted. In the model developed in section 2, the only side effect of such a change of basis is to change the angle of the vector $\boldsymbol{k_0}$. As a consequence, by applying the corresponding change of basis on $\boldsymbol{k_0}$, we can focus our study only on flows defined by equation (1.88).

Each flow can be viewed as a step in a continuum axis parametrised by $\delta \in [0\,;1]$. The hyperbolic flow corresponds to a value of $\delta = 1$ and the rotation flow to $\delta = 0$. It is worth noticing that the plane Couette flow is the middle point $\delta = 1/2$ for which contributions of hyperbolic and rotation flows are equal. The reason of our choice concerning θ and s, is to obtain this plane Couette flow oriented horizontally as it is usually presented.

C Computation of X and k

In this appendix is described how are computed $\boldsymbol{X}$ and $\boldsymbol{k}$, defined in equations (1.4) and (1.7) respectively, which both rely on the exponential of the matrix B. To compute this exponential, we decompose B using the Pauli matrices

$$\sigma_1 = \begin{bmatrix} 0 & 1 \\ 1 & 0 \end{bmatrix} \qquad \sigma_2 = \begin{bmatrix} 0 & -i \\ i & 0 \end{bmatrix} \qquad \sigma_3 = \begin{bmatrix} 1 & 0 \\ 0 & -1 \end{bmatrix} . \tag{1.89}$$

According to appendix A, we write the matrix B in the form

$$\mathsf{B} = \delta\sigma_1 + i(1-\delta)\sigma_2 . \tag{1.90}$$

We define $\Lambda = \sqrt{2\delta - 1}$ which can be imaginary. Then, using the well known Pauli matrices properties

$$\begin{aligned} {\sigma_1}^2 = {\sigma_2}^2 &= {\sigma_3}^2 = \mathsf{Id} \ , & (1.91)\\ \sigma_1\sigma_2 = i\sigma_3 \qquad & \sigma_3\sigma_1 = i\sigma_2 \ , & (1.92)\\ \sigma_2\sigma_3 = i\sigma_1 \qquad & \sigma_\mathsf{m}\sigma_\mathsf{n} = -\sigma_\mathsf{n}\sigma_\mathsf{m} \ , & (1.93) \end{aligned}$$

we get the following relations

$$\mathsf{B}^{2n} = \Lambda^{2n}\mathsf{Id} \qquad , \qquad \mathsf{B}^{2n+1} = \Lambda^{2n}\mathsf{B} \ , \tag{1.94}$$

which allows us to express the matrix exponential in the form

$$\exp(\mathsf{B}) = \cosh(\Lambda)\mathsf{Id} + \frac{\sinh(\Lambda)}{\Lambda}\mathsf{B} \ . \tag{1.95}$$

In equation (1.7), $\boldsymbol{k}$ is defined by

$$\boldsymbol{k}(\tau) = \exp\left(-\mathsf{B}^\mathsf{T}\tau\right)\boldsymbol{k_0} \ , \tag{1.96}$$

therefore, using (1.95), we finally obtain

$$\boldsymbol{k}(\tau) = \left[\cosh(\Lambda\tau)\mathsf{Id} - \frac{\sinh(\Lambda\tau)}{\Lambda}\mathsf{B}^\mathsf{T}\right]\boldsymbol{k_0} \ , \tag{1.97}$$

which gives explicit formulas to compute $\boldsymbol{k}$, α, β , k, and also, thanks to (1.96), $\dot{k} = -2\alpha\beta\delta/k$.

The same method is used to compute the transformation matrix between fixed coordinates $\boldsymbol{x}$ and convected coordinates $\boldsymbol{X}$. It yields

$$\boldsymbol{X} = \left[\cosh(\Lambda At)\mathsf{Id} - \frac{\sinh(\Lambda At)}{\Lambda}\mathsf{B}\right]\boldsymbol{x} \ . \tag{1.98}$$

References

Bakas, N. A. 2009 Mechanisms underlying transient growth of planar perturbations in unbounded compressible shear flow. *J. Fluid Mech.* **639**, 479–507. (doi: 10.1017/S0022112009991273)

Batchelor, G. K. & Proudman, I. 1954 The effect of rapid distortion of a fluid in turbulent motion. *Q. J. Mech. Appl. Math.* **7**, 83–103. (doi: 10.1093/qjmam/7.1.83)

Berry, M. V. 1990 Histories of adiabatic quantum transitions. *Proc. R. Soc. Lond. A* **429**, 61–72.

Bonnet-BenDhia, A.-S., Duclairoir, E.-M., Legendre, G. & Mercier, J.-F. 2007 Time-harmonic acoustic propagation in the presence of a shear flow. *J. Comput. Appl. Math* **204(2)**, 428–439. (doi: 10.1016/j.cam.2006.02.048)

Bonnet-BenDhia, A.-S., Mercier, J.-F., Millot, F., Pernet, S. & Peynaud, E. 2012 Time-harmonic acoustic scattering in a complex flow : a full coupling between acoustics and hydrodynamics. *Commun. Comput. Phys.* **11(2)**, 555–572. (doi: 10.4208/cicp.221209.030111s)

Bretherton, F. P. & Garrett, C. J. R. 1968 Wavetrains in inhomogeneous moving media. *Proc. R. Soc. Lond. Ser. A* **302**, 529–554. (doi: 10.1098/rspa.1968.0034)

Buhler, O. 2009 *Waves and mean flows.* Cambridge : Cambridge University Press.

Butler, K. M. & Farrell, B. F. 1992 Three-dimensional optimal perturbations in viscous shear flow. *Phys. Fluids A : Fluid Dyn.* **4**, 1637–1650. (doi: 10.1063/1.858386)

Cambon, C., Benoit, J.-P., Shao, L. & Jacquin, L. 1994 Stability analysis and large-eddy simulation of rotating turbulence with organized eddies. *J. Fluid Mech.* **278**, 175–200. (doi: 10.1017/S0022112094003666)

Cambon, C. & Scott, J. F. 1999 Linear and nonlinear models of anisotropic turbulence. *Annu. Rev. Fluid Mech.* **31**, 1–53. (doi: 10.1146/annurev.fluid.31.1.1)

Chagelishvili, G. D. 2002 New linear mechanisms of acoustic wave generation in smooth shear flows - (Nonmodal study). In *Sound-flow interactions* (ed. Y. Auregan, A. Maurel, V. Pagneux & J. Pinton), pp. 210–237. Berlin : Springer-Verlag.

Chagelishvili, G. D., Hristov, T. S., Chanishvili, R. G. & Lominadze, J. G. 1993 Mechanism of energy transformations in shear magnetohydrodynamic flows. *Phys. Rev. E* **47**, 366–374. (doi: 10.1103/PhysRevE.47.366)

Chagelishvili, G. D., Khujadze, G. R., Lominadze, J. G. & Rogava, A. 1997*a* Acoustic waves in unbounded shear flows. *Phys. Fluids* **9**, 1955–1962. (doi: 10.1063/1.869314)

Chagelishvili, G. D., Rogava, A. D. & Segal, I. N. 1994 Hydrodynamic stability of compressible plane couette flow. *Phys. Rev. E* **50**, R4283–R4285. (doi: 10.1103/PhysRevE.50.R4283)

Chagelishvili, G. D., Tevzadze, A. G., Bodo, G. & Moiseev, S. S. 1997*b* Linear mechanism of wave emergence from vortices in smooth shear flows. *Phys. Rev. Lett.* **79**, 3178–3181. (doi: 10.1103/PhysRevLett.79.3178)

Craik, A. D. D. & Criminale, W. O. 1986 Evolution of wavelike disturbances in shear flows : A class of exact solutions of the navier-stokes equations. *Proc. R. Soc. Lond. A* **406**, 13–26. (doi: 10.1098/rspa.1986.0061)

Criminale, W. O. & Drazin, P. G. 1990 The evolution of linearized perturbations of parallel flows. *Stud. Appl. Math.* **83**, 123–157.

Davis, J. P. & Pechukas, P. 1976 Nonadiabatic transitions induced by a time dependent hamiltonian in the semiclassical/adiabatic limit : The two state case. *J. Chem. Phys.* **64**, 3129–3137. (doi: 10.1063/1.432648)

Folguera, A. & Harris, J. 1999 Coupled rayleigh surface waves in a slowly varying elastic waveguide. *Proc. R. Soc. Lond. A* **455**, 917–931.

Friedlander, S. & Lipton-Lifschitz, A. 2003 Localized instabilities in fluids. In *Handbook of mathematical fluid dynamics* (ed. S. Friedlander & D. Serre), vol. 2, pp. 289–353. Elsevier. (doi: 10.1016/S1874-5792(03)80010-1)

Gabard, G., Astley, R., Gamallo, P. & Kennedy, G. 2010 Physics-based computational methods for aero-acoustics. *Procedia Eng.* **6**, 183 – 192. (doi: 10.1016/j.proeng.2010.09.020)

George, J. & Sujith, R. I. 2009 Emergence of acoustic waves from vorticity fluctuations : Impact of non-normality. *Phys. Rev. E* **80**, 046 321. (doi: 10.1103/PhysRevE.80.046321)

Gogoberidze, G., Chagelishvili, G. D., Sagdeev, R. Z. & Lominadze, D. G. 2004 Linear coupling and overreflection phenomena of magnetohydrodynamic waves in smooth shear flows. *Phys. Plasmas* **11**, 4672–4685. (doi: 10.1063/1.1789998)

Goldstein, M. E. 1976 *Aeroacoustics*. McGraw-Hill.

Goldstein, M. E. 1978 Unsteady vortical and entropic distortions of potential flows round arbitrary obstacles. *J. Fluid Mech.* **89**, 433–468. (doi: 10.1017/S0022112078002682)

Gridin, D. & Craster, R. V. 2003 Quasi–modes of a weakly curved waveguide. *Proc. R. Soc. Lond. A* **459**, 2909–2931. (doi: 10.1098/rspa.2003.1141)

Hagedorn, G. A. & Joye, A. 2004 Time development of exponentially small nonadiabatic transitions. *Commun. Math. Phys.* **250**, 393–413. (doi: 10.1007/s00220-004-1124-5)

Hinch, E. J. 1991 *Perturbation methods*. Cambridge texts in applied mathematics. Cambridge : Cambridge University Press.

Holmes, M. H. 1995 *Introduction to perturbation methods*. Texts in applied mathematics. Springer-Verlag.

Huerre, P. & Monkewitz, P. A. 1990 Local and global instabilities in spatially developing flows. *Annu. Rev. Fluid Mech.* **22**, 473–537. (doi: 10.1146/annurev.fl.22.010190.002353)

Huerre, P. & Rossi, M. 1998 Hydrodynamic Instabilities in Open Flows. In *Hydrodynamics and nonlinear instabilities* (ed. C. Godrèche & P. Manneville), pp. 81–294. Cambridge : Cambridge University Press. (doi: 10.1017/CBO9780511524608)

Iserles, A., Marthinsen, A. & Nørsett, S. P. 1999 On the implementation of the method of magnus series for linear differential equations. *BIT* **39**, 281–304. (doi: 10.1023/A :1022393913721)

Landau, L. & Lifshitz, E. 1977 *Quantum mechanics : non-relativistic theory*, vol. 3 of *Course of theoretical physics*. Butterworth-Heinemann.

Landau, L. D. 1932 Zur theorie der energieubertragung. ii. *Phys. Z. Sowjetunion* **2**, 46.

Lim, R. & Berry, M. V. 1991 Superadiabatic tracking of quantum evolution. *J. Phys. A : Math. Gen.* **24**, 3255–3264.

Mahajan, S. M. & Rogava, A. D. 1999 What can the kinematic complexity of astrophysical shear flows lead to ? *Astrophys. J.* **518**, 814–820. (doi: 10.1086/307319)

Mohring, W., Muller, E. & Obermeier, F. 1983 Problems in flow acoustics. *Rev. Mod. Phys.* **55**, 707–724. (doi: 10.1103/RevModPhys.55.707)

Pagneux, V. 2010 Multimodal admittance method in waveguides and singularity behavior at high frequencies. *J. Comp. Appl. Math.* **234**, 1834–1841. (doi: 10.1016/j.cam.2009.08.034)

Pagneux, V. & Maurel, A. 2006 Lamb wave propagation in elastic waveguides with variable thickness. *Proc. R. Soc. A* **462**, 1315–1339.

Reddy, S. C., Schmid, P. J. & Henningson, D. S. 1993 Pseudospectra of the orr-sommerfeld operator. *SIAM J. Appl. Math.* **53**, 15–47. (doi: 10.1137/0153002)

Rogava, A., Poedts, S. & Mahajan, S. 2001 Acoustics of kinematically complex shear flows. *J. Comput. Acoust.* **9**, 869–888. (doi: 10.1142/S0218396X01001078)

Rogava, A. D. & Mahajan, S. M. 1997 Coupling of sound and internal waves in shear flows. *Phys. Rev. E* **55**, 1185–1188. (doi: 10.1103/PhysRevE.55.1185)

Schmid, P. J. 2007 Nonmodal stability theory. *Annu. Rev. Fluid Mech.* **39**, 129–162. (doi: 10.1146/annurev.fluid.38.050304.092139)

Schmid, P. J. & Henningson, D. S. 2001 *Stability and transition in shear flows*, vol. 142 of *Applied Mathematical Science*. New York : Springer-Verlag.

Smith, R. 1977 Propagation in slowly-varying waveguides. *SIAM J. Appl. Math.* **33**, 39–50. (doi: 10.1137/0133004)

Thomson, W. L. K. 1887 Stability of fluid motion (continued from the may and june numbers).-rectilineal motion of viscous fluid between two parallel planes. *Philos. Mag.* **24**, 188.

Trefethen, L. N., Trefethen, A. E., Reddy, S. C. & Driscoll, T. A. 1993 Hydrodynamic stability without eigenvalues. *Science* **261**, 578–584. (doi: 10.1126/science.261.5121.578)

Zener, C. 1932 Non-adiabatic crossing of energy levels. *Proc. R. Soc. Lond. Ser. A* **137**, 696–702. (doi: 10.1098/rspa.1932.0165)

2

Evolution superadiabatique de perturbations compressibles au sein d'un écoulement de Couette plan

Ce deuxième chapitre se présente sous la forme d'un article qui, à l'heure où ce manuscrit de thèse est rédigé, sera prochainement soumis au *Physics Letter A*.

Dans le précédent chapitre nous avons mis en œuvre la méthode WKB à l'ordre 0 et à l'ordre 1 dans le cadre de l'étude de l'évolution de perturbations compressibles dans des écoulements linéaires incompressibles. La méthode WKB nous a fourni trois solutions approchées qui correspondent à trois modes de perturbation, deux modes acoustiques et un mode de vorticité. L'utilisation de la base constituée de ces trois modes pour représenter la solution exacte permet de mettre en évidence des phénomènes de couplages qui se caractérisent par l'émergence de modes non excités initialement. Le parallèle entre ces phénomènes de couplages, et les phénomènes de transitions non-adiabatiques en mécanique quantique a été soulevé. Berry (1990) a montré que, dans le cas de l'équation de Schrödinger, l'utilisation des bases superadiabatiques, qui sont composées des solutions approchées WKB aux ordres supérieurs, a pour effet de lisser les amplitudes des modes émergeant lors des transitions non-adiabatiques. Lorsque l'ordre de la base superadiabatique augmente ces amplitudes tendent à prendre la forme de la fonction d'erreur de Gauss. Une fois un ordre optimum atteint, les amplitudes commencent alors à diverger. Ce résultat est d'une portée très générale car il ne dépend pas de la dépendance temporelle des coefficients apparaissant dans l'équation de Schrödinger.

Nous nous intéressons dans ce chapitre à l'utilisation des bases superadiabatiques dans l'étude du couplage entre le mode de vorticité et les modes acoustique au sein de l'écoulement de Couette. Nous constaterons que les résultats prédits par Berry s'appliquent aussi dans notre cas : les amplitudes des modes acoustiques générés par le mode de vorticité tendent à prendre la forme de la fonction d'erreur de Gauss lorsqu'elles sont exprimées dans les bases superadiabatiques. Ainsi, l'utilisation de ces bases d'ordres supérieurs permet de suivre plus précisément l'apparition des modes acoustiques.

Superadiabatic evolution of compressible perturbations in Couette flow [1]

Abstract : We explore the effect of higher order WKB asymptotics on the study of the coupling between the vorticity and the acoustic modes inside a plane Couette flow. In the case of the Schrödinger equation, it has been shown that looking at the solution expressed in the superadiabatic base, composed of higher order asymptotic solutions, smoothes quantum state transitions. In a first time, increasing the order of the superadiabatic base makes these transitions to tend to the Gauss error function. Then, once an optimal order is reached, the asymptotic process starts to diverge. We show that in the Couette flow, similar results can be applied on the amplitudes of the vorticity and acoustic modes. This allows one a finer tracking of the emergence of the acoustic modes in presence of the vorticity mode.

1 Introduction

The propagation of acoustic waves in the Couette plane flow (and a fortiori in shear flows) allows the existence of subtle phenomena of couplings between acoustic and vorticity perturbations (for a review see Chagelishvili, 2002). In another paper (Favraud & Pagneux, 2012) we show that using the WKB method gives an efficient frame to describe the different types of perturbations in a general incompressible planar flow. This method relies on the existence of a small parameter ε to provide approximate asymptotic solutions. Here, ε is the ratio of the shear rate of the flow to the typical frequency of the perturbation. At order ε, the solutions given by the WKB method are able to describe very closely the exact solution. The only phenomena which are not taken into account are sudden emergences of non excited modes which occur near the complex degeneracies of the equation governing the time evolution of the perturbations. Similar phenomena, called non adiabatic transitions, has been studied in quantum mechanics since the works of Landau (1932), Landau & Lifshitz (1977) and Zener (1932). The use of higher order approximations provides a base of asymptotic approximate solutions, or modes, which is called the *superadiabatic* base. Berry (1990) has shown that looking at the exact solution expressed in this superadiabatic base allows a finer tracking of the emerging mode amplitudes by smoothing them. There is an optimal order at which the time evolution of the amplitude of the emerging mode renormalizes to a general shape, which is the Gauss error function. Then, as in many asymptotic processes (Boyd, 1999), it starts to diverge once this optimal order is reached. This has been predicted in the case of a two state system by Berry (1990) and Lim & Berry (1991) on the basis of the work done by Dykhne (1962) and Davis & Pechukas (1976). More recently a mathematical proof has

1. To be submitted to *Physics Letter A*. Authors: Gael Favraud and Vincent Pagneux.

been proposed by Hagedorn & Joye (2004). Similar renormalizations of amplitudes are depicted, among others, by Betz *et al.* (2009), or by Lim (1993) concerning a two level system crossing two successive coupling areas, and by Elk (1995) concerning a three level system.

In this paper, we focus on the coupling between the vorticity and acoustic perturbations of a planar Couette flow, where superadiabatic bases can be used. The coupling phenomena between vorticity and acoustic perturbation in the Couette flow has been already widely studied with other methods (Chagelishvili, 2002, Chagelishvili *et al.*, 1993, 1994, 1996, 1997*a*,*b*, Rogava & Mahajan, 1997, Mahajan & Rogava, 1999, Rogava *et al.*, 2001, Gogoberidze *et al.*, 2004, George & Sujith, 2009). In the first section the equations governing the evolution of the perturbations are derived. The derivation of the governing equations is based on the so called non-modal methods. These methods, initiated by Kelvin (Thomson, 1887), were developed for the analysis of flows stability to incompressible perturbations. In the case of the plane Couette flow we are interested in, these methods allows a great number of simplifications. In the second section the WKB method is applied. The first order asymptotic solution gives us a base of three modes, two acoustic modes and one vorticity mode. We show that this base is close to the exact solution and permits to track the emergences of non excited modes. In the last section, we derive the bases corresponding to the following orders asymptotic. The predictions of Berry are investigated in our case.

2 Model

Let be a mean plane Couette flow $\boldsymbol{u_0}(x,y) = (Ay;0)$ where A is the shear rate of the flow. The main interest of this choice is that in this case the non-modal method is reduced to two major steps : the first one is to introduce a new set of independent variables which will be a frame of convected coordinates, and the second one is to apply the spatial Fourier transform to the equations. A more detailed step-by-step derivation can be found in (Chagelishvili, 2002, Chagelishvili *et al.*, 1994).

Then we consider compressible perturbations of pressure p and velocity $\boldsymbol{u} = (u;v)$. The time evolution of these perturbations is governed by the linearized Euler equations in the small Mach number approximation

$$\left(\frac{\partial}{\partial t} + Ay\frac{\partial}{\partial x}\right)u + Av = -\frac{1}{\rho_0}\frac{\partial}{\partial x}p\ , \tag{2.1a}$$

$$\left(\frac{\partial}{\partial t} + Ay\frac{\partial}{\partial x}\right)v = -\frac{1}{\rho_0}\frac{\partial}{\partial y}p\ , \tag{2.1b}$$

$$\left(\frac{\partial}{\partial t} + Ay\frac{\partial}{\partial x}\right)p = -\rho_0 c_0^2\left(\frac{\partial}{\partial x}u + \frac{\partial}{\partial y}v\right)\ , \tag{2.1c}$$

where c_0 is the adiabatic speed of sound linking the density and pressure of the perturbations by $p = c_0^2\rho$.

We focus on the evolution of dimensionless spatial Fourier harmonics in the convected

coordinate frame which follows the flow. Namely we look for solutions under the form

$$\begin{bmatrix} u(x,y,t) \\ v(x,y,t) \\ p(x,y,t) \end{bmatrix} = \begin{bmatrix} c_0 U(T) \\ c_0 V(T) \\ \rho_0 c_0^2 P(T) \end{bmatrix} \exp\Big(i\alpha_0 (x - Ayt) + i\beta_0 y) \Big) \ , \tag{2.2}$$

where $T = c_0\alpha_0 t$ is the dimensionless time with respect to the product of the speed of sound and the horizontal Fourier wave number in the convected coordinates. For any perturbed quantity f within u, v, and p, this as the effect to transform the derivatives such as $(\partial/\partial t + Ay\partial/\partial x) f(x,y,t) \mapsto \alpha_0 c_0 F'(T) \exp(\dots)$, $\partial f(x,y,t)/\partial x \mapsto i\alpha_0 F(T) \exp(\dots)$, and $\partial f(x,y,t)/\partial x \mapsto i(\beta_0 - Ay\alpha_0 t) F(t) \exp(\dots)$, where the argument of the exponentials is the same as in the right hand side of equation (2.2), and $F(t)$ stands for $c_0 U(t)$, $c_0 V(T)$ and $\rho_0 c_0^2 P(T)$ respectively. Equations (2.1) then become

$$U'(T) + \varepsilon V(T) = -iP(T) \ , \tag{2.3a}$$

$$V'(T) = -i\beta(\varepsilon T) P(T) \ , \tag{2.3b}$$

$$P'(T) = -iU(T) - i\beta(\varepsilon T) V(T) \ , \tag{2.3c}$$

where $\beta(\varepsilon T) = (\beta_0 - \alpha_0 A t)/\alpha_0 = \beta_0/\alpha_0 - \varepsilon T$, and where appear the dimensionless parameter

$$\varepsilon = \frac{A}{c_0 \alpha_0} \ . \tag{2.4}$$

This ε is the ratio of the shear rate of the mean flow to the frequency of the perturbation. The system of equations (2.3) forms an ordinary differential equation of dimension 3 with respect to the dimensionless time.

When $\varepsilon = 0$, the classical wave equation can be derived from equations (2.3). Hereafter, in order to construct asymptotic solutions by use of the WKB method, we focus on small values of ε, namely $\varepsilon \ll 1$ but not zero. This corresponds to a small shearing assumption, that is a weak shear rate of the mean flow compared to the frequency of the perturbations. In that case the characteristic time scale of the variation of β is εT (slow variation), whereas it is known from classical acoustics that the solution oscillates on the T time scale. Hence we introduce the slow time defined by

$$\tau = \varepsilon T \ , \tag{2.5}$$

and rewrite equations (2.3) in terms of τ. This yields

$$\varepsilon \boldsymbol{X}'(\tau) = \Big(\mathsf{H}_0(\tau) + \varepsilon \mathsf{H}_1 \Big) \boldsymbol{X}(\tau) \ , \tag{2.6}$$

where $\boldsymbol{X}(\tau) = (U(\tau); V(\tau); iP(\tau))$, and

$$\mathsf{H}_0(\tau) = \begin{bmatrix} 0 & 0 & -1 \\ 0 & 0 & -\beta(\tau) \\ 1 & \beta(\tau) & 0 \end{bmatrix} \ , \ \mathsf{H}_1 = \begin{bmatrix} 0 & -1 & 0 \\ 0 & 0 & 0 \\ 0 & 0 & 0 \end{bmatrix} \ . \tag{2.7}$$

Note that multiplying equation (2.6) by i yields a Schrödinger equation whose Hamiltonian $(i\mathsf{H}_0 + i\varepsilon\mathsf{H}_1)$ is *not* hermitian due to the $i\varepsilon\mathsf{H}_1$ part.

3 The adiabatic base

The WKB method consists in looking for solution under the form :

$$\boldsymbol{X}^{(n)}(\tau) = e^{\frac{i}{\varepsilon}\sigma(\tau)}\Big(\boldsymbol{\varphi}^{(0)}(\tau) + \cdots + \varepsilon^n \boldsymbol{\varphi}^{(n)}(\tau)\Big) \tag{2.8}$$

Inserting (2.8) into (2.6) yields the successive equations for each order of power of ε

$$\Big(i\sigma' - \mathsf{H}_0\Big) \qquad \boldsymbol{\varphi}^{(0)} = \mathbf{0} \qquad , \tag{2.9}$$

$$\Big(i\sigma' - \mathsf{H}_0\Big) \qquad \boldsymbol{\varphi}^{(n+1)} = \mathsf{H}_0\boldsymbol{\varphi}^{(n)} - \varepsilon \mathsf{H}_1 \boldsymbol{\varphi}'^{(n)} \qquad . \tag{2.10}$$

According to the order 0 equation (equation (2.9)), $i\sigma'$ is an eigenvalue of the H_0 matrix, and $\boldsymbol{\varphi}^{(0)}$ is its associated eigenvector. These eigenvalues are

$$\lambda_H = 0 \ , \ \lambda_\pm = \pm ik \ , \tag{2.11}$$

where $k = \sqrt{1+\beta^2}$. The evolution of the eigenvalues (imaginary part) is represented on figure 2.1. The particular time $\tau_\star = \beta_0/\alpha_0$ minimises k, and is the point where the three eigenvalues are the closest. It is actually the time on the real τ axis which is the closest to the complex zeros $\tau_c = \beta_0/\alpha_0 \pm i$ of k. As detailed later this particular time is of crucial interest as couplings occur at this time.

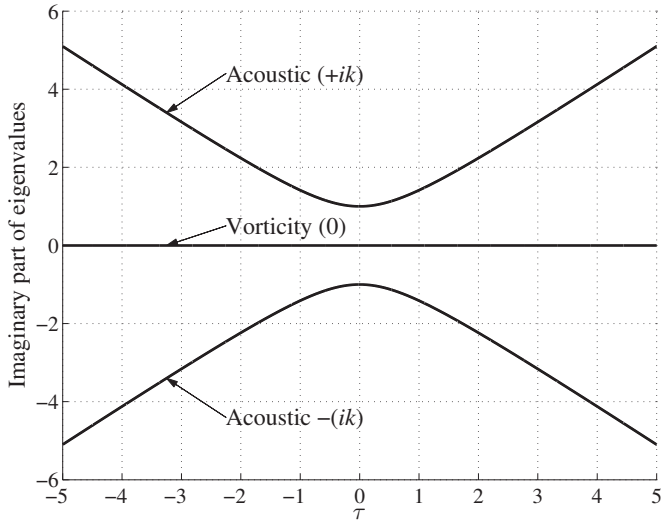

FIGURE 2.1 – Time evolution of the imaginary parts of the eigenvalues of H_0 (real parts are zeros). $\alpha_0 = \beta_0 = 1, \varepsilon = 0.1$.

The associated modes are

$$\boldsymbol{\varphi}_H^{(0)} = \frac{1}{k^2}\begin{bmatrix}\beta\\-1\\0\end{bmatrix} \ , \ \boldsymbol{\varphi}_\pm^{(0)} = \frac{1}{\sqrt{k}}\begin{bmatrix}\alpha\\\beta\\\mp ik\end{bmatrix} \ , \tag{2.12}$$

where the scalar pre-factors comes from the compatibility condition imposed by equation (2.10) at order $n = 1$. Finally, the three order 0 WKB approximate solutions, that we call order 0 WKB modes, are

$$\boldsymbol{X}_{\pm}^{(0)}(\tau) = e^{\int^{\tau} \pm \frac{i}{\varepsilon} k(s)ds}\, \boldsymbol{\varphi}_{\pm}^{(0)}(\tau)\ , \tag{2.13}$$

$$\boldsymbol{X}_{H}^{(0)}(\tau) = \boldsymbol{\varphi}_{H}^{(0)}(\tau)\ . \tag{2.14}$$

We identify two acoustic modes (subscripts $-$ and $+$) and a vorticity modes (subscript H). These three modes form a base $\left\{\boldsymbol{X}_{-}^{(0)}; \boldsymbol{X}_{H}^{(0)}; \boldsymbol{X}_{+}^{(0)}\right\}$ called the *adiabatic base*. Looking at the solution in this adiabatic base gives us the amplitude of each WKB mode. By writing $\boldsymbol{Y}^{(0)}(\tau) = (Y_{-}^{(0)}(\tau); Y_{H}^{(0)}(\tau); Y_{+}^{(0)}(\tau))$ the coordinates in this base of the real solution $\boldsymbol{X}(\tau)$, and by defining the transformation matrix $\Phi^{(0)}(\tau) = \left[\boldsymbol{X}_{-}^{(0)}\ \boldsymbol{X}_{H}^{(0)}\ \boldsymbol{X}_{+}^{(0)}\right]$ we get

$$\boldsymbol{X}(\tau) = \Phi^{(0)}(\tau)\boldsymbol{Y}^{(0)}(\tau)\ , \tag{2.15}$$

or equivalently $\boldsymbol{X} = Y_{-}^{(0)}\boldsymbol{X}_{-}^{(0)} + Y_{H}^{(0)}\boldsymbol{X}_{H}^{(0)} + Y_{+}^{(0)}\boldsymbol{X}_{+}^{(0)}$.

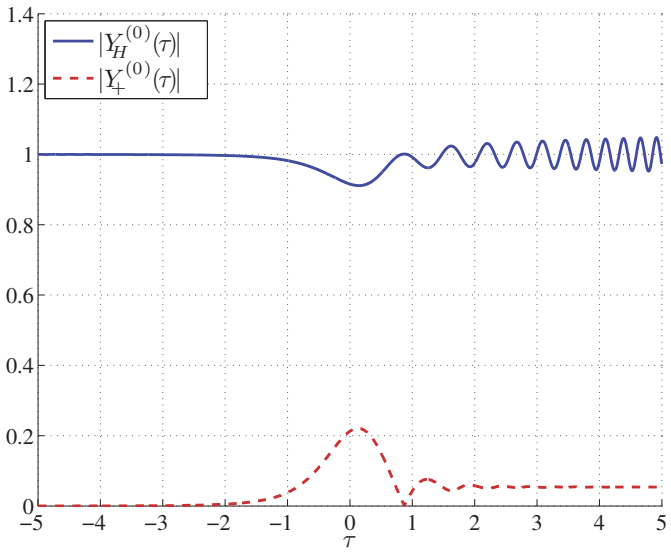

FIGURE 2.2 – Time evolution of the modulus of the WKB mode amplitudes for initial condition $\boldsymbol{X}(\tau_i) = \boldsymbol{X}_{H}^{(0)}(\tau_i)$ (incident acoustic + mode) with $\beta_0 = 0$, $\tau_i = -5$, and $\varepsilon = 0.2$. The $|Y_{-}^{(0)}|$ mode amplitude is not represented as it is equal to $|Y_{+}^{(0)}|$.

Some subtle phenomena can be understood from the form of these modes and from the time evolution of their amplitudes (Favraud & Pagneux, 2012). In this paper the emphasis is put on the coupling between the vorticity mode and the acoustic modes, that is, what happens when the initial condition is imposed on the vorticity mode : $\boldsymbol{X}(\tau_i) = \boldsymbol{X}_{H}^{(0)}(\tau_i)$. The figure 2.2 shows the time evolution of the modulus of the mode amplitudes $|Y_{H}^{(0)}|$ and $|Y_{+}^{(0)}|$ in that case for an initial time $\tau_i = -10$ and $\varepsilon = 0.2$.

This figure shows results similar to the ones obtained by Lim & Berry (1991). In a first time the vorticity mode amplitude stays close to 1 meaning that the modes succeeded in clinging to a solution. Then near $\tau_\star$, the acoustics modes emerges. This emergence is masked by strong oscillations. Then it stabilises to a final amplitude which is small compared to the one of the vorticity mode. This an a non-adiabatic transition that the asymptotic process cannot predicts as it is an exponentially small phenomenon – of order $\exp(-C/\varepsilon)$. The only remarkable difference with the case studied by Lim & Berry (1991) is the oscillating behaviour that the vorticity mode acquires once the acoustic modes emerged. This is an asymptotic error of order ε^n and is discussed by Favraud & Pagneux (2012).

4 The super-adiabatic bases

In the following the WKB modes at order $n \geqslant 1$ are sought, in the same way as done by Berry (Berry, 1990, Lim & Berry, 1991) in the field of quantum mechanics. Berry showed that the behaviour of the amplitudes is dominated by the effects of singularities present in the equations determining the first orders. These singularities are the complex zeros of the eigenvalues. For higher order, by mean of successive integrations, their effect become of significative order even on the real axis. There is a particular order for which the amplitudes tends to the Gauss error function. At following order,the asymptotic development starts diverging.

To apply this result in our case we look for next order WKB modes, that is determining the $\boldsymbol{\varphi}_j^{(n)}$ (with $j \in \{-, H, +\}$) for $n \geqslant 1$ in the WKB *ansatz* (2.8). The starting point is equation (2.10) with the expression (2.12) of each $\boldsymbol{\varphi}_j^{(n)}$. To perform this calculus it is convenient to express the $\boldsymbol{\varphi}_{\boldsymbol{j}}^{(\boldsymbol{n})}$ vectors in the base of the eigenvectors $\boldsymbol{\varphi}_j^{(0)}$ of $\mathsf{H_0}$:

$$\boldsymbol{\varphi}_j^{(n)} = \mathsf{S}\ \boldsymbol{c}_j^{(n)} \qquad \text{for} j \in \{-, H, +\}\ , \tag{2.16}$$

$$\text{where } \mathsf{S} = \left[\boldsymbol{\varphi}_-^{(0)}\ \boldsymbol{\varphi}_H^{(0)}\ \boldsymbol{\varphi}_+^{(0)}\right]\ , \tag{2.17}$$

and where $\boldsymbol{c}_j^{(n)}$ is the representation of $\boldsymbol{\varphi}_j^{(n)}$ in this basis. Note that the matrix S differs from the adiabatic base matrix $\Phi^{(0)}$ because of the exponentials terms. Also for convenience, and following the method of Berry, we express the components of $\mathsf{H_0}$ (which are the horizontal and vertical wavenumber) in polar coordinates :

$$\begin{bmatrix} 1 \\ \beta(\tau) \end{bmatrix} = k(\tau) \begin{bmatrix} \sin\theta(\tau) \\ \cos\theta(\tau) \end{bmatrix} \tag{2.18}$$

Projecting equation (2.10) into this base yields

$$\Big(\lambda_j \mathsf{I} - \mathsf{D}\Big)\boldsymbol{c}_j^{(n+1)} = \left(\mathsf{S}^{-1}\mathsf{H_1}\mathsf{S} - \mathsf{S}^{-1}\mathsf{S}' - \frac{\mathrm{d}}{\mathrm{d}\,\tau}\right)\boldsymbol{c}_j^{(n)}\ , \tag{2.19}$$

where I is the identity matrix and $\mathsf{D} = \mathrm{diag}(\lambda_-, \lambda_H, \lambda_+)$ is the diagonal matrix composed of the eigenvalues of $\mathsf{H_0}$. A detailed expression of equation (2.19) is given in equation (2.25) of A. This allows us to compute all the $\boldsymbol{c}_j^{(n)}$ through the scheme

$$c_{j,k}^{(n+1)} = \frac{1}{\lambda_j - \lambda_k} \sum_l M_{j,l} c_{j,l}^{(n)} - \dot{c}_{j,k}^{(n)} \qquad \text{for } j \neq k \ , \tag{2.20a}$$

$$\dot{c}_{j,j}^{(n+1)} = \sum_l M_{j,l} c_{j,l}^{(n+1)} \qquad \text{for } j = k \ , \tag{2.20b}$$

where $M_{j,k}$ are the coefficients of the matrix $\mathsf{M} = \mathsf{S}^{-1}\mathsf{H_1}\mathsf{S} - \mathsf{S}^{-1}\mathsf{S}'$ which has a null diagonal. Of course, expressions of the $\boldsymbol{c}_j^{(n)}$ at order 0 are $\boldsymbol{c}_-^{(0)} = (1;0;0)$, $\boldsymbol{c}_H^{(0)} = (0;1;0)$, and $\boldsymbol{c}_+^{(0)} = (0;0;1)$. The constants coming form the integration of equation (2.20b) are chosen in order to cancel terms which differs between $\boldsymbol{c}^{(n)}$ and $\boldsymbol{c}^{(0)}$ at $\tau = \pm\infty$, so that ideally $\boldsymbol{c}^{(0)}(\pm\infty) = \boldsymbol{c}^{(n)}(\pm\infty)$. However, some terms appearing while solving the scheme (2.20a) cannot be canceled because they does not have a finite limit at $\pm\infty$. They are the source of non-uniformities discussed by Favraud & Pagneux (2012). The order $n = 1$ components can be easily obtained :

$$\boldsymbol{c}_-^{(1)} = \begin{bmatrix} -i\cos^3\theta/24 + i\cos\theta - 23i/24 \\ -i\alpha^{1/2}\sin^{-1/2}\theta \\ -i\cos\theta\sin^2\theta/4 \end{bmatrix} \ , \tag{2.21}$$

$$\boldsymbol{c}_H^{(1)} = \begin{bmatrix} -i\sin^{9/2}\theta \\ 0 \\ i\sin^{9/2}\theta \end{bmatrix} \ , \tag{2.22}$$

$$\boldsymbol{c}_+^{(1)} = \begin{bmatrix} i\cos\theta\sin^2\theta/4 \\ i\sin^{-1/2}\theta \\ i\cos^3\theta/24 - i\cos\theta + 23i/24 \end{bmatrix} \ . \tag{2.23}$$

Because of their increasing complexity, the following terms are computed with a symbolic computation software (*Maxima* version 5.19.2).

In the same manner as in the preceding section we look at the mode amplitudes in the bases formed by these new WKB modes at order n. We define the *super-adiabatic base of order n* as the base formed by the order n WKB modes $\left\{\boldsymbol{X}_-^{(n)}; \boldsymbol{X}_H^{(n)}; \boldsymbol{X}_+^{(n)}\right\}$, where each $\boldsymbol{X}_j^{(n)}$ includes now the asymptotic power series from $\boldsymbol{\varphi}_j^{(0)}$ to $\boldsymbol{\varphi}_j^{(n)}$. We define the transformation matrix $\Phi^{(n)} = \left[\boldsymbol{X}_-^{(n)}\boldsymbol{X}_H^{(n)}\boldsymbol{X}_+^{(n)}\right]$ and write similarly to equation (2.15)

$$\boldsymbol{X} = \Phi^{(n)}\boldsymbol{Y}^{(n)} \ . \tag{2.24}$$

The figure 2.3 shows the modulus of the acoustic "+" WKB modes amplitudes at different order n from 0 to 7 (still with vorticity mode "H" incident). Of course the curve at $n = 0$ is the same as on figure 2.2. As the order of the basis grows, two phenomena can be noticed. The first one is the smoothing of the oscillations during the

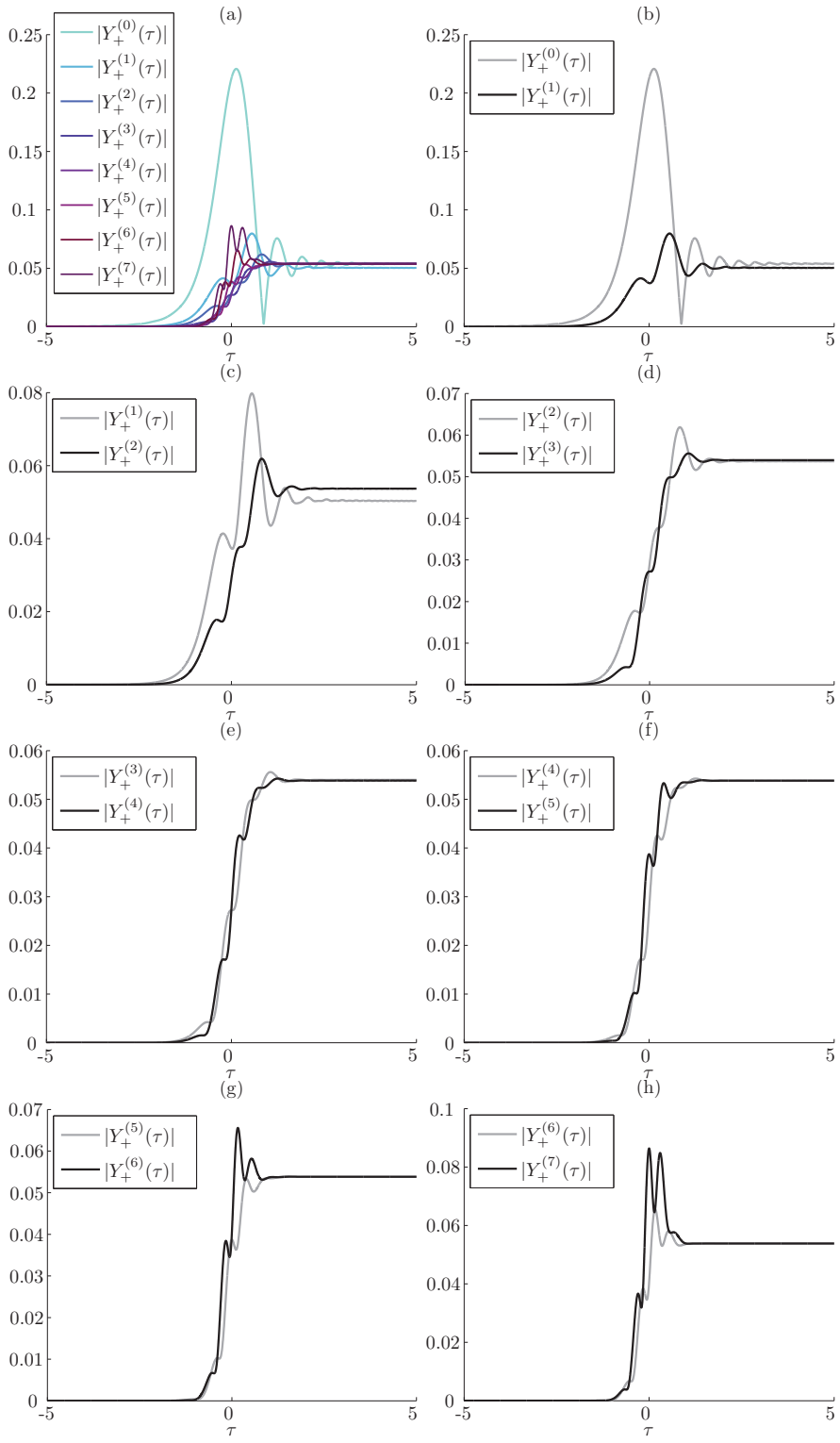

FIGURE 2.3 – Time evolution of the amplitude of acoustic "+" WKB modes at orders from $n = 0$ to 7 (a). Details of successive orders (b-h). Same configuration as figure 2.2.

transition until the order $n = 4$ which is the optimal order. At this order the shape of the transition is close to the Gauss error function as predicted by Berry (1990). At the following orders $n = 5$, 6 and 7 the oscillations grow again and the process starts to diverge. The superadiabatic base never describes this transition as it is an exponentially small quantity of order $\sim \exp(-\mathcal{C}/\varepsilon)$ which cannot be described in terms of powers of ε. Yet, it provides a frame that emphasises the transition. The second phenomenon is the asymptotic convergence of the superadiabatic base revealed by the slight change of the final amplitude. This is due to the fact that the modes are not the same at $\tau = \pm\infty$. This point is tackled by Favraud & Pagneux (2012). However the base rapidly converges and starting from order $n = 3$ the final amplitude does not change. On the figure 2.4 is represented the final amplitude $|Y_+^{(7)}(+\infty)|$ of the acoustic mode as a function of ε (bold line). The curve is indeed asymptotic to $\mathcal{A}e^{-\mathcal{C}/\varepsilon}$ (thin line). Physically, it represents the amount of acoustic waves created by a vorticity wave as a function of the ratio of the shearing of the steady flow to the frequency of the wave. It is remarkable that for small values of this ratio ($\varepsilon < 0.1$) the coupling is almost nonexistent.

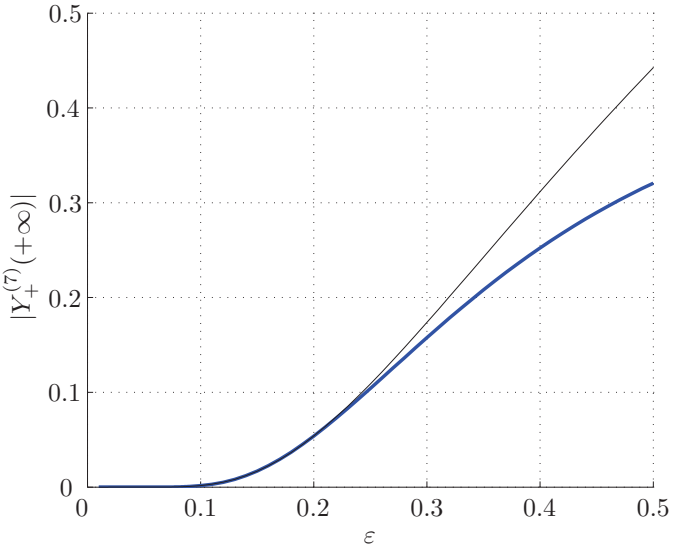

FIGURE 2.4 – Final amplitude $|Y_+^{(7)}(+\infty)|$ as a function of ε. Computation (bold line), fitted $\mathcal{A}e^{-\mathcal{C}/\varepsilon}$ curve (thin line).

5 Concluding remarks

The WKB modes constitute a well suited base to represent acoustic and vorticity perturbations in a Couette plane flow. Examining the time evolution of the modes in the frame of the superadiabatic bases shows results similar to those obtained by Berry (1990) in the field of quantum mechanics. Namely, it allows a smooth tracking of the exponentially small emergences of the non excited modes which, for an optimal order, take

the form the Gauss error function. The derivation of analytical approximate expression of these emergences will constitute a sequel to this work.

A Detail of equation (2.19)

$$\begin{bmatrix} \lambda_j - \lambda_- & 0 & 0 \\ 0 & \lambda_j - \lambda_z & 0 \\ 0 & 0 & \lambda_j - \lambda_+ \end{bmatrix} \begin{bmatrix} c_{j,-}^{(n+1)} \\ c_{j,H}^{(n+1)} \\ c_{j,+}^{(n+1)} \end{bmatrix} = \begin{bmatrix} -\frac{\mathrm{d}}{\mathrm{d}\,\tau} & \frac{\sin^2\theta}{k^{3/2}} & -\frac{\cos\theta\sin\theta}{2} \\ -k^{3/2} & -\frac{\mathrm{d}}{\mathrm{d}\,\tau} & -k^{3/2} \\ -\frac{\cos\theta\sin\theta}{2} & \frac{\sin^2\theta}{k^{3/2}} & -\frac{\mathrm{d}}{\mathrm{d}\,\tau} \end{bmatrix} \begin{bmatrix} c_{j,-}^{(n)} \\ c_{j,H}^{(n)} \\ c_{j,+}^{(n)} \end{bmatrix} \quad (2.25)$$

References

Berry, M. V. 1990 Histories of adiabatic quantum transitions. *Proc. R. Soc. Lond. A* **429**, 61–72.

Betz, V., Goddard, B. D. & Teufel, S. 2009 Superadiabatic transitions in quantum molecular dynamics. *Proc. R. Soc. A* **465**, 3553–3580. (doi: 10.1098/rspa.2009.0337)

Boyd, J. P. 1999 The devil's invention : Asymptotic, superasymptotic and hyperasymptotic series. *Acta Appl. Math.* **56**, 1–98.

Chagelishvili, G. D. 2002 New linear mechanisms of acoustic wave generation in smooth shear flows - (Nonmodal study). In *Sound-flow interactions* (ed. Y. Auregan, A. Maurel, V. Pagneux & J. Pinton), pp. 210–237. Berlin : Springer-Verlag.

Chagelishvili, G. D., Hristov, T. S., Chanishvili, R. G. & Lominadze, J. G. 1993 Mechanism of energy transformations in shear magnetohydrodynamic flows. *Phys. Rev. E* **47**, 366–374. (doi: 10.1103/PhysRevE.47.366)

Chagelishvili, G. D., Khujadze, G. R., Lominadze, J. G. & Rogava, A. 1997*a* Acoustic waves in unbounded shear flows. *Phys. Fluids* **9**, 1955–1962. (doi: 10.1063/1.869314)

Chagelishvili, G. D., Rogava, A. D. & Segal, I. N. 1994 Hydrodynamic stability of compressible plane couette flow. *Phys. Rev. E* **50**, R4283–R4285. (doi: 10.1103/PhysRevE.50.R4283)

Chagelishvili, G. D., Rogava, A. D. & Tsiklauri, D. G. 1996 Effect of coupling and linear transformation of waves in shear flows. *Phys. Rev. E* **53**, 6028–6031. (doi: 10.1103/PhysRevE.53.6028)

Chagelishvili, G. D., Tevzadze, A. G., Bodo, G. & Moiseev, S. S. 1997*b* Linear mechanism of wave emergence from vortices in smooth shear flows. *Phys. Rev. Lett.* **79**, 3178–3181. (doi: 10.1103/PhysRevLett.79.3178)

Davis, J. P. & Pechukas, P. 1976 Nonadiabatic transitions induced by a time dependent hamiltonian in the semiclassical/adiabatic limit : The two state case. *J. Chem. Phys.* **64**, 3129–3137. (doi: 10.1063/1.432648)

Dykhne, A. 1962 Adiabatic perturbation of discrete spectrum states. *Sov. Phys. JETP* **14**, 941–943.

Elk, M. 1995 Adiabatic transition histories of population transfer in the λ system. *Phys. Rev. A* **52**, 4017–4022.

Favraud, G. & Pagneux, V. 2012 Acoustic-vorticity coupling in linearly varying shear flows using the WKB method (Revised manuscript submitted for publication to *Proc. R. Soc. A*, Chapter 1 of this thesis).

George, J. & Sujith, R. I. 2009 Emergence of acoustic waves from vorticity fluctuations : Impact of non-normality. *Phys. Rev. E* **80**, 046 321. (doi: 10.1103/PhysRevE.80.046321)

Gogoberidze, G., Chagelishvili, G. D., Sagdeev, R. Z. & Lominadze, D. G. 2004 Linear coupling and overreflection phenomena of magnetohydrodynamic waves in smooth shear flows. *Phys. Plasmas* **11**, 4672–4685. (doi: 10.1063/1.1789998)

Hagedorn, G. A. & Joye, A. 2004 Time development of exponentially small non-adiabatic transitions. *Commun. Math. Phys.* **250**, 393–413. (doi: 10.1007/s00220-004-1124-5)

Landau, L. & Lifshitz, E. 1977 *Quantum mechanics : non-relativistic theory*, vol. 3 of *Course of theoretical physics*. Butterworth-Heinemann.

Landau, L. D. 1932 Zur theorie der energieubertragung. ii. *Phys. Z. Sowjetunion* **2**, 46.

Lim, R. 1993 Overlapping stokes smoothings in adiabatic quantum transitions. *J. Phys. A* **26**, 7615.

Lim, R. & Berry, M. V. 1991 Superadiabatic tracking of quantum evolution. *J. Phys. A : Math. Gen.* **24**, 3255–3264.

Mahajan, S. M. & Rogava, A. D. 1999 What can the kinematic complexity of astrophysical shear flows lead to ? *Astrophys. J.* **518**, 814–820. (doi: 10.1086/307319)

Rogava, A., Poedts, S. & Mahajan, S. 2001 Acoustics of kinematically complex shear flows. *J. Comput. Acoust.* **9**, 869–888. (doi: 10.1142/S0218396X01001078)

Rogava, A. D. & Mahajan, S. M. 1997 Coupling of sound and internal waves in shear flows. *Phys. Rev. E* **55**, 1185–1188. (doi: 10.1103/PhysRevE.55.1185)

Thomson, W. L. K. 1887 Stability of fluid motion (continued from the may and june numbers).-rectilineal motion of viscous fluid between two parallel planes. *Philos. Mag.* **24**, 188.

Zener, C. 1932 Non-adiabatic crossing of energy levels. *Proc. R. Soc. Lond. Ser. A* **137**, 696–702. (doi: 10.1098/rspa.1932.0165)

Deuxième partie

Conditions limites de géométries complexes et application à l'acoustique et aux couches limites visqueuses

3

Réflexion d'une onde acoustique par une surface rigide de géométrie complexe

Cette seconde partie de ce manuscrit de thèse traite de la modélisation de problèmes incluant une condition limite appliquée sur une frontière dont la géométrie est complexe. L'approche proposée repose sur l'application d'une transformation conforme aux équations du problème considéré, puis en l'utilisation d'une méthode multimodale pour résoudre les équations ainsi obtenues. Dans ce chapitre nous développons cette méthode dans le cas de la réflection d'une onde acoustique par une surface de géométrie complexe. Ce chapitre se présente sous la forme d'un article qui sera prochainement soumis pour publication au *Journal of the Acoustical Society of America*.

L'utilisation d'une transformation conforme permet de transformer une géométrie complexe dans le plan d'origine (X, Y) en une géométrie plus simple dans le plan transformé (x, y). De plus, le caractère conforme de la transformation implique que les angles sont localement conservés. Ainsi, les conditions limites, qu'elles soient de type Dirichlet ou de type Neumann, conservent une forme simple et peuvent être appliquées sur des géométries plus simples. Mais il existe bien évidemment un coût à payer pour cette simplification : la complexification des équations en volume. Le grand intérêt des transformations conformes est que ce coût est moindre lorsque le problème considéré fait intervenir un opérateur Laplacien. En effet, une transformation conforme transforme ce Laplacien en un autre Laplacien multiplié par une fonction de l'espace (le carré du

module de la dérivée de la transformation conforme). La principale difficulté pour la résolution des équations est ainsi déplacée de l'application des conditions limites sur une géométrie complexe à la résolution d'équations en volume avec coefficients variables.

Trouver la transformation conforme qui permet de transformer une géométrie complexe donnée en une géométrie plane peut s'avérer être un tâche difficile. Il existe pour cela des méthodes, dépendant du type de géométrie, qui permettent d'obtenir la transformation conforme idoine. A titre d'exemple, Floryan (1986) propose une telle méthode pour les configurations constituées d'une suite de segments droits. Dans ce travail, nous portons une attention particulière à la transformation conforme proposée par Vandembroucq & Roux (1997*a*,*b*) ainsi qu'à la méthode qui permet d'en définir les paramètres. Cette transformation concerne les géométries périodiques dont la pente reste inférieure à 1.

Dans notre étude, nous considérons l'équation de Helmholtz, qui régit l'évolution du champ de pression en régime harmonique. Nous étudions d'abord la réflection d'une onde dans un guide d'onde ayant une terminaison de géométrie complexe, puis, nous nous intéressons à la réflection d'une onde en espace libre par une surface périodique de géométrie complexe. Dans ces deux cas, la transformation conforme est choisie de façon à ce que la surface de géométrie complexe par laquelle l'onde est réfléchie soit transformée en la droite $y = 0$. L'application de cette transformation conforme fait apparaître un indice qui varie en fonction de l'espace dans l'équation de Helmholtz. Ces deux problèmes sont alors traités comme des guides d'onde dans la direction y, orthogonale à la surface, et sont résolus au moyen de la méthode multimodale.

La méthode multimodale a d'abord été développée en acoustique par Pagneux *et al.* (1996) afin de résoudre de façon semi-analytique l'équation de Helmholtz dans un guide de section variable. Elle consiste en la projection des équations sur la base des modes propres rigides transverses. Ces modes rigides ont l'avantage de pouvoir être déterminés de façon analytique *a priori*, alors que la détermination des véritables modes propres d'une section du guide peut parfois nécessiter l'usage de méthodes numériques dans certains cas complexes, comme par exemple en présence de traitements à réaction non-localisée. Il est alors possible d'obtenir une équation différentielle ordinaire sur l'évolution le long du guide des amplitudes modales de la pression et de sa dérivée axiale. La connaissance d'une expression analytique de la base de fonctions considérée fait que tous les termes intervenant dans cette équation sont connus analytiquement. Cette équation ne peut être intégrée directement par des méthodes numériques pour deux raisons. La première est que la présence de modes évanescents peut induire des instabilités numériques et faire diverger l'erreur (Pagneux *et al.*, 1996). La seconde est que le problème est posé comme un problème aux conditions limites imposées aux deux extrémités du guide : condition initiale en entrée du guide et condition de rayonnement en sortie du guide. Le problème ne peut de ce fait être intégré comme un problème de Cauchy. Pour cette raison une matrice d'impédance, reliant les amplitudes modales de la pression et de sa dérivée est introduite. Son évolution le long du guide vérifie alors une équation de Riccati, connue pour posséder des singularités dépendant de la condition initiale (ou *movable singularities* en anglais, Schiff & Shinider, 1999). Cette équation peut cependant

être intégrée numériquement de façon efficace, y compris au travers des singularités, en utilisant un schéma de “Magnus–Möbius” (Iserles *et al.*, 1999, Iserles & Norsett, 1999). Ces singularités revêtent un caractère important car elle correspondent à des modes piégés du guide (Pagneux, 2010).

Nous adaptons ici la méthode proposée par Pagneux (2010) pour trouver des modes quasi-piégés dans un guide d'onde de section variable. La méthode que nous proposons permet de trouver les géométries ayant des modes quasi-piégés en évoluant au sein d'une famille de géométries donnée. La particularité de cette méthode est qu'elle permet de trouver ces géométries en fonction de la fréquence, et non pas, pour une géométrie donnée, de rechercher la fréquence et le mode piégé associé.

Reflection of an acoustic wave on a geometrically complex boundary by use of conformal mapping [1]

Abstract : The reflection of an acoustic wave on a geometrically complex boundary is considered. The proposed method relies on the use of conformal mappings to model the boundary and of the multimodal impedance method to solve the resulting equations. The use of conformal mappings allows one to reduce the problem of the complex boundary condition into a simpler plane boundary condition, but adds a spatially varying index to the governing equations. These equations are then treated with the multimodal impedance method. They are reduced into a Riccati equation for the modal impedance matrix which is solved numerically with a Magnus–Möbius scheme. This Riccati equation is known to have quasi-singularities (or movable singularities) which corresponds to quasi-trapped modes of the geometry. We describe a method to find geometries having such trapped-modes at a given frequency, by looking for these quasi-singularities. The whole method is first described in the case of a wave in a semi infinite rigid waveguide reflected by a geometrically complex termination. Then it is applied on the reflection of a wave by periodic geometrically complex surface in semi-infinite free space.

1 Introduction

The reflection and the scattering of a wave by a rough surface, or more generally by a geometrically complex surface, is a subject which has been intensively studied in acoustics but also in optics and electromagnetism. As a result, a very large literature exists on the subject, including several books which deal with this only topic (for instance Ogilvy, 1991, Voronovich, 1999). Among the different methods yet proposed, some rely on the use of conformal mappings to treat the Helmholtz equation governing the wave propagation in harmonic regime. This allows one to map the rough surface onto a plane surface. Such a transformation has the advantage of preserving the Laplacian operator, which is simply replaced by another Laplacian multiplied by a function of space. The challenging difficulty is then moved from applying the boundary condition on a complex geometry, to solving the Helmholtz equations with a varying index. Different methods has been proposed to solve this new problem, such as, for instance, differential methods (Depine & Simon, 1982, 1983), integral methods (Takakura, 1995), or asymptotic methods for low frequencies (Sabina & Babich, 2001).

1. To be submitted to *The Journal of the Acoustical Society of America*. Authors: Gael Favraud and Vincent Pagneux.

In this paper we propose a method based on the use of a conformal mapping and of a multimodal impedance method to solve the problem of the reflection of a wave by a geometrically complex boundary in harmonic regime. The term "geometrically complex boundary" is preferred here to the term "rough boundary" as the method proposed here requires no assumption on the relative length scale of the boundary roughness in comparison to the wavelength. The Helmholtz problem with varying index, obtained by applying the conformal mapping, is viewed as a waveguide problem in the y direction, orthogonal to the boundary. This problem is solved with the multimodal impedance method which was first developed to solve the Helmholtz equation in an irregular waveguide by Pagneux *et al.* (1996). It has since been applied to different problems such as, for instance, acoustic waveguides with bends (Felix & Pagneux, 2001, 2002), or with non-uniform lining (Bi *et al.*, 2006, 2007). It relies on the projection of the governing equations on the basis of the local transverse rigid eigenmodes. The equations obtained cannot be solved directly because they are numerically unstable due to the presence of evanescent modes. To obtain an equation that can be integrated numerically, an admittance/impedance matrix is introduced. Its variation in the y direction (along the waveguide) is governed by a Riccati equation of the form $\frac{\mathrm{d}}{\mathrm{d}\,y}\mathsf{Y} = f(\mathsf{Y}, y)$ which is solved numerically. This Riccati equation is known to be subject to movable singularities in the complex y plane (Schiff & Shinider, 1999). They are responsible for very high peaks of the admittance matrix (quasi-singularities) on the real y axis. Despites these quasi-singularities, the Riccati equation can be integrated very efficiently using a Magnus–Möbius scheme (Schiff & Shinider, 1999, Iserles *et al.*, 1999, Iserles & Norsett, 1999). Whereas these singularities can be considered as problematic, they present a great interest in order to find quasi-trapped modes. Indeed, the existence of a trapped mode is linked to a singularity of the admittance/impedance matrix (Pagneux, 2010) (the admittance matrix cannot be defined at the point where such a trapped mode exists). In this paper, we adapt this method in order to compute the reflected field and to find quasi-trapped modes of geometrically complex surfaces. The particularity of this method is that it allows one to find, among a given family of geometries, the geometries having quasi-trapped modes at a given frequency.

The case of a wave inside a vertical rigid waveguide reflected by a geometrically complex rigid termination at the bottom is first considered in Secs. 2 to 5. In Sec. 2, the governing equations are first presented. Then the conformal mapping is introduced. The multimodal method is detailed in Sec. 3. One of the major difficulty of the method proposed in this paper is to find the appropriate mapping corresponding to a given geometry. Depending on the type of the geometry, some straightforward methods exist to determine the relevant mapping. Section 4 focuses on a particular mapping proposed by Vandembroucq & Roux (1997*a*), and provides some examples of results that can be obtained. In Sec. 5, the method to find particular geometries having quasi-trapped modes is exposed. Eventually, in Sec. 6, the methods and tools developed earlier in the paper are adapted to the case of a wave in a semi-infinite space reflected on a geometrically complex surface.

2 The governing equations

We first consider the case of a wave inside a vertical rigid waveguide reflected by a geometrically complex rigid termination at the bottom end. The Helmholtz equation is to be solved inside the domain $\mathcal{D}_0$ which represents the waveguide. The space coordinates (X, Y) are supposed to be non-dimensionalized so that the waveguide width is 2π. The boundary $\partial\mathcal{D}_0$ is constituted of the two side walls at $X = 0$ and $X = 2\pi$ and of the complex termination.which is defined by the curve $\mathcal{C}_0 = \{(X, Y) \mid X = U(s), Y = V(s), s \in [0, 2\pi]\}$ where U and V are two real functions. In this paper, both the sidewalls and the termination are supposed to be rigid (Neumann boundary condition), but other boundary conditions like Dirichlet or Robin (impedance) boundary conditions may be considered. The governing equations are the Helmholtz equation in harmonic regime together with Neumann boundary conditions on $\partial\mathcal{D}_0$ (the time dependence $e^{-i\omega t}$ where ω is the pulsation is omitted in the following). These are written as

$$\Delta_X P + k^2 P = 0 \qquad \text{in } \mathcal{D}_0 \ , \tag{3.1a}$$

$$\boldsymbol{\nabla}_X P \cdot \boldsymbol{n} = 0 \qquad \text{on } \partial\mathcal{D}_0 \ , \tag{3.1b}$$

where Δ_X and $\boldsymbol{\nabla}_X$ are the Laplacian and the gradient operators with respect to the (X, Y) coordinates, and where $\boldsymbol{n}$ is the vector normal to $\partial\mathcal{D}_0$. The total field P is split into the sum of an incident field p_{in} and of a reflected field p :

$$P = p_{in} + p \ . \tag{3.2}$$

The incident field is supposed to be known and to satisfy itself the Helmholtz equation with rigid boundary condition on the side walls

$$\Delta_X p_{in} + k^2 p_{in} = 0 \qquad \text{in } \mathcal{D}_0 \ , \tag{3.3a}$$

$$\frac{\partial}{\partial X} p_{in} = 0 \qquad \text{for } X = 0,\ 2\pi \ . \tag{3.3b}$$

Therefore, the reflected field, which is the unknown to be found, satisfies

$$\Delta_X p + k^2 p = 0 \qquad \text{in } \mathcal{D}_0 \ , \tag{3.4a}$$

$$\boldsymbol{\nabla}_X p \cdot \boldsymbol{n} = -\boldsymbol{\nabla}_X p_{in} \cdot \boldsymbol{n} \qquad \text{on } \partial\mathcal{D}_0 \ . \tag{3.4b}$$

The most challenging issue to solve these equations comes from applying the boundary condition on $\mathcal{C}_0$. One interesting method to deal with this difficulty is by using a conformal mapping which maps the domain $\mathcal{D}_0$ in the *physical plane* (X, Y) to a simpler domain $\mathcal{D}$ in the *computational plane* (x, y). Namely, the mapping function is defined by

$$\Omega : z \mapsto Z = \Omega(z) \ , \tag{3.5}$$

where $z = x+iy$, and $Z = X+iY$. The mapping function Ω is chosen so that the domain $\mathcal{D}_0$ is the image of the domain $\mathcal{D} = \{(x, y) \mid 0 \leqslant x \leqslant 2\pi; y \geqslant 0\}$. Therefore, the two side walls remain unchanged by the mapping whereas the complex boundary $\mathcal{C}_0$ is the image

of the straight segment $\mathcal{C} = \{(x, 0) \mid 0 \leqslant x \leqslant 2\pi\}$. For convenience of the upcoming resolution of this problem, we impose as a last condition that the mapping tends to the identity at infinity, that is $\Omega(z) \to z$ for $y \to \infty$. The more rapidly the mapping tends to the identity is the better, because in that case the effect of the mapping is localized in a small region near $y = 0$ (the mapping functions considered in the following tends exponentially to the identity). The first interest of a conformal mapping is that it locally conserve the angles. Thus the complex boundary condition (3.4b) simply reduces to $\partial p/\partial y = -\partial p_{in}/\partial y$ on $\mathcal{C}$ in the computational plane. The other advantage is that it transforms the Laplacian operator into another Laplacian operator :

$$\Delta_X = \left|\frac{\mathrm{d}\, z}{\mathrm{d}\, Z}\right|^2 \Delta_x \ , \tag{3.6}$$

where Δ_x is the Laplacian operator with respect to the (x, y) variables. Defining

$$V(x, y) = \left|\frac{\mathrm{d}\, Z}{\mathrm{d}\, z}\right|^2 \ , \tag{3.7}$$

the governing equations (3.4) are therefore rewritten as

$$\Delta_x p + k^2 V p = 0 \qquad \text{in } \mathcal{D} \ , \tag{3.8a}$$

$$\frac{\partial}{\partial x} p = 0 \qquad \text{for } x = 0,\ 2\pi \ , \tag{3.8b}$$

$$\frac{\partial}{\partial y} p = -\frac{\partial}{\partial y} p_{in} \qquad \text{for } y = 0 \ . \tag{3.8c}$$

This new problem to solve is a Helmholtz equation with a spatially varying index but with boundary conditions imposed on a simpler geometry. In the end, the mapping moves the difficulty arising from the complex boundary condition into the bulk equations.

To close the problem, it is also imposed a radiation condition : it is supposed that p contains no wave coming from $y = +\infty$. Figure 3.1 summarizes the problem to solve and the link between physical and computational plane. In the following, the problem (3.8) is solved by using the multimodal method (Pagneux *et al.*, 1996). This article mainly follows the methods and ideas presented by Pagneux (2010), and apply them to the problem (3.8).

3 Multimodal resolution

In this section, a method to solve Eqs. (3.8), based on the multimodal method, is presented. The reflected field p and its axial derivative $q(x, y) = \frac{\partial p}{\partial y}$ are decomposed as infinite series on the basis of the normalized rigid transverse eigenmodes φ_m of the straight waveguide $\mathcal{D}$ in the (x, y) plane

$$p = \sum_{m \geqslant 0} p_m(y)\varphi_m(x) \ , \tag{3.9a}$$

$$q = \sum_{m \geqslant 0} q_m(y)\varphi_m(x) \ . \tag{3.9b}$$

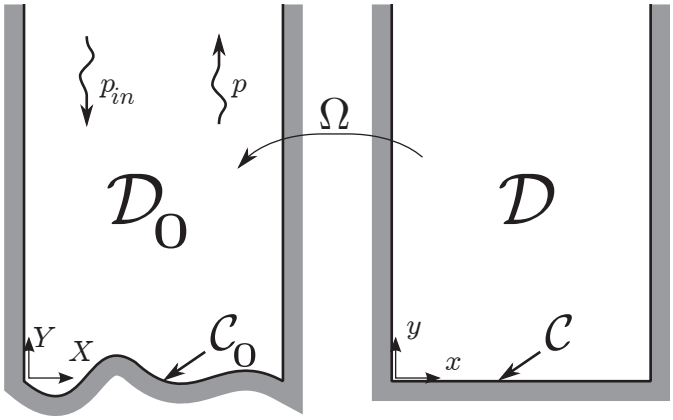

FIGURE 3.1 – Representation of the studied problem in the physical (X, Y) and computational (x, y) planes.

These modes are solutions of the transverse problem

$$\left(\frac{\mathrm{d}^2}{\mathrm{d}x^2} + \alpha_m^2\right) \varphi_m = 0 \qquad \text{for } 0 \leqslant x \leqslant 2\pi \ , \tag{3.10a}$$

$$\frac{\mathrm{d}}{\mathrm{d}x} \varphi_m = 0 \qquad \text{for } x = 0,\ 2\pi \ . \tag{3.10b}$$

They are

$$\varphi_0(x) = \frac{1}{\sqrt{2\pi}} \ , \tag{3.11a}$$

$$\varphi_m(x) = \frac{\cos(\alpha_m x)}{\sqrt{\pi}} \qquad \text{for } m > 0 \ , \tag{3.11b}$$

with $\alpha_m = m/2$. They satisfy the orthogonality relation

$$\int_0^{2\pi} \varphi_n(x)\varphi_m(x)\mathrm{d}x = \delta_{n,m} \ . \tag{3.12}$$

The projection of Eq. (3.8a) on the basis of the φ_m takes advantages of the orthogonality relation and of the rigid boundary conditions of the modes. This yields

$$p_n'(y) = q_n(y) \ , \tag{3.13a}$$

$$q_n'(y) = -k_n^2 p_n(y) - k^2 \sum_{m \geqslant 0} \Gamma_{n,m}(y) p_m(y) \ , \tag{3.13b}$$

where $k_n = \sqrt{k^2 - \alpha_n^2}$, and

$$\Gamma_{n,m}(y) = \int_0^{2\pi} (V(x,y) - 1)\varphi_n(x)\varphi_m(x)\mathrm{d}x \ . \tag{3.14}$$

By defining the vectors $\boldsymbol{p} = (p_m)_m$ and $\boldsymbol{q} = (q_m)_m$, as well as the matrices $\mathsf{K} = (k_n\delta_{n,m})_{n,m}$ and $\mathsf{\Gamma} = (\Gamma_{n,m})_{n,m}$, Eqs. (3.13) are rewritten as the vectorial first order ordinary differential equation

$$\frac{\mathrm{d}}{\mathrm{d}\,y}\begin{bmatrix}\boldsymbol{p}\\ \boldsymbol{q}\end{bmatrix} = \begin{bmatrix}0 & \mathsf{Id}\\ -(\mathsf{K}^2 + k^2\mathsf{\Gamma}) & 0\end{bmatrix}\begin{bmatrix}\boldsymbol{p}\\ \boldsymbol{q}\end{bmatrix} \ . \tag{3.15}$$

This equation cannot be integrated numerically because of the presence of evanescent modes which are responsible for exponential divergence of the error (Pagneux *et al.*, 1996). Besides, it cannot be integrated as an initial value problem because the boundary conditions are imposed respectively at $y = 0$ and $y = +\infty$. Following the method proposed by Pagneux *et al.* (1996), an equation on the admittance matrix has to be considered. The admittance matrix Y is defined by the relation

$$\boldsymbol{q} = \mathsf{Y}\boldsymbol{p} \ , \tag{3.16}$$

which can be seen as a matrix formulation of the Dirichlet to Neumann operator. The equation governing the variation of the admittance matrix along the waveguide is obtained by injecting its definition (3.16) into Eq. (3.15). This gives the Riccati equation

$$\mathsf{Y}' = -\mathsf{Y}^2 - k^2\mathsf{\Gamma} - \mathsf{K}^2 \ . \tag{3.17}$$

This ODE of order 1 can be integrated as an initial value problem with just one initial condition. In order to impose the direction of the decay of the evanescent modes, this initial condition has to be imposed at $y = +\infty$. It derives from the radiation condition and from the fact that the mapping function is the identity at infinity. This latter condition induces that the $\mathsf{\Gamma}$ matrix is zero at infinity. In that case, Eq.(3.17) reduces to $\mathsf{Y}' = -\mathsf{Y}^2 - \mathsf{K}^2$ at $y = +\infty$.

Therefore, in order to fulfill the radiation condition, the initial condition on Y has to be

$$\mathsf{Y}(y = +\infty) = +\mathsf{Y_c} \ , \tag{3.18}$$

where $\mathsf{Y_c}$ is the characteristic admittance matrix $\mathsf{Y_c} = i\mathsf{K}$.

Once the admittance matrix is known, to compute the reflected field p, Eq.(3.8c) has also to be projected on the modes φ_m. This requires to switch between the physical and the computational plane because the incident field p_{in} is most usually known as a function of the physical plane coordinates (X, Y) in which the initial problem (3.4) is stated. It is supposed hereafter that p_{in} is the rigid mode numbered n_0 :

$$p_{in}(X, Y) = e^{-ik_{n_0}Y}\varphi_{n_0}(X) \ . \tag{3.19}$$

This makes no loss generality as the problem solved here is linear. The projection of Eq. (3.8c) on the modes $\varphi_m(x)$ in the computational plane yields

$$\begin{aligned} q_m(0) = \int_0^{2\pi}\Big[&- \frac{\partial\Omega_R}{\partial y}(x)\varphi'_{n_0}(\Omega_R(x)) \\ &+ ik_{n_0}\frac{\partial\Omega_I}{\partial y}(x)\varphi_{n_0}(\Omega_R(x))\Big] \\ &\times \varphi_m(x)e^{-ik_{n_0}\Omega_I(x)}\mathrm{d}\,x \ , \end{aligned} \tag{3.20}$$

where Ω_R and Ω_I are the real and imaginary parts of the mapping function. From Eq. (3.20), and knowing the admittance matrix at zero $\mathsf{Y}(0)$, the initial pressure $\boldsymbol{p}(0)$ can directly be obtained, and the pressure can be computed everywhere.

In practice, the infinite series has to be truncated. The number of modes which has to be retained depends on both the frequency and on the mapping used. In all cases, all the propagative modes has to be kept. But for the calculation to converge, a certain number of evanescent modes has also to be considered. The best way to see if such a method has converged is to make two calculation with a different number of modes and compare the results (Pagneux *et al.*, 1996). If there is no significant difference in the results, then the code has converged. Looking at the relative amplitude of the last evanescent modes may also give relevant information on the convergence. The admittance matrix is computed numerically with a Magnus-Möebius scheme (Pagneux, 2010). This method is based on the Möbius scheme (Schiff & Shinider, 1999), which consists in solving the linear system (3.15) instead of the Riccati equation (3.17). It allows one to compute the Riccati equation very efficiently through the movable (and even true) singularities. The Magnus method (Iserles *et al.*, 1999, Iserles & Norsett, 1999) is used to solve this linear system. For a detailed expression of the scheme at orders 2 and 4 see Pagneux (2010). The initial condition on the admittance is imposed at a point $y = L$ where L is sufficiently large so that $\mathsf{\Gamma}(L)$ can be neglected in comparison with K, and the initial condition (3.18) is used. The use of a mapping which tends exponentially to the identity, as it is done hereafter, makes that L can have a reasonable value. The admittance matrix is then computed from $y = L$ to $y = 0$. The initial condition on the pressure (3.20) is then computed numerically as it may be very difficult to compute it analytically. The *Chebfun* package (Trefethen *et al.*, 2011), based on Chebyshev expansions (Battles & Trefethen, 2004), is used here as it provides a rapid and accurate computational tool. However, any other numerical method would do fine. Eventually, the pressure is calculated in the reverse order from $y = 0$ to $y = L$ as described in (Pagneux, 2010), by using the resolvent operator numerically obtained while integrating Y with the Magnus–Möbius scheme.

4 A general mapping based on Fourier series

The major difficulty of the method presented in this paper is to find the appropriate mapping to model a given particular boundary geometry. Provided the rough termination $\mathcal{C}_0$ can be described by

$$Y = h(X) \qquad 0 \leqslant X \leqslant 2\pi \ , \tag{3.21}$$

and under the assumption that $h'(X) < 1$, it is possible to find an appropriate mapping based on a Fourier series (Vandembroucq & Roux, 1997*a*,*b*). The mapping is defined by

$$Z = \Omega(z) = z + \sum_{l=1}^{N} \omega_l e^{ilz} \ . \tag{3.22}$$

Owing to the exponentials this mapping tends exponentially to the identity when $y \to +\infty$ as required in the preceding section. As the description of the boundary is usually

given as a function of the X variable in the physical plane, the determination of the coefficients ω_l is not straight forward. Vandembroucq & Roux (1997*a*) proposed an iterative method to find these coefficients. This method requires that the slope of the boundary remains less than 1 to converge.

The Γ matrix corresponding to this mapping is

$$\begin{aligned}\Gamma_{n,m}(y) = &\sum_l l^2 e^{-2ly}|\omega_l|^2\delta_{n,m} \\ &- 2\sum_l l e^{-ly}\Big(\Im(\omega_l)F_{n,m}(l) + \Re(\omega_l)G_{n,m}(l)\Big) \\ &+ 2\sum_{l,r>l} lr e^{-(l+r)y}\Big(\Re(\omega_l\overline{\omega}_r)F_{n,m}(l-r) \\ &\qquad - \Im(\omega_l\overline{\omega}_r)G_{n,m}(l-r)\Big)\ , \end{aligned} \tag{3.23}$$

where

$$\begin{aligned} F_{n,m}(l) &= \int_{x=0}^{2\pi} \cos lx\ \varphi_n(x)\varphi_m(x)\mathrm{d}\,x \\ &= \frac{\delta_{n,m+2l} + \delta_{n,m-2l} + \delta_{n,-m+2l} + \delta_{n,-m-2l}}{2\sqrt{1+\delta_{n,0}}\sqrt{1+\delta_{m,0}}}\ , \end{aligned} \tag{3.24a}$$

$$\begin{aligned} G_{n,m}(l) &= \int_{x=0}^{2\pi} \sin lx\ \varphi_n(x)\varphi_m(x)\mathrm{d}\,x \\ &= \frac{1}{\pi\sqrt{1+\delta_{n,0}}\sqrt{1+\delta_{m,0}}} \\ &\times \Big(\frac{1}{2l+n+m} + \frac{1}{2l+n-m} \\ &\quad + \frac{1}{2l-n+m} + \frac{1}{2l-n-m}\Big)\ , \end{aligned} \tag{3.24b}$$

$$G_{n,m}(l) = 0 \qquad \text{when } (m+n) \text{ is even}\ . \tag{3.24c}$$

As an example of application of the proposed method, we now consider a waveguide terminated by a "parabolic reflector". The boundary, defined by the equation $Y = (X-\pi)^2/(4f_0)$, is described with the mapping (3.22) using 15 Fourier components. Figures 3.2(a) and (b) present the considered geometry with $f_0 = \pi$ in the physical plane, and the associated variation of the index added by the mapping in the computational plane respectively. The total field $|P|$ corresponding to an incident plane wave at $k = 40.3$ is represented on fig. 3.3(a). It can be seen that the reflected wave focuses at the point $(\pi/2, f_0)$. For this calculation, 81 modes are propagating, and 119 modes evanescent modes were kept in the calculation, leading to a total of 200 modes. The amplitude of each modes at the boundary $y = 0$ is represented on fig. 3.3(b) in logarithmic scale. The method starts converging from the 100th mode. This shows that about 40 evanescent modes at least has to be retained in this case. Figure 3.4 displays, for the same geometry, the pressure field associated to an incident mode 4 at a lower frequency $k = 20.3$. This time the interactions at the focusing point of the reflector are destructive.

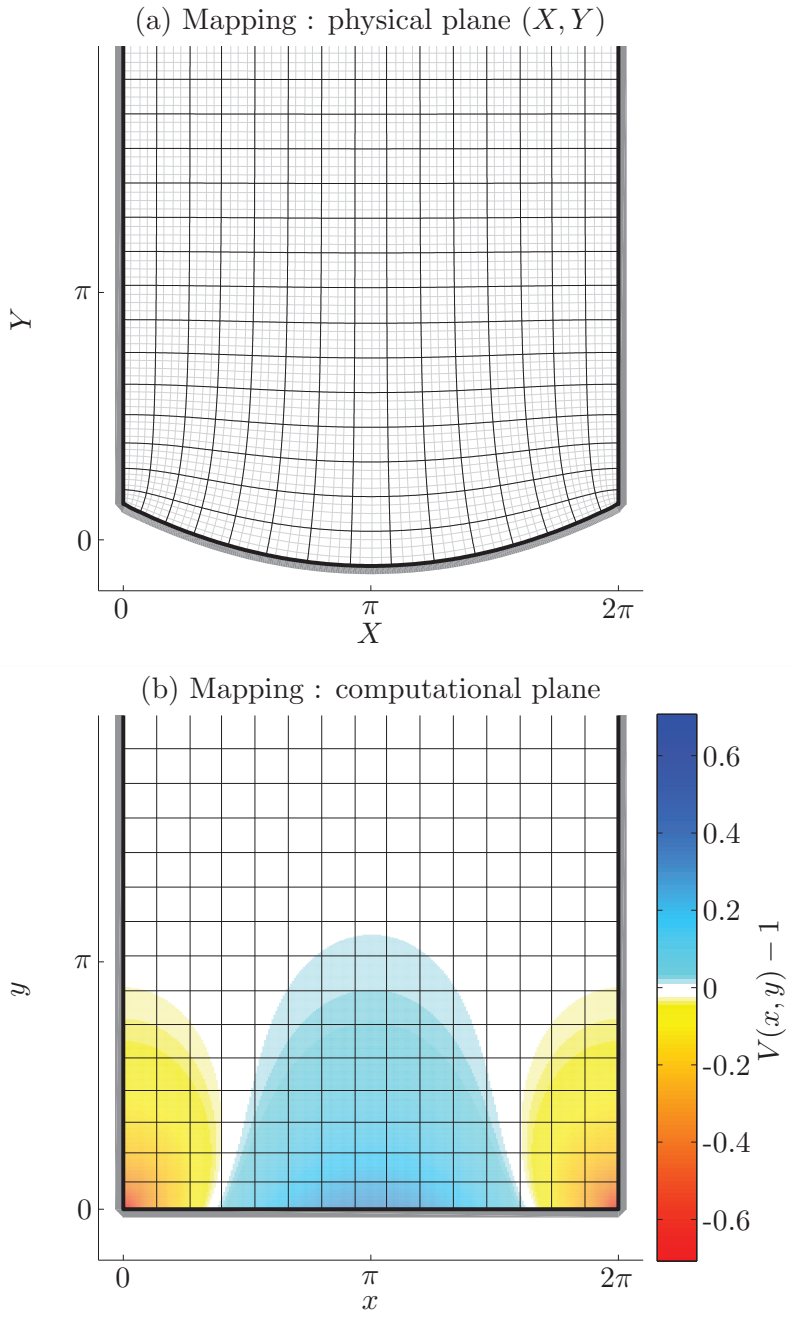

FIGURE 3.2 – Mapping of a duct terminated by a parabolic reflector discretized with 15 Fourier components and with $f_0 = \pi$. Physical plane (a), and computational plane (b). The color values represent the variation of the index $V(x, y) - 1$.

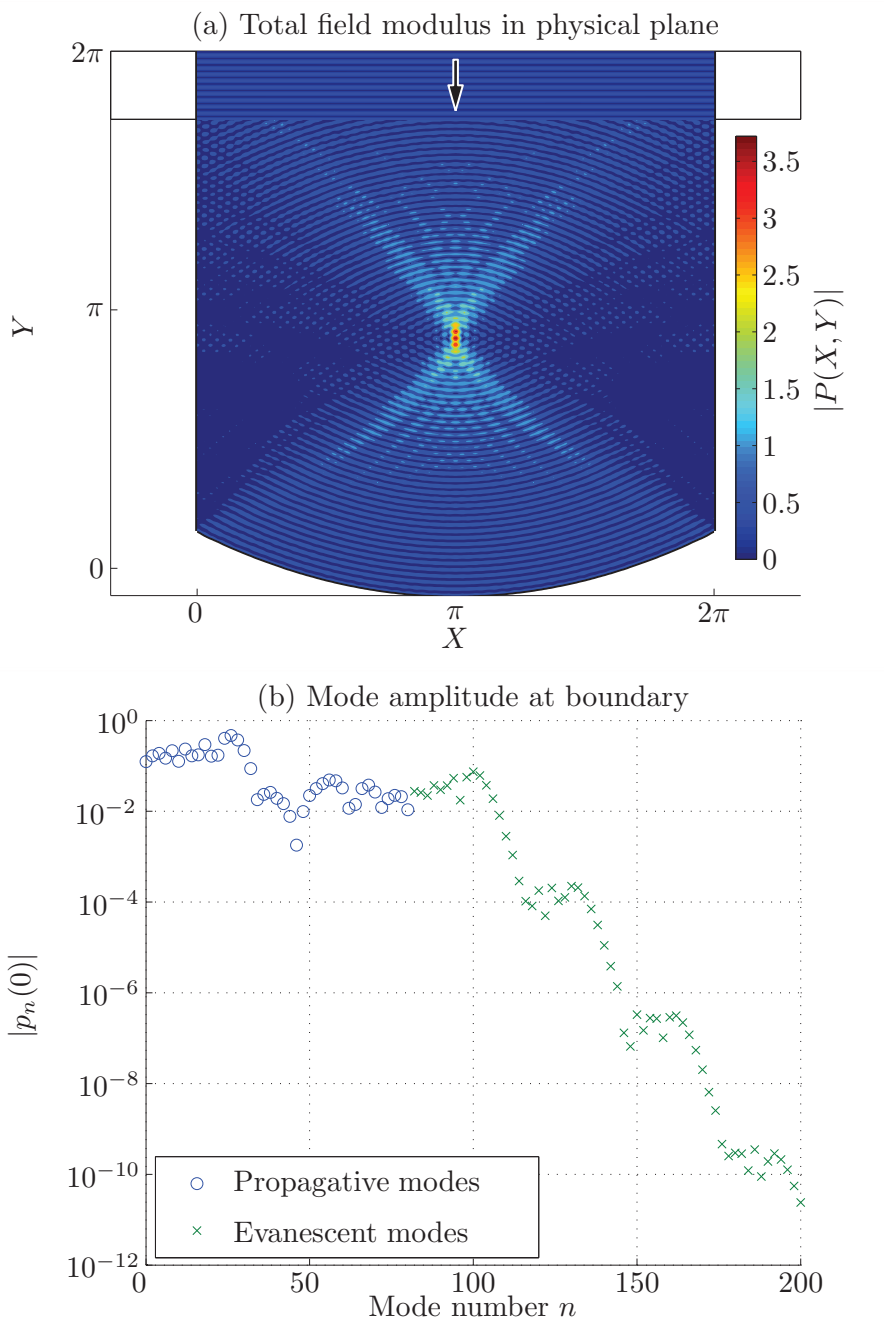

FIGURE 3.3 – Pressure field in a duct terminated by a parabolic reflector (same configuration as fig. 3.2). Total field modulus $|P| = |p_{in} + p|$ for incident plane wave at $k = 40.3$ (a). Inset : modulus of real part of incident field. Mode amplitudes $|p_n(0)|$ at $y = 0$ (b).

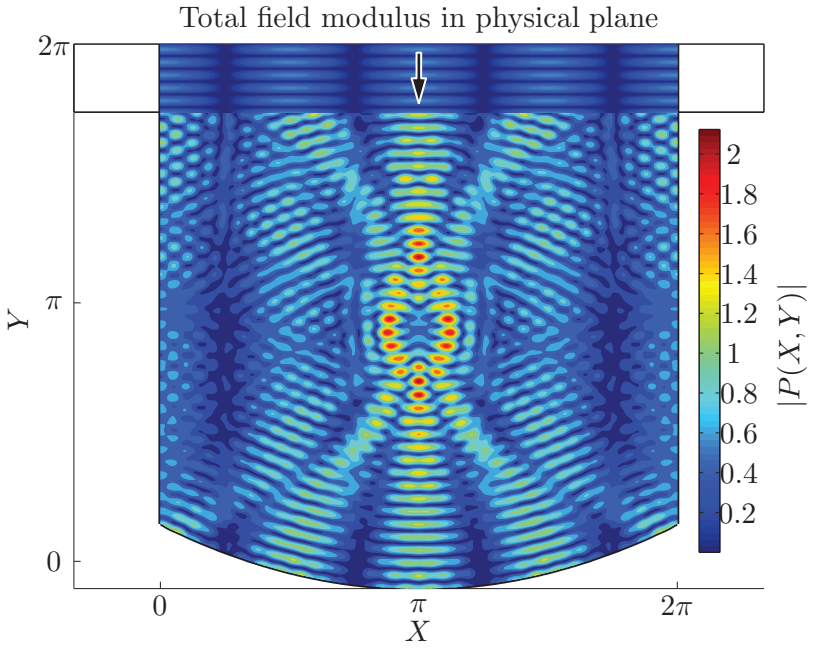

FIGURE 3.4 – Pressure field in a duct terminated by a parabolic reflector (same configuration as fig. 3.2). Total field modulus $|P| = |p_{in} + p|$ for mode 4 incident at $k = 20.3$. Inset : modulus of real part of incident field.

5 Quasi-trapped modes

As mentioned earlier, the Riccati equation (3.17) is known to possess singularities. These singularities are usually seen as a source of issues for the integration process. However, as pointed out by Pagneux (2010), these singularities turn out to be an efficient way to find trapped modes. This section focuses on these (quasi) trapped modes [2]

In general, the singularities of the Riccati equation (3.17) lie in the complex y–plane. When they are close to the real y–axis they are responsible for high peaks of the diagonal component of Y. At the same point, a peak of the modulus of one of the eigenvalues occur. The eigenvector, say $\boldsymbol{\psi}_c$, associated to the eigenvalue, say λ_c, satisfies $\mathsf{Y}\boldsymbol{\psi}_c = \lambda_c\boldsymbol{\psi}_c$. If the initial condition on $\boldsymbol{p}$ is imposed at the (quasi) singularity $y = y_c$ by imposing $\boldsymbol{q}(y_c) = \boldsymbol{\psi}_c$ then $\boldsymbol{p}(y_c) = \frac{1}{\lambda_c}\boldsymbol{\psi}_c$. Supposing the eigenvector is normalized (or at least finite), and because $\lambda_c \to \infty$ due to the singularity, $\boldsymbol{p}(y_c) \to 0$. Therefore the solution almost fulfills the Dirichlet boundary condition on $y = y_c$, and the Sommerfeld radiation condition at $y = +\infty$ while not being trivial. Taking this solution in the physical plane (X, Y) and considering the image of the line $y = y_c$ as the boundary provides a geometry

2. A trapped mode is a solution of the homogeneous Helmholtz equation with waves radiating towards infinity

having a trapped mode at the considered frequency. In the same manner, the singularities of the impedance matrix $\mathsf{Z} = \mathsf{Y}^{-1}$ (or near zeros of the eigenvalues of Y) can be used to find geometries having trapped modes with respect to the Neumann boundary condition at $y = y_c$. Note that to apply this method, a particular mapping must be chosen before. This determines a family of geometries on which trapped modes will be sought. This family is composed of all the geometries in the physical plane corresponding to the segments $y = \text{const.}$ in the computational plane. In the end, this method permits one to find trapped modes as a function of a given frequency, rather than finding the frequencies at which trapped modes exists.

In the following of this section, some trapped modes associated to a geometry having an open cavity are presented. This cavity is defined by the following conformal mapping

$$Z = \Omega(z) = z - i\frac{a}{e^{iz} + b} + i\frac{a}{b} \ . \tag{3.25}$$

It is represented on fig. 3.5(c). The associated $\mathsf{\Gamma}$ matrix is defined by

$$\begin{aligned}
\Gamma_{n,m} =& \left(\frac{a(\frac{a}{b} - 4)\gamma^2}{b}(I_{n+m} + I_{n-m}) \right. \\
& \left. - \frac{a(1+\gamma^2)\gamma}{b}(I_{n+m+2} + I_{n-m+2} + I_{n+m-2} + I_{n-m-2}) \right) \\
& \times \frac{1}{\sqrt{1+\delta_{n,0}}\sqrt{1+\delta_{m,0}}} \ , \qquad (3.26) \\
I_m =& (-1)^{\frac{|m|}{2}} \gamma^{\frac{|m|}{2}+2} \ \frac{2 + \left(\frac{|m|}{2} + 1\right)\frac{1-\gamma^2}{\gamma^2}}{(1-\gamma^2)^3} \ , \qquad (3.27) \\
\gamma =& \frac{e^{-y}}{b} \ . \qquad (3.28)
\end{aligned}$$

On fig. 3.5(a) is represented the variation of the component $Y_{6,6}(y)$ of the admittance matrix depending on y for a value of $k = 2.1$. A quasi-singularity is present at $y_c = 0.0051$ (this abscissa is represented by the vertical dotted line). It corresponds to a very high value of one of its eigenvalue which is represented on fig. 3.5(b). The pressure field of the associated quasi-trapped mode is represented on fig. 3.6, in both physical and computational planes. The typical length scale of this quasi-trapped mode in the computational plane is very small as can be seen from fig. 3.6(b). For this reason an important number of evanescent modes must be taken into account in the calculation for the singularity to occur.

Figure 3.7 shows some various quasi-trapped modes corresponding to Dirichlet (quasi-singularities of Y) and to Neumann (quasi-singularities of Z) boundary conditions on $\mathcal{C}_0$.

We now briefly tackle the localization of the quasi-trapped modes. Still considering the same cavity geometry, fig 3.8 represents the modulus of the highest eigenvalue of the impedance matrix Z as a function of the frequency k and of the position y in the waveguide. Some singularities we can see on this figure are linked to the cutoff frequencies of

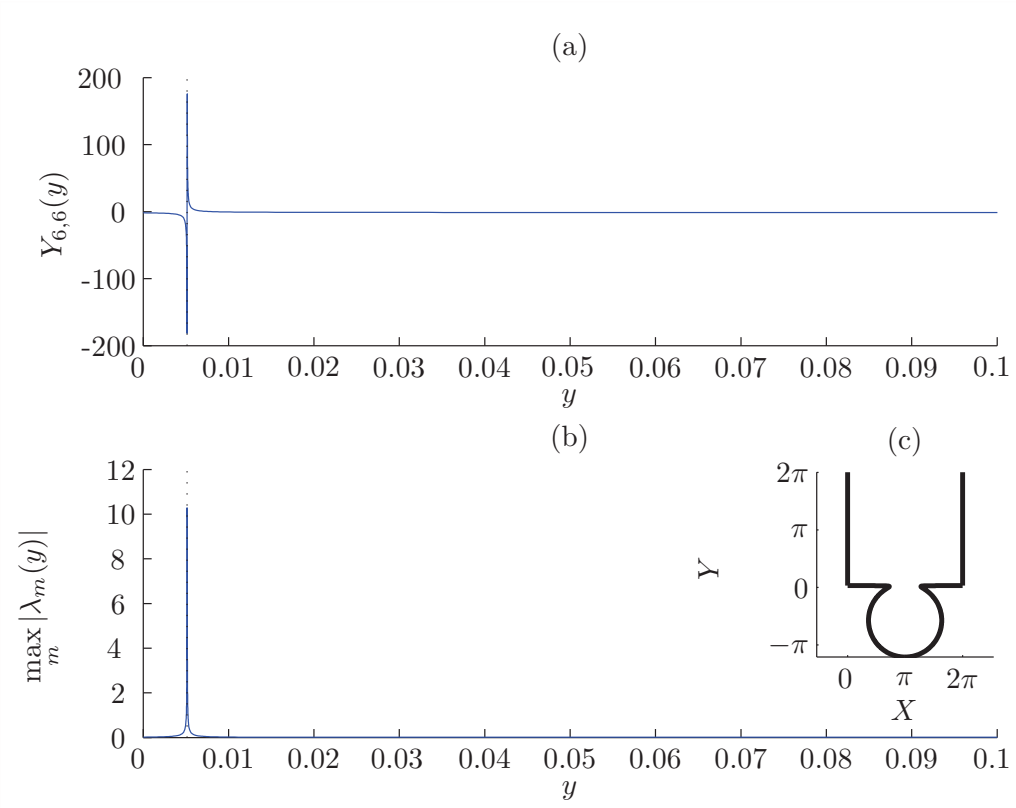

FIGURE 3.5 – Variation of the $Y_{6,6}$ component (a), and of the maximum $\max_m |\lambda_m(y)|$ of the eigenvalues (b) of the admittance matrix with $k = 2.1$ (6 propagative modes) for mapping (3.25) with values $a = 0.2$, $b = 1.05$. Geometry of the mapping (c).

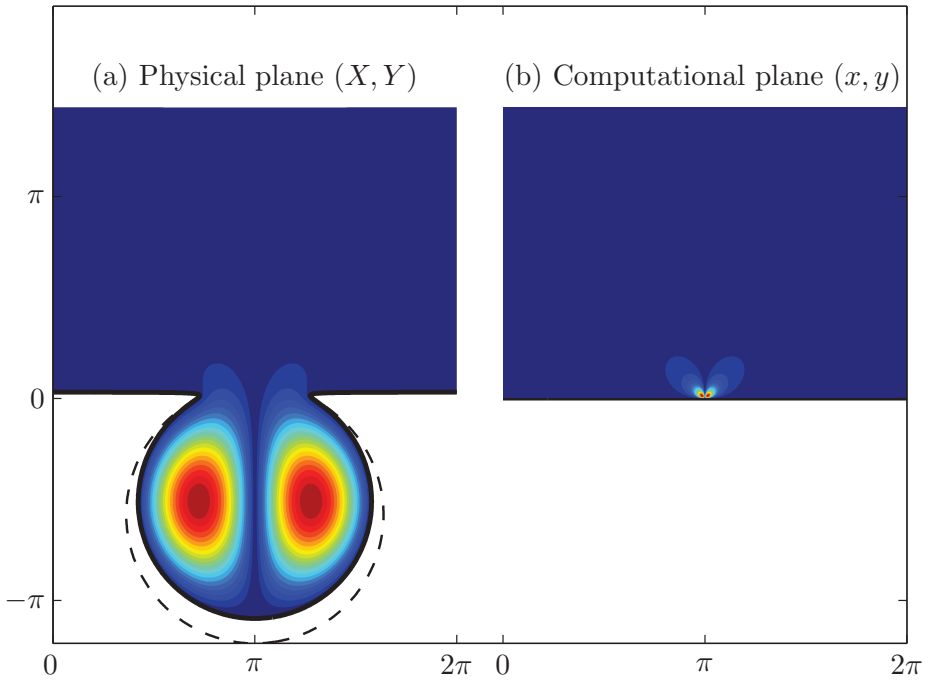

FIGURE 3.6 – Modulus of the pressure field in the physical plane $|p(X, Y)|$ (a), and in the computational plane $|p(x, y)|$ (b), of the quasi-trapped mode associated to the quasi-singularity of the admittance matrix Y at $y_c = 0.0051$. Same geometrical configuration as on fig. 3.5. The dashed line represents the boundary corresponding to $y = 0$.

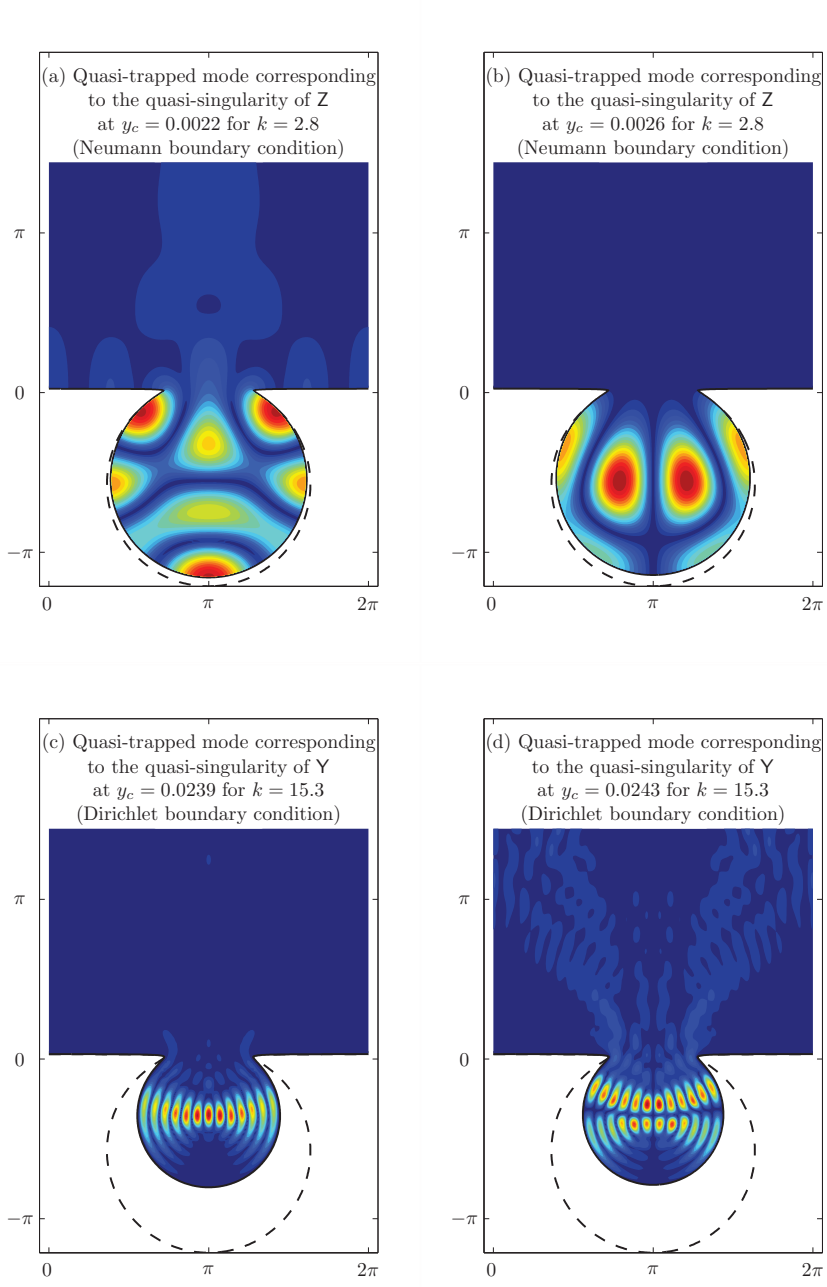

FIGURE 3.7 – Modulus of pressure field of some quasi-trapped modes associated to quasi-singularities of the impedance matrix Z (a-b), and to the admittance matrix Y (c-d). Same geometrical configuration as on fig. 3.5.

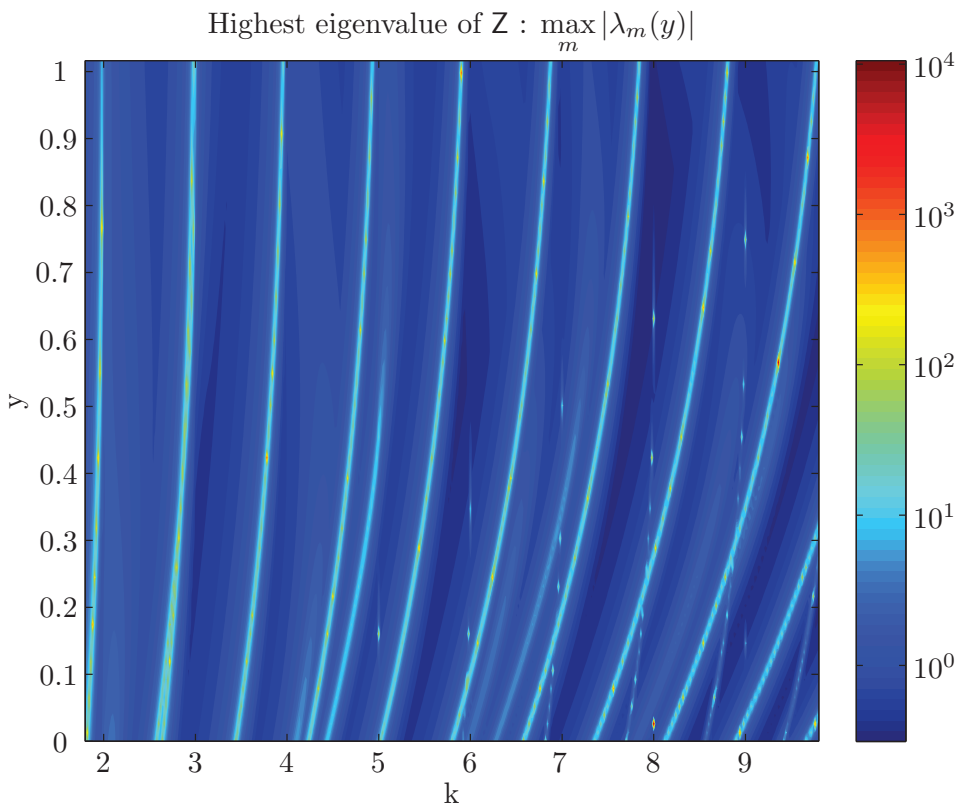

FIGURE 3.8 – Modulus of the highest eigenvalue of the impedance matrix Z as a function of the frequency k and of the position y in the waveguide. Same configuration (cavity) as on fig. 3.5(c).

the straight waveguide. The localization in terms of frequency of these singularities evolve depending on y. For high values of y, the conformal mapping, which tends to the identity, has an effect which tends to be null. As a consequence, the quasi-singularities tends to be true singularities localized at the cutoff frequencies of the waveguide. For small values of y, the effect of the conformal mapping is important. The quasi-singularities are then of finite amplitudes, their frequencies are moved as an effect of the conformal mapping, and they divide. The conformal mapping stretch out the boundary at $y = 0$ between the computational plane (x, y) and the physical plane (X, Y). The quasi-singularities are then moved to smaller values of the frequency k near the boundary at $y = 0$. The method presented in this section allows us to find a quasi-trapped mode at a given frequency when one of these quasi-singularities crosses the line $k = \text{Const.}$ on which we are looking. So, finding a quasi-trapped mode would be easier at frequencies close to the waveguide cutoff frequencies but strictly inferior. As an example, the two quasi-trapped modes presented on figures 3.7(a) et (b) correspond to quasi-singularities linked to the cutoff frequency $k = 3$ of the waveguide : the line $k = 2.8$ crosses these singularities at $y = 0.0022$ and $y = 0.0026$ (merged on this figure).

6 Wave reflected by a geometrically complex boundary in a semi-infinite free space

The method proposed earlier in this paper can be adapted to the reflection of a plane wave in a semi-infinite free space by a periodic geometrically complex boundary. We consider that the geometrically complex boundary is 2π–periodic. The incident field is taken under the form of a plane wave

$$p_{in} = e^{i\alpha X - i\beta Y} \ , \tag{3.29}$$

where

$$\beta = k^2 - \alpha^2 \ . \tag{3.30}$$

Assuming that the total field is quasi-periodic the problem to solve is

$$\Delta_X P + k^2 P = 0 \ , \tag{3.31a}$$

$$P(X, Y) = P(X + 2\pi, Y) e^{2i\pi\alpha} \ , \tag{3.31b}$$

$$\boldsymbol{\nabla}_X P \cdot \boldsymbol{n} = 0 \qquad \text{on } \mathcal{C}_0 \ , \tag{3.31c}$$

where $\mathcal{C}_0 = \{(X, Y) \mid X = U(s), Y = V(s)\}$ defines the boundary, and where U and V are 2π–periodic. Owing to the quasi-periodicity assumption, it only has to be solved on one period of the boundary in the X direction. Introducing the conformal mapping in the same manner as in Sec. 2, the reflected field on one period has to satisfy

$$\Delta_x p + k^2 V p = 0 \qquad \text{for } y \geqslant 0 \ , \tag{3.32a}$$

$$p(0, y) = p(2\pi, y) e^{2i\pi\alpha} \qquad \text{for } y \geqslant 0 \ , \tag{3.32b}$$

$$\frac{\partial p}{\partial y}(x, 0) = -\frac{\partial p_{in}}{\partial y}(x, 0) \qquad \text{at } y = 0 \ . \tag{3.32c}$$

The unknown reflected field p is decomposed as a Fourier series

$$p(x,y) = \sum_{m\in\mathbb{Z}} p_m(y)\varphi_m(x) \ , \tag{3.33}$$

where

$$\varphi_m(x) = \frac{e^{imx}}{\sqrt{2\pi}} e^{i\alpha x} \qquad m \in \mathbb{Z} \ . \tag{3.34}$$

This is the analog of Eq. (3.9) of Sec. 3, where the reflected field inside the waveguide is projected on the basis of the transverse eigenmodes. Indeed, Eq. (3.33) could also be viewed as the projection of the solution onto the transverse eigenmodes of the vertical waveguide with boundary condition of quasi-periodicity, which are precisely the φ_m of Eq. (3.34). Applying the multimodal method as in Sec. 3 leads to the same equation as Eq. (3.13), but where here and hereafter the matrices $\mathsf{\Gamma}$ and K are defined by

$$\Gamma_{n,m}(y) = \int_0^{2\pi} (V(x,y)-1)\overline{\varphi_n}(x)\varphi_m(x)\mathrm{d}\,x \ , \tag{3.35a}$$

$$K_{n,m} = \beta_n \delta_{n,m} \ . \tag{3.35b}$$

The $\mathsf{\Gamma}$ matrix corresponding to the mapping (3.22) projected on this new basis is given by

$$\begin{aligned}\Gamma_{n,m}(y) = &\sum_l l^2 e^{-2ly}|\omega_l|^2\delta_{n,m} \\ &+ \sum_l il e^{-ly}\Big(\omega_l\delta_{n-l,m} - \overline{\omega}_l\delta_{n+l,m}\Big) \\ &+ \sum_{l,r>l} lr e^{-(l+r)y}\Big(\omega_l\overline{\omega}_r\delta_{n-l+r,m} \\ &\qquad + \omega_r\overline{\omega}_l\delta_{n+l-r,m}\Big) \ ,\end{aligned} \tag{3.36}$$

Then, the equations satisfied by the admittance matrix Y are the same as Eqs. (3.17) and (3.18) where the matrices $\mathsf{\Gamma}$ and K have to be replaced by those given by Eq. (3.35). Therefore, Y can be computed using the same Magnus–Möbius scheme as previously. To compute the reflected field, the initial condition at $y = 0$ must be derived. It yields

$$\begin{aligned}q_m(0) = \frac{1}{\sqrt{2\pi}}\int_0^{2\pi} \Big[&- i\alpha\frac{\partial\Omega_R}{\partial y}(x) + i\beta\frac{\partial\Omega_I}{\partial y}(x)\Big] \\ &\times e^{i\alpha\Omega_R(x) - i\beta\Omega_I(x) - imx}\mathrm{d}\,x \ .\end{aligned} \tag{3.37}$$

Eventually, the reflected field can be fully computed.

Figure 3.9 shows the total pressure field due to an oblique incident wave reflected on a boundary having a crest. The boundary corresponds to the mapping (3.22) with the only one nonzero component $w_1 = -0.9i$. A shadowing phenomenon can be noticed at

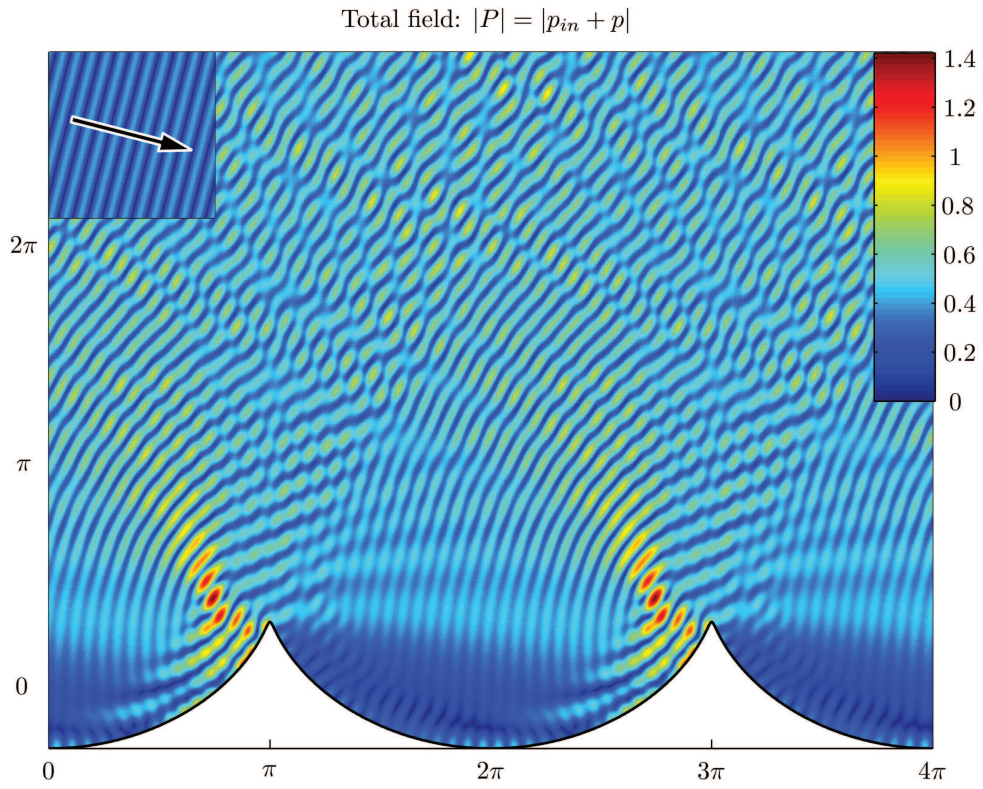

FIGURE 3.9 – Total field (modulus) $|P(X,Y)| = |p_{in} + p|$ for incident plane wave corresponding to $\alpha = 15$ with $k = 15.48$. Mapping (3.22) with $w_1 = -0.9i$. Inset : Modulus of real part of incident field $|\Re\{p_{in}\}|$ and direction of propagation (arrow).

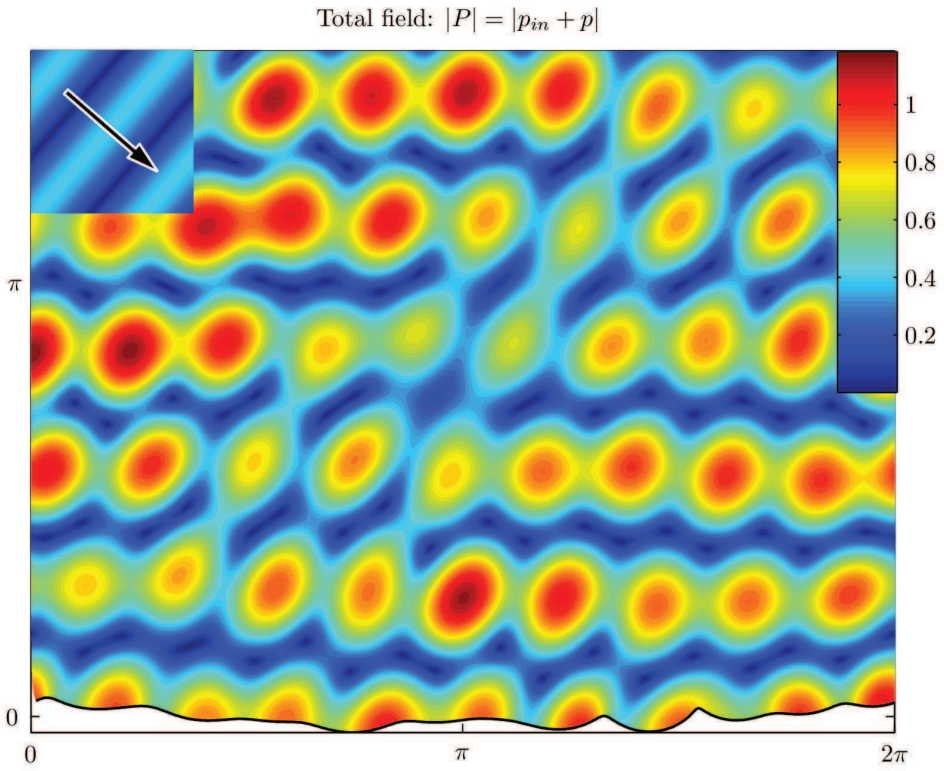

FIGURE 3.10 – Total field (modulus) $|P(X,Y)| = |p_{in} + p|$ for incident plane wave corresponding to $\alpha = 4$ with $k = 5.3$. Mapping (3.22) for a rough surface. Inset : Modulus of real part of incident field $|\Re\{p_{in}\}|$ and direction of propagation (arrow).

the right of the crest. The case of a rough surface obtained with the method proposed by Vandembroucq & Roux (1997*a*) is displayed on fig. 3.10.

The method described in Sec.5 can also be used here to find quasi-trapped modes. Indeed, fig. 3.11 represents a quasi-trapped found while using the same geometry as the one used on fig. 3.9. Note that in this case the quasi-trapped mode is in fact a stationary surface wave.

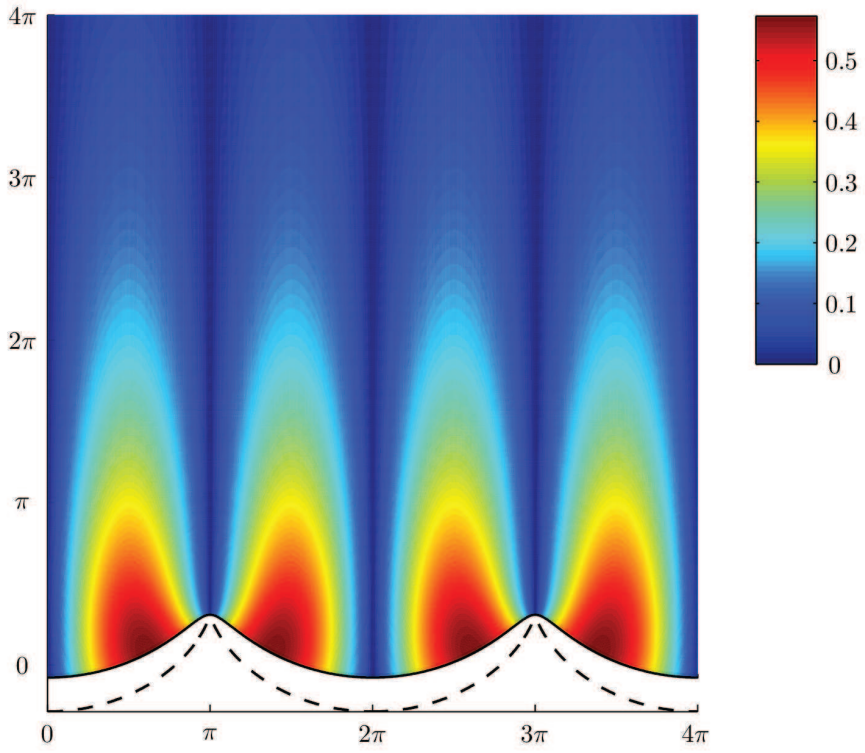

FIGURE 3.11 – Quasi-trapped mode associated to the singularity of Z at $y_c = 0.39$ for mapping (3.22) with $w_1 = -0.9i$.

7 Concluding remarks

A method to compute the pressure field associated to a wave reflected by a geometrically complex boundary has been developed. It has been applied to the case of a waveguide with a complex termination, and to a particular case of plane waves in free space. The method we proposed in this paper requires no assumption on the relative orders of the characteristic lengthscale of the boundary geometry and of the wavelength.

A method to find particular geometries having quasi-trapped modes has also been proposed, and some examples of quasi-trapped modes have been showed. The particularity of this method is that it provides the geometry having a quasi-trapped mode as a function of the frequency, instead of finding the frequencies at which a quasi-trapped mode exist inside a particular geometry Work is under progress to use this method to find traveling surface waves.

References

Battles, Z. & Trefethen, L. 2004 An extension of matlab to continuous functions and operators. *SIAM J. Sci. Comput.* **25**, 1743–1770. (doi: 10.1137/S1064827503430126)

Bi, W., Pagneux, V., Lafarge, D. & Auregan, Y. 2006 Modelling of sound propagation in a non-uniform lined duct using a multi-modal propagation method. *J. Sound Vibr.* **289**, 1091–1111. (doi: 10.1016/j.jsv.2005.03.021)

Bi, W., Pagneux, V., Lafarge, D. & Auregan, Y. 2007 An improved multimodal method for sound propagation in nonuniform lined ducts. *J. Acoust. Soc. Am.* **122**, 280–290. (doi: 10.1121/1.2736785)

Depine, R. A. & Simon, J. 1982 Diffraction grating efficiencies conformal mapping method for a good real conductor. *Opt Acta : Int. J.Opt.* **29**, 1459–1473. (doi: 10.1080/713820790)

Depine, R. A. & Simon, J. 1983 Surface impedance boundary condition for metallic diffraction gratings in the optical and infrared range. *Opt Acta : Int. J.Opt.* **30**, 313–322. (doi: 10.1080/713821187)

Felix, S. & Pagneux, V. 2001 Sound propagation in rigid bends : A multimodal approach. *J. Acoust. Soc. Am.* **110**, 1329–1337.

Felix, S. & Pagneux, V. 2002 Multimodal analysis of acoustic propagation in three-dimensional bends. *Wave Motion* **36**, 157–168. (doi: 10.1016/S0165-2125(02)00009-4)

Floryan, J. 1986 Conformal-mapping- based coordinate generation method for flows in periodic configurations. *J. Comput. Phys.* **62**, 221 – 247. (doi: 10.1016/0021-9991(86)90108-7)

Iserles, A., Marthinsen, A. & Nørsett, S. P. 1999 On the implementation of the method of magnus series for linear differential equations. *BIT* **39**, 281–304. (doi: 10.1023/A :1022393913721)

Iserles, A. & Norsett, S. P. 1999 On the solution of linear differential equations in lie group. *Phil. Trans. R. Soc. A* **357**, 983–1019.

Ogilvy, J. 1991 *Theory of wave scattering from random rough surfaces.* A. Hilger.

Pagneux, V. 2010 Multimodal admittance method in waveguides and singularity behavior at high frequencies. *J. Comp. Appl. Math.* **234**, 1834–1841. (doi: 10.1016/j.cam.2009.08.034)

Pagneux, V., Amir, N. & Kergomard, J. 1996 A study of wave propagation in varying cross-section waveguides by modal decomposition .1. theory and validation. *J. Acoust. Soc. Am.* **100**, 2034–2048. (doi: 10.1121/1.417913)

Sabina, F. J. & Babich, V. M. 2001 Low-frequency scattering of acoustic waves by a bounded rough surface in a half-plane. *J. Acoust. Soc. Am.* **109**, 878–885. (doi: 10.1121/1.1348297)

Schiff, J. & Shinider, S. 1999 A natural approach to the numerical integration of riccati differential equations. *SIAM J. Numer. Anal.* **36**, 1392–1413.

Takakura, Y. 1995 Rigorous integral approach to the problem of scattering from a modulated periodic medium obtained through conformal mapping. *J. Opt. Soc. Am. A* **12**, 1283–1289. (doi: 10.1364/JOSAA.12.001283)

Trefethen, L. N. *et al.* 2011 *Chebfun Version 4.2.* The Chebfun Development Team.

Vandembroucq, D. & Roux, S. 1997*a* Conformal mapping on rough boundaries. i. applications to harmonic problems. *Phys. Rev. E* **55**, 6171–6185. (doi: 10.1103/PhysRevE.55.6171)

Vandembroucq, D. & Roux, S. 1997*b* Conformal mapping on rough boundaries. ii. applications to biharmonic problems. *Phys. Rev. E* **55**, 6186–6196. (doi: 10.1103/PhysRevE.55.6186)

Voronovich, A. 1999 *Wave scattering from rough surfaces.* Springer series on wave phenomena. Springer.

4

Couche limite visqueuse d'un fluide oscillant à proximité d'une surface rigide de géométrie complexe

Dans le chapitre précédent, nous avons exposé une méthode pour calculer le champ de pression correspondant à une onde réfléchie par une surface de géométrie complexe. Dans le chapitre qui suit, en vue de l'étude de l'effet de la couche limite visco-thermique sur l'onde acoustique, nous appliquons la même démarche pour modéliser la couche limite visqueuse d'un fluide incompressible oscillant à proximité d'une paroi de géométrie complexe périodique selon x. Nous considérons le problème sous la formulation vorticité–fonction de courant. Nous y appliquons une transformation conforme et décomposons les inconnues en séries de Fourier selon x. En introduisant une matrice d'impédance reliant la vorticité à sa dérivée selon y, il est alors possible d'obtenir une équation de Riccati, comparable à celle obtenue dans le chapitre précédent (équation (3.17)), qui régie l'évolution de cette matrice d'impédance selon y. Cette dernière équation peut être résolue par un schéma de Magnus–Möbius comme précédemment. Nous explorons au moyen de cette méthode les différentes géométries que nous avons déjà considérées dans le chapitre précédent, à savoir une cavité (figure 3.7), une crête (figure 3.9), et une surface rugueuse (figure 3.10). Nous mettons en évidence l'existence de zones de recirculation.

Dans le cas de la transformation conforme proposée par Vandembroucq & Roux (1997*a*), que nous avons déjà utilisée pour modéliser la crête ainsi que la surface rugueuse, les équations et les conditions limites que satisfont les coefficients des séries de Fourier

revêtent une forme relativement simple. Pour le cas simple de la géométrie en forme de crête, où la transformation conforme ne comporte qu'un seul terme, nous proposons une méthode perturbative qui permet de résoudre le problème analytiquement. Cette solution analytique est en parfait accord avec la solution numérique. Par ailleurs, elle nous donne des indications sur la convergence de la méthode numérique.

Ce chapitre est lui aussi présenté sous la forme d'un article en langue anglaise destiné à être soumis prochainement au *Journal of Fluid Mechanics*.

Viscous boundary layer of an incompressible oscillating fluid near a geometrically complex boundary by use of conformal mapping [1]

Abstract : The viscous boundary layer of an oscillating incompressible fluid (second Stokes problem) near a geometrically complex boundary is considered. This problem is first stated in the vorticity–stream function formulation. Then, the use of a conformal mapping transforms the geometrically complex boundary into a plane boundary, but it makes to appear varying coefficients in the bulk equations. These equations are then solved with a multimodal method. For a particular conformal mapping, a perturbative approach provides approximate solutions. The existence of recirculation areas for some boundary geometries is investigated.

1 Introduction

In this paper, the laminar Stokes boundary layer of an incompressible fluid oscillating near a periodic geometrically complex boundary in the small Reynolds number limit is considered. The term "geometrically complex boundary" is preferred here to "rough boundary" as the method proposed can embrace rough boundaries but can also consider more general boundaries. Many previous works on the subject of rough boundaries cannot take into account arbitrary roughness as they are based on asymptotic approaches (Lyne, 1971, Kaneko & Honji, 1979). The effect of a strong curvature on the vorticity distribution over the boundary, which has been studied by Pozrikidis (1993) using a Boundary Element Method, cannot be taken into account by such methods. The aim of this paper is to propose a multimodal approach based on the use of a conformal mapping. The effect of such a mapping is to map the complex geometry on a plane geometry. This moves the difficulty of applying the boundary condition on a complicated geometry into solving the bulk equations with varying coefficients. The main interest of the method we propose is to offer the possibility of an efficient numerical treatment, which can be used for any geometry, but also to open the possibility of an analytical perturbative resolution.

In Sec. 2 the governing equations are presented and the conformal mapping is applied to them. The proposed multimodal approach is exposed in Sec. 3. The most difficult part of the use of conformal mappings is to find the appropriate mapping corresponding to a given geometry. In Sec. 4 we focus on a particular mapping, proposed by Vandembroucq & Roux (1997*a*,*b*), which allows us to overcome this difficulty under some assumptions. The multimodal approach together with the rather simple expression of this mapping

1. To be submitted to *Journal of Fluid Mechanics*. Authors: Gael Favraud and Vincent Pagneux.

opens the possibility of an analytic treatment of the laminar Stokes boundary layer by a perturbative approach which is discussed in Sec.5. In Sec. 6, recirculation phenomena inside cavities are discussed as an application of the proposed method. Some concluding remarks are given in Sec. 7.

2 Governing equations

We wish to solve the second Stokes problem in presence of a geometrically complex boundary. We consider in the (X, Y) plane an incompressible viscous fluid oscillating in the X direction near a boundary of complex geometry which is supposed to be periodic in the X direction. Far from the boundary the flow is a uniformly oscillating flow $\boldsymbol{u}_\infty = U_0 \exp(i\sigma t)\boldsymbol{e}_X$, where σ is the time frequency of the oscillation. We consider that U_0 is small enough to neglect non linear terms in the governing equations. The vorticity created due to the presence of the boundary is localized in a boundary layer whose thickness is of order $\delta = \sqrt{\nu/\sigma}$ where ν is the kinematic viscosity of the flow. In this boundary layer, the problem to solve is the second Stokes problem *i.e.* an incompressible viscous flow in contact of a wall. It is governed by the linearized unstationary Stokes equations in harmonic regime

$$\boldsymbol{\nabla}_X \cdot \boldsymbol{u} = 0 \ , \tag{4.1a}$$

$$i\sigma \boldsymbol{u} = -\frac{1}{\rho}\boldsymbol{\nabla}_X p + \nu \boldsymbol{\nabla}_X^2 \boldsymbol{u} \ , \tag{4.1b}$$

where $\boldsymbol{\nabla}_X$ is the gradient operator with respect to the X and Y variables. Because far from the wall the flow tends to be the uniformly oscillating flow mentioned before, it has to satisfy the boundary condition

$$\boldsymbol{u} \to U_\infty \boldsymbol{e}_X \qquad \text{for } Y \to +\infty \ . \tag{4.2}$$

The second boundary condition needed to obtain a well posed problem is that the flow is null at the wall. This wall is periodic in the X direction. For convenience, we supposed that the distances are non-dimensionalized in such way that the periodicity of the wall is of 2π. Consequently, we suppose that the flow is also 2π–periodic, so that the problem is solved on one period only. The wall is described as a curve $\mathcal{C}_0 = \{(X, Y)/X = \zeta_X(s), Y = \zeta_Y(s), s \in [0, 2\pi]\}$. We also suppose that the two real functions ζ_X and ζ_Y are differentiable. Therefore the second boundary condition is

$$\boldsymbol{u}(X, Y) = \boldsymbol{0} \qquad \text{for } (X, Y) \in \mathcal{C}_0 \ . \tag{4.3}$$

We state this problem in the vorticity — stream function formulation (ω — ψ) by writing

$$\omega = (\boldsymbol{\nabla}_X \times \boldsymbol{u}) \cdot \boldsymbol{e}_z \ , \qquad \boldsymbol{u} = \boldsymbol{\nabla}_X \times (\psi \boldsymbol{e}_z) \ . \tag{4.4}$$

It yields

$$\boldsymbol{\nabla}_X^2 \psi = -\omega \tag{4.5a}$$

$$\boldsymbol{\nabla}_X^2 \omega = \lambda_0^2 \omega \ , \tag{4.5b}$$

where $\lambda_0 = \sqrt{i/\delta^2}$. The boundary conditions become

$$\left.\begin{aligned} \omega &\longrightarrow 0 \\ \frac{\partial \psi}{\partial Y} &\longrightarrow U_\infty \\ \frac{\partial \psi}{\partial X} &\longrightarrow 0 \end{aligned}\right\} \qquad \text{for } Y \to +\infty \ , \tag{4.6a}$$

$$\frac{\partial \psi}{\partial Y} = \frac{\partial \psi}{\partial X} = 0 \qquad \text{for } (X,Y) \in \mathcal{C}_0 \ . \tag{4.6b}$$

The main difficulty comes from the second boundary condition (4.6b) (imposing a Neumann boundary condition on a complex geometry) and is the reason why we introduce conformal mappings.

Conformal mappings allows us to map the physical domain $\mathcal{E}$ in which is posed the original problem (4.5,4.6) to a computational domain $\mathcal{D}$ in which the problem to solve is more convenient. The interests of conformal mappings are twice. The first one is that it maps the geometrically complex boundary condition at the wall to another simpler boundary condition on a straight boundary. By choosing a mapping which tends to the identity for $Y \to +\infty$ the other boundary condition remains unchanged. The second interest is that it transforms the Laplacian operator into another Laplacian operator multiplied by the modulus of the complex derivative of the mapping function. Therefore, the effect of the geometry of the wall is no more expressed by the boundary condition, but inside the bulk equations by adding space varying coefficients. Namely, we introduce new variables x, y and the mapping function

$$w : \begin{array}{c} \mathcal{D} \mapsto \mathcal{E} \\ z = x + iy \mapsto w(z) = X + iY \ . \end{array} \tag{4.7}$$

The function w is analytical on the domain $\mathcal{D} = \{(x,y) | 0 \leq x \leq 2\pi, 0 \leq y\}$. We impose two restrictions on w. The first one is that it maps the straight boundary $y = 0$ in the computational domain to the rough boundary $\mathcal{C}_0$ in the physical domain. The second one is that it tends to the identity for $y \to +\infty$, such that the boundary condition at infinity is preserved. It is also supposed that it is a bijection from $\mathcal{D}$ into $\mathcal{E}$. As mentioned before, the effect of the mapping on the equations is to transform the Laplacian into another Laplacian :

$$\boldsymbol{\nabla}_X^2 = \left| \frac{\mathrm{d}\, z}{\mathrm{d}\, w} \right|^2 \boldsymbol{\nabla}_x^2 \ , \tag{4.8}$$

where $\boldsymbol{\nabla}_x$ is the gradient with respect to the x and y variables. Consequently, if we define

$$V(x,y) = \left| \frac{\mathrm{d}\, w}{\mathrm{d}\, z} \right|^2 \ , \tag{4.9}$$

the original problem (4.5,4.6) is equivalent to

$$\boldsymbol{\nabla}_x^2 \psi = -V\omega \tag{4.10a}$$

$$\boldsymbol{\nabla}_x^2 \omega = \lambda_0^2 V \omega \tag{4.10b}$$

$$\left.\begin{aligned} \omega &\longrightarrow 0 \\ \frac{\partial \psi}{\partial y} &\longrightarrow U_\infty \\ \frac{\partial \psi}{\partial x} &\longrightarrow 0 \end{aligned}\right\} \qquad \text{for } y \to +\infty \ , \tag{4.11a}$$

$$\frac{\partial \psi}{\partial y} = \frac{\partial \psi}{\partial x} = 0 \qquad \text{at } y = 0 \ . \tag{4.11b}$$

This problem can be written in a simpler form by introducing the function

$$g = \psi - U_0 y + \frac{1}{\lambda_0^2}\omega \ . \tag{4.12}$$

Indeed, Eqs. (4.10,4.11) finally reduce to

$$\boldsymbol{\nabla}_x^2 g = 0 \ , \tag{4.13a}$$

$$\boldsymbol{\nabla}_x^2 \omega - \lambda_0^2 \omega = \lambda_0^2 (V-1)\omega \ , \tag{4.13b}$$

$$\left.\begin{aligned} \omega &\longrightarrow 0 \\ \frac{\partial g}{\partial x} &\longrightarrow 0 \\ \frac{\partial g}{\partial y} &\longrightarrow 0 \end{aligned}\right\} \qquad \text{for } y \to +\infty \ , \tag{4.14a}$$

$$\left.\begin{aligned} \frac{\partial g}{\partial x} &= \frac{1}{\lambda_0^2}\frac{\partial \omega}{\partial x} \\ \frac{\partial g}{\partial y} &= \frac{1}{\lambda_0^2}\frac{\partial \omega}{\partial y} - U_0 \end{aligned}\right\} \qquad \text{at } y = 0 \ . \tag{4.14b}$$

In the end, the effect of the mapping is to add the spatially varying right hand side term $\lambda_0^2(V(x,y)-1)$. This term vanishes at infinity as the mapping tends to the identity (and so $V(x,y)$ tends to 1).

3 Multimodal resolution

The method proposed to solve problem (4.13,4.14) is inspired by the multimodal method used to solve the Helmholtz equation in acoustical waveguides and developed by Pagneux (Pagneux *et al.*, 1996, Pagneux, 2010). It relies on the projection of the governing equations onto the transverse rigid eigenmodes of the waveguide. Note that problem (4.13,4.14) could be view as a waveguide in the y direction with boundary

condition of periodicity on the side walls. Here, we decompose the unknowns ω and g as Fourier series

$$g(x,y) = \sum_{m=-\infty}^{+\infty} g_m(y) e_m(x) \ , \tag{4.15}$$

$$\omega(x,y) = \sum_{m=-\infty}^{+\infty} \omega_m(y) e_m(x) \ , \tag{4.16}$$

where

$$e_m(x) = \frac{1}{\sqrt{2\pi}} e^{imx} \ . \tag{4.17}$$

The projection of Eq.(4.13) onto the base of the e_m yields

$$g_n'' - n^2 g_n = 0 \ , \tag{4.18a}$$

$$\omega_n'' - \lambda_n^2 \omega_n = \lambda_0^2 \sum_m \Gamma_{nm} \omega_m \ , \tag{4.18b}$$

where $\lambda_n^2 = \lambda_0^2 + n^2$, and where

$$\Gamma_{n,m}(y) = \int_{x=0}^{2\pi} (V(x,y) - 1) \overline{e_n}(x) e_m(x) \mathrm{d}\, x \ . \tag{4.19}$$

The general form of the g_n can directly be determined from Eq. (4.18a) and from the boundary condition at infinity (4.14a) :

$$g_n(y) = g_n(0) e^{-|n|y} \ . \tag{4.20}$$

Using (4.20), the projection of the boundary conditions (4.14b) at $y = 0$ gives

$$g_n(0) = \frac{\omega_n(0)}{\lambda_0^2} \ , \tag{4.21a}$$

$$|n| g_n(0) = -\frac{\omega_n'(0)}{\lambda_0^2} + U_0 \sqrt{2\pi} \delta_{n,0} \ . \tag{4.21b}$$

This fully determines the expression of the g_n in terms of the ω_n :

$$g_n(y) = \frac{\omega_n(0)}{\lambda_0^2} e^{-|n|y} \ . \tag{4.22}$$

To determine the ω_n we need to solve Eqs. (4.18b) and (4.21) that we write in the matrix form

$$\boldsymbol{\omega}'' - \mathsf{\Lambda}^2 \boldsymbol{\omega} = \lambda_0^2 \mathsf{\Gamma} \boldsymbol{\omega} \ , \tag{4.23a}$$

$$\boldsymbol{\omega}'(0) + \mathsf{N} \boldsymbol{\omega}(0) = -\lambda_0^2 U_\infty \sqrt{2\pi} \boldsymbol{e_0} \qquad \text{at } y = 0 \ , \tag{4.23b}$$

$$\boldsymbol{\omega} \to \mathbf{0} \qquad \text{for } y \to \infty \ , \tag{4.23c}$$

where $\boldsymbol{\omega}(y) = (\omega_m(y))_m$, $\mathsf{\Gamma}(y) = (\Gamma_{n,m}(y))_{n,m}$, $\mathsf{\Lambda} = (\lambda_n \delta_{n,m})_{n,m}$, $\mathsf{N} = (|n|\delta_{n,m})_{n,m}$ and $\boldsymbol{e_0} = (\delta_{n,0})_n$. This problem cannot be directly solved numerically for two reasons. The first one is that this equation is not numerically stable because of the presence of evanescent modes which are responsible for exponential divergence of the error (Pagneux *et al.*, 1996). The second reason is that the problem is posed as a boundary value problem, with boundary conditions being imposed at two opposite boundaries. So it cannot be integrated as an initial value problem. For these two reasons, following the multimodal method, we introduce the admittance matrix Y linking $\boldsymbol{\omega}$ and its derivative by the relation

$$\boldsymbol{\omega}' = \mathsf{Y}\boldsymbol{\omega} \ . \tag{4.24}$$

This can be viewed as a matrix equivalent of the Dirichlet to Neumann operator. Then, Eq. (4.23a) is equivalent to the Riccati equation

$$\mathsf{Y}' = -\mathsf{Y}^2 + \mathsf{\Lambda}^2 + \lambda_0^2 \mathsf{\Gamma} \ . \tag{4.25}$$

This latter ordinary differential equation of order 1 can be integrated as an initial value problem with only one initial condition. This initial condition has to be taken at $y = \infty$ to impose the direction of the decay of the evanescent modes. As the mapping tends to the identity, infinitely far from the wall we have $\mathsf{Y}' = \mathsf{\Gamma} = \mathsf{0}$. Therefore Eq. (4.25) with Eq. (4.14a) imply the initial condition

$$\mathsf{Y} = -\mathsf{\Lambda} \qquad \text{for } y \to +\infty \ . \tag{4.26}$$

The Riccati equation (4.25) is known to possess movable singularities in the complex plane (Schiff & Shinider, 1999). For this reason, it is integrated with a Magnus-Möbius scheme (Iserles *et al.*, 1999, Pagneux, 2010). It is based on the Möbius scheme which permits us to integrate such an equation even through (true) singularities (Schiff & Shinider, 1999). The details of the scheme at orders 2 and 4 are given by Pagneux (2010). The admittance matrix Y is computed from the infinite end of the guide to the wall at $y = 0$. Then, the resolvent operator obtained numerically form the integration of Y is used to compute the vorticity $\boldsymbol{\omega}$ in the opposite direction. The initial condition used to compute $\boldsymbol{\omega}$ is obtained from (4.23b) and from the definition of Y. It yields

$$\boldsymbol{\omega}(0) = -\lambda_0^2 U_\infty \sqrt{2\pi} \Big(\mathsf{Y}(0) + \mathsf{N} \Big)^{-1} \boldsymbol{e_0} \ . \tag{4.27}$$

In practice, the infinite series (4.15) has to be truncated. The number of modes (component of the Fourier series) must be sufficiently high for the solution to converge. The convergence depends on the value of λ_0 and on the mapping used. A good method to check the convergence is to compare the results of two different computations with a different number of modes (Pagneux *et al.*, 1996). If these two results have no significant differences, then the code has converged. Looking at the relative amplitudes of the last modes of the truncation in comparison to the other modes may also give important information on the convergence (they should be small if the code has converged). The integration of Y is done from a sufficiently large distance L such that we can assume

$(x, y) \simeq (X, Y)$ so that $\Gamma \simeq 0$. Then the initial condition (4.26) is used at $Y = L$. This can be done since the mapping is supposed to tend to the identity at infinity. In the following of this paper, the considered mappings tend exponentially to the identity.

4 A general mapping based on Fourier series

The most challenging step of the method proposed in this paper is to find the mapping suitable for a given geometry. Vandembroucq & Roux (1997*a*,*b*) proposed a method to find an appropriate mapping to a particular geometry provided this geometry fulfills certain assumptions. The mapping he proposed is defined by

$$w(z) = z + \sum_{m=1}^{N} w_m e^{imz} \ . \tag{4.28}$$

It is composed of the sum of the identity function and of a Fourier series which decays exponentially as $y \to \infty$. It can be applied on a boundary which can be described by $\mathcal{C}_0 = \{(X, Y) \mid Y = h(X), X \in [0, 2\pi]\}$. An iterative procedure to determine the w_m coefficients is given by Vandembroucq & Roux (1997*a*) provided $|h'(x)| \leqslant 1$.

The Γ matrix corresponding to the mapping (4.28) is given by

$$\begin{aligned}\Gamma_{n,m}(y) = &\sum_{l} |w_l|^2 \delta_{n,m} l^2 e^{-2ly} + \sum_{l} \Big(w_l \delta_{n-l,m} - \overline{w_l} \delta_{n+l,m} \Big) i l e^{-ly} \\ &+ \sum_{l,r>l} \Big(w_l \overline{w_r} \delta_{n-l+r,m} + w_r \overline{w_l} \delta_{n+l-r,m} \Big) l r e^{-(l+r)y} \ .\end{aligned} \tag{4.29}$$

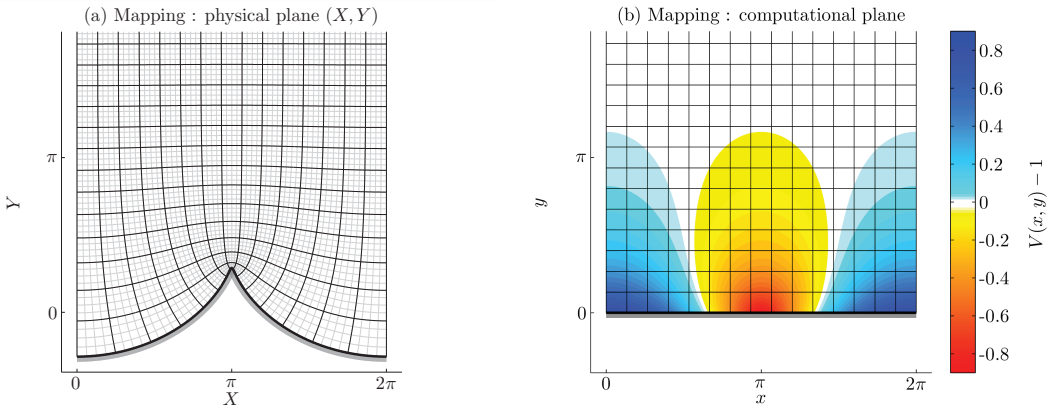

FIGURE 4.1 – Geometry defined by mapping (4.28) with only one non-zero component $w_1 = -0.9i$ in the physical plane (a). Value of the additional term $V(x, y) - 1$ added by the mapping in the computational plane (b).

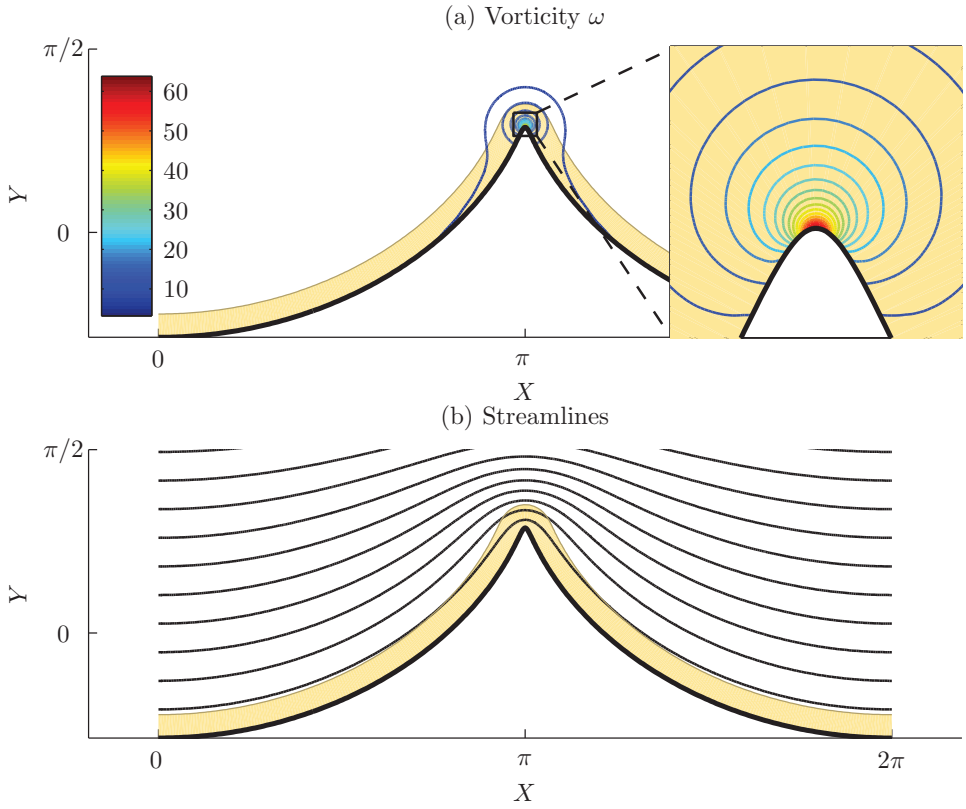

FIGURE 4.2 – Vorticity contours (a) and streamlines (b) of geometry defined by mapping (4.28) with only one non-zero component $w_1 = -0.9i$ for $\delta = 0.2$. The width δ of the boundary layer is represented by the coloured area.

As an example, fig. 4.1(a) shows the geometry corresponding to the mapping (4.28) having only one Fourier component $w_1 = -0.9i$. This geometry corresponds to a crest. Note that in the case of only one Fourier component, for the mapping to be a bijection, w_1 has to satisfy $|w_1| \leqslant 1$. The effect of the mapping on the equations, that is the term $(V-1)$, is represented on figure 4.1(b). The vorticity contours and streamlines obtained by our method are shown on figure 4.2. It can be noticed that the vorticity is concentrated near the crest and that the streamlines become closer to each others at this place.

On fig. 4.3 the streamlines patterns for a rough geometry are represented for different time steps. The geometry is modeled with the mapping (4.28). The coefficients of the mapping has been obtained with the method proposed by Vandembroucq & Roux (1997*a*). It can noticed that recirculation areas are created due to the roughness of the boundary. They are then convected toward the upper part of the flow and disappear.

5 Analytical perturbative approach

A particularity of the mapping (4.28) is that the solution of the Riccati equation (4.31) can be approximated analytically. The case where there is only one component in the Fourier series of the mapping (4.28) is considered. In this case, the mapping (4.28) reduces to

$$w(z) = z - iae^{iz} \ . \tag{4.30}$$

The Γ matrix then takes the form

$$\Gamma_{n,m}(y) = a^2 e^{-2y}\delta_{n,m} + ae^{-y}(\delta_{n,m-1} + \delta_{n,m+1}) \ .$$

Therefore, the equation (4.23a) that the ω_n has to satisfy becomes

$$\omega_n'' - \lambda_n^2\omega_n = \lambda_0^2 a^2 e^{-2y}\omega_n + \lambda_0^2 ae^{-y}(\omega_{n-1} + \omega_{n+1}) \ , \tag{4.31}$$

with initial condition

$$\omega_n'(0) + |n|\omega_n(0) = \lambda_0^2 U_0\sqrt{2\pi}\delta_{n,0} \ . \tag{4.32}$$

The basic idea is to solve this equation using a perturbative approach based on the parameter a, supposed to be small. The components of the $\boldsymbol{\omega}$ vector are sought under the form of the power series

$$\omega_n = \omega_{n,0} + a\omega_{n,1} + a^2\omega_{n,2} + \dots \ . \tag{4.33}$$

Injecting this power series and identifying terms of same order in a in Eq. (4.31) yields the recursive equation

$$\omega_{n,m}'' - \lambda_n^2\omega_{n,m} = \omega_{n,m-2}\lambda_0^2 e^{-2y} + (\omega_{n-1,m-1} + \omega_{n+1,m-1})\lambda_0^2 e^{-y} \ , \tag{4.34}$$

while the initial condition (4.32) becomes

$$\omega_{n,0}'(0) + |n|\omega_{n,0}(0) = \lambda_0^2 U_0\sqrt{2\pi}\delta_{n,0} \ , \tag{4.35a}$$

$$\omega_{n,m}'(0) + |n|\omega_{n,m}(0) = 0 \qquad \text{for } m \neq 0 \ . \tag{4.35b}$$

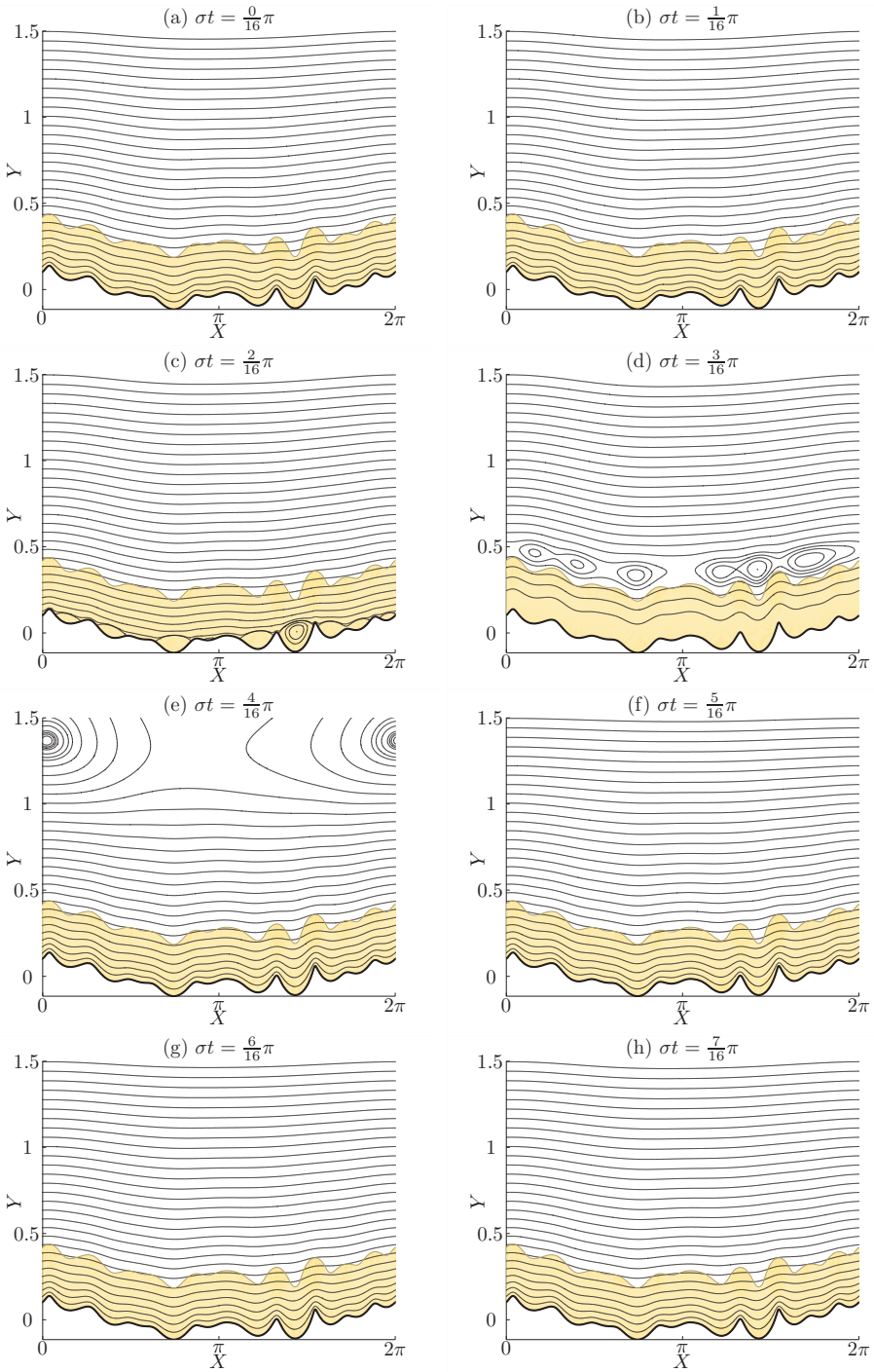

FIGURE 4.3 – Streamlines patterns for a rough geometry modeled with mapping (4.28) at different time steps from $\sigma t = 0$ (a) to $\sigma t = 7\pi/16$ (h). The boundary layer width $\delta = 0.3$ is represented by the coloured area.

Thanks to the structure of Eqs. (4.34) and (4.35) the process is simplified in several ways. The first thing to notice is that at order 0, the only term which is non zero is $\omega_{0,0}$. Indeed solving Eqs. (4.34) and (4.35a) at order 0 gives

$$\omega_{0,0} = -\lambda_0 U_0 \sqrt{2\pi}\, e^{-\lambda_0 y} \ , \tag{4.36a}$$

$$\omega_{n,0} = 0 \qquad \forall n \neq 0 \ . \tag{4.36b}$$

The second thing to notice is that each term $\omega_{n,m}$ depends only on $\omega_{n,m-2}$ and $\omega_{n\pm1,m-1}$, so that all terms are recursively generated with $\omega_{0,0}$ being the source term. Solving this problem eventually yields that the only other non zero terms are

$$\omega_{n,n+2m} = \sum_{j=0}^{m} \sum_{l=0}^{n+m-j} C_{n,m,j,l} e^{-(\lambda_l - l + n + 2(m-j))y} \tag{4.37a}$$

$$\omega_{-n,n+2m} = \omega_{n,n+2m} \ , \tag{4.37b}$$

where $n \geqslant 0$, $m \geqslant 0$ and where the coefficients $C_{n,m,j,l}$ are given by

$$\begin{matrix} 0 \leq j \leq m-1 \\ 0 \leq l \leq n+m-j-1 \end{matrix} \quad C_{n,m,j,l} = \frac{\lambda_0^2 (C_{n,m-1,j,l} + C_{n+1,m-1,j,l} + C_{n-1,m,j,l})}{(\lambda_l - l + n + 2(m-j))^2 - \lambda_n^2} \tag{4.38}$$

$$\begin{matrix} 0 \leq j \leq m-1 \\ l = n+m-j \end{matrix} \quad C_{n,m,j,n+m-j} = \frac{\lambda_0^2 C_{n+1,m-1,j,n+m-j}}{(\lambda_{n+m-j} + m - j)^2 - \lambda_n^2} \tag{4.39}$$

$$\begin{matrix} j = m \\ 0 \leq l \leq n-1 \end{matrix} \quad C_{n,m,m,l} = \frac{\lambda_0^2 C_{n-1,m,m,l}}{(\lambda_l - l + n)^2 - \lambda_n^2} \tag{4.40}$$

$$\begin{matrix} j = m \\ l = n \end{matrix} \quad C_{n,m,m,n} = -\sum_{\tilde{j}=0}^{m} \sum_{\substack{\tilde{l}=0 \\ (\tilde{j},\tilde{l}) \neq (m,n)}}^{n+m-\tilde{j}} \frac{\lambda_{\tilde{l}} - \tilde{l} + 2(m-\tilde{j})}{\lambda_n - n} C_{n,m,\tilde{j},\tilde{l}} \ . \tag{4.41}$$

It is worth noting that this perturbative solution also shows that the contribution of a mode m is of order $O(a^{|m|})$.

Figure 4.4 shows the vorticity contours and streamlines in the same configuration as the one used for the numerical result displayed on figure 4.2. This shows a very good agreement despite the value of $a = 0.9$ being very close to 1.

Whereas the calculations would rapidly become fastidious, and the final solution more complicated, the same king of treatment may be applied in the general case where there are an arbitrary number of Fourier components in the mapping (4.37).

6 Recirculation phenomenon inside cavities

In this section, as an example of application of our method, the existence of recirculation phenomena is investigated in a particular geometry. These recirculations are similar to Moffatt eddies of stationary Stokes flows, except that here the fluid is oscillating (Moffatt, 1964). The mapping considered in the following is defined by

$$w(z) = z - \frac{ia}{e^{iz} + b} + i\frac{a}{b} \ . \tag{4.42}$$

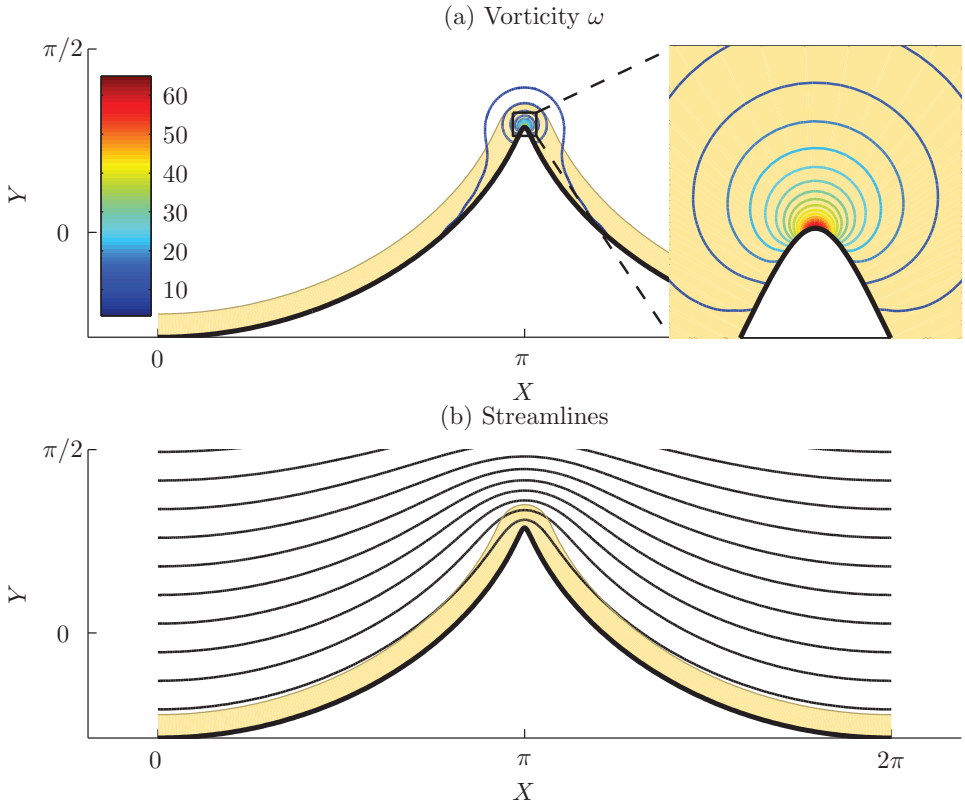

FIGURE 4.4 – Vorticity contours (a) and streamlines (b) for the geometry defined by mapping (4.28) computed with the analytical perturbative solution (4.37) (same configuration as figure 4.2). Terms $\omega_{n,m}$ from order $m = 0$ to 30 where considered (*i.e.* 31 modes are considered).

It corresponds to an almost plane wall having a cavity. It is represented on figure 4.5. Note that because of the symmetry of the problem it is possible to decompose the functions g and ω on the base of the

$$\varphi_m(x) = \frac{1}{\sqrt{\pi(1+\delta_{m,0})}} \cos(mx) \ , \tag{4.43}$$

with $m \in \mathbb{N}$ instead of using the exponentials with $m \in \mathbb{Z}$.

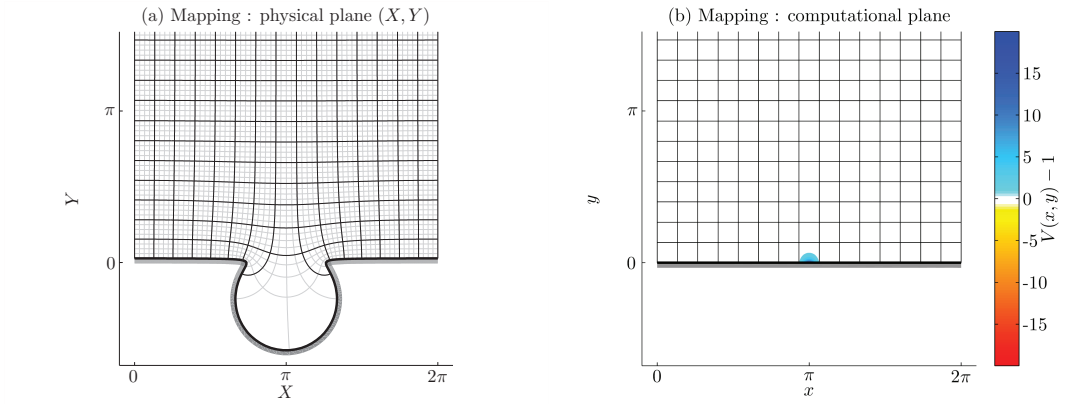

FIGURE 4.5 – Representation of mapping (4.42) with values $a = 0.2$ and $b = 1.1$. (a) Actual shape in the physical plane. (b) Computational plane. The colour map represents $\log|\frac{\mathrm{d}\,w}{\mathrm{d}\,z}|$.

The coefficients of the Γ matrix corresponding to this mapping and to this new basis are given by

$$\begin{aligned}\Gamma_{n,m} =&\left(\frac{a(\frac{a}{b}-4)\alpha^2}{b}(I_{n+m}+I_{n-m})\right.\\ &\left.-\frac{a(1+\alpha^2)\alpha}{b}(I_{n+m+2}+I_{n-m+2}+I_{n+m-2}+I_{n-m-2})\right)\\ &\times\frac{1}{\sqrt{1+\delta_{n,0}}\sqrt{1+\delta_{m,0}}} \qquad (4.44)\\ I_m =&(-1)^{\frac{|m|}{2}}\alpha^{\frac{|m|}{2}+2}\,\frac{2+\left(\frac{|m|}{2}+1\right)\frac{1-\alpha^2}{\alpha^2}}{(1-\alpha^2)^3} \qquad (4.45)\\ \alpha =&\frac{e^{-y}}{b} \qquad (4.46)\end{aligned}$$

The streamlines obtained are displayed on figure 4.6 for values varying between $\delta = 0.1$ and $\delta = 0.4$. For $\delta = 0.1$, on figure 4.6(a), the streamlines follows the boundary with accuracy. But starting from $\delta = 0.2$ two recirculation areas appear near the wall on the left and on the right of the cavity. As δ grows, the two recirculation areas become wider and wider, and merge into one recirculation centered inside the cavity. Eventually, for values of $\delta \geq 4$, the recirculation occupy the whole cavity, and the flow barely enter the cavity.

7 Concluding remarks

We proposed a modal method based on a conformal mapping to compute the boundary layer of an incompressible viscous flow in presence of a geometrically complex boundary. Recirculation phenomena inside cavities has been exposed as an application of our approach. A method proposed by Vandembroucq & Roux (1997*a*,*b*) gives the possibility of finding the appropriate mapping to a particular geometry under some assumptions. This particular mapping, permits us to obtain numerical results as well as analytical results based on a perturbative approach.

It is worth noting that Eqs. (4.1a) are those which describe the viscous boundary layer that would generate an acoustic wave grazing a wall with complex geometry, in the limit where the wavelength is big compared to the length scale of the boundary geometry and of the boundary layer. An interesting development in the future would be the study of such an acoustic wave taking into account this boundary layer. The fact that recirculations can exist in such configurations, as shown in section 6, could be of important consequences to acoustic waves. For instance, the attenuation of on acoustic wave due to a the boundary layer near a rough boundary may strongly be affected by the presence of recirculations. An investigation of these effects could constitute a sequel to this work.

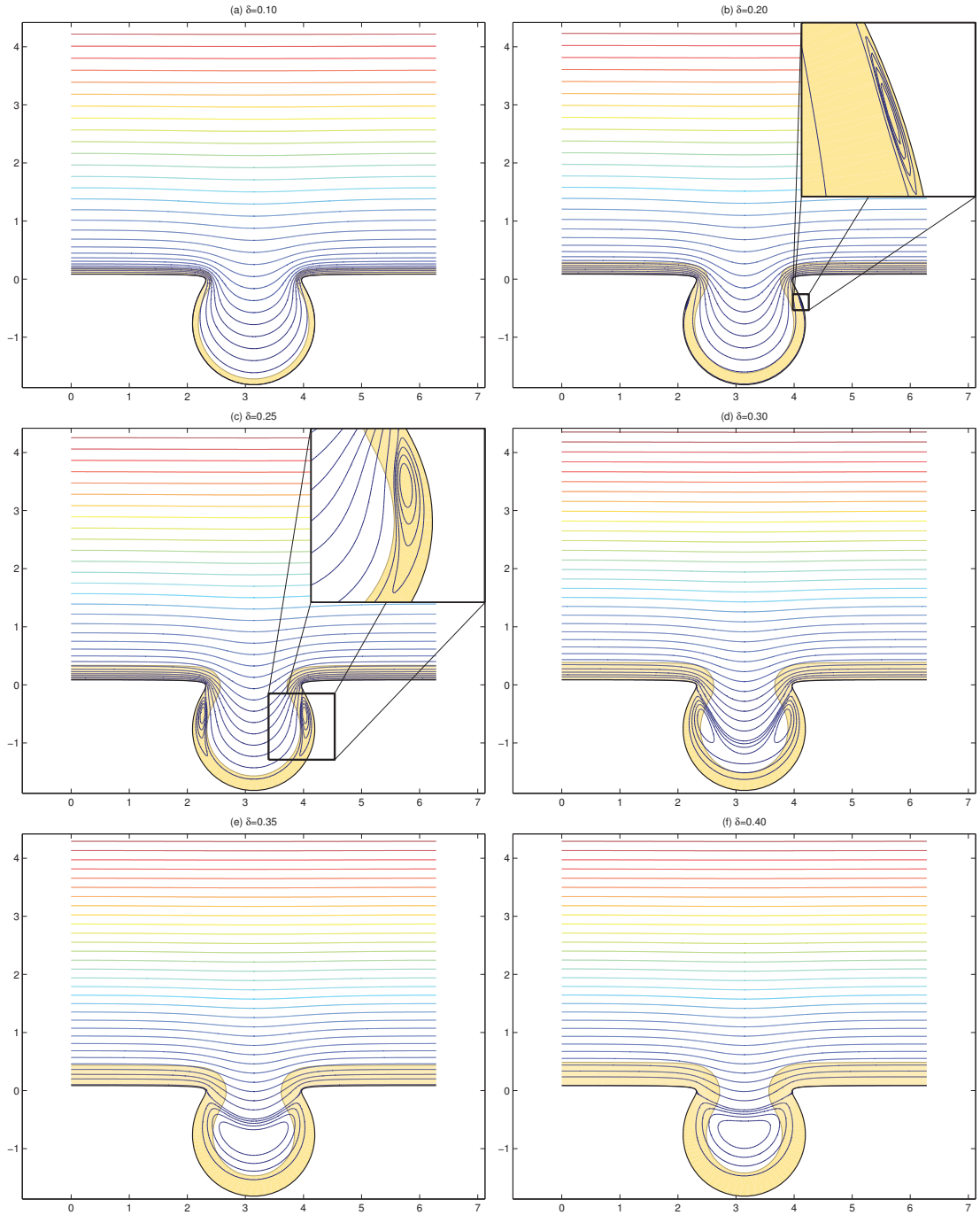

FIGURE 4.6 – Streamlines corresponding to the mapping (4.42) for different values of the boundary layer width δ, $\delta = 0.1$ (a), $\delta = 0.2$ (b), $\delta = 0.25$ (c), $\delta = 0.3$ (d) $\delta = 0.35$ (e) and $\delta = 0.4$ (f). The boundary layer width is symbolised by the coloured area near the boundary. (The distance between two streamlines is arbitrary)

References

Iserles, A., Marthinsen, A. & Nørsett, S. P. 1999 On the implementation of the method of magnus series for linear differential equations. *BIT* **39**, 281–304. (doi: 10.1023/A :1022393913721)

Kaneko, A. & Honji, H. 1979 Double structures of steady streaming in the oscillatory viscous-flow over a wavy wall. *J. Fluid Mech.* **93**, 727–&. (doi: 10.1017/S0022112079001993)

Lyne, W. 1971 Unsteady viscous flow over a wavy wall. *J. Fluid Mech.* **50**, 33–&. (doi: 10.1017/S0022112071002441)

Moffatt, H. K. 1964 Viscous and resistive eddies near a sharp corner. *J. Fluid Mech.* **18**, 1–18. (doi: 10.1017/S0022112064000015)

Pagneux, V. 2010 Multimodal admittance method in waveguides and singularity behavior at high frequencies. *J. Comp. Appl. Math.* **234**, 1834–1841. (doi: 10.1016/j.cam.2009.08.034)

Pagneux, V., Amir, N. & Kergomard, J. 1996 A study of wave propagation in varying cross-section waveguides by modal decomposition .1. theory and validation. *J. Acoust. Soc. Am.* **100**, 2034–2048. (doi: 10.1121/1.417913)

Pozrikidis, C. 1993 Unsteady viscous-flow over irregular boundaries. *J. Fluid Mech.* **255**, 11–34. (doi: 10.1017/S002211209300237X)

Schiff, J. & Shinider, S. 1999 A natural approach to the numerical integration of riccati differential equations. *SIAM J. Numer. Anal.* **36**, 1392–1413.

Vandembroucq, D. & Roux, S. 1997*a* Conformal mapping on rough boundaries. i. applications to harmonic problems. *Phys. Rev. E* **55**, 6171–6185. (doi: 10.1103/PhysRevE.55.6171)

Vandembroucq, D. & Roux, S. 1997*b* Conformal mapping on rough boundaries. ii. applications to biharmonic problems. *Phys. Rev. E* **55**, 6186–6196. (doi: 10.1103/PhysRevE.55.6186)

5

Conclusion et perspectives

Dans la première partie nous avons étudié les phénomènes de couplages entre acoustique et vorticité dans les écoulements incompressibles cisaillés linéaires. Ces écoulements ont la particularité de pouvoir être décomposés comme la somme d'une partie hyperbolique et d'une partie rotation solide. La méthode WKB a été utilisée pour étudier l'évolution de perturbations compressibles. Cette méthode repose sur l'existence d'un petit paramètre ε qui représente le rapport entre le taux de cisaillement de l'écoulement et la fréquence des perturbations. Elle nous a permis de dégager une base de trois modes, composée de deux modes acoustiques et d'un mode de vorticité. Cette base, proche de la solution exacte, permet de suivre les évolutions des amplitudes de ces modes au cours du temps. Nous avons mis en évidence la génération des modes acoustiques par le mode de vorticité, qui semble être liée à la partie hyperbolique de l'écoulement. Ce phénomène de couplage est comparable aux phénomènes de transitions non-adiabatiques en mécanique quantique, discipline au sein de laquelle la méthode WKB a été développée. Ce couplage apparaît être une quantité exponentiellement faible, d'ordre $e^{-C/\varepsilon}$, et ne peut être approché par une méthode asymptotique, y compris en considérant des approximations d'ordres supérieurs. Une suite à ce travail peut consister à obtenir une expression analytique de l'amplitude de ce couplage en s'inspirant de travaux réalisés notamment par Davis & Pechukas (1976) ou par Berry (1990) en mécanique quantique. Les travaux présentés ici soulignent que ces effets de couplage sont d'un ordre de grandeur très faible (exponentiellement faible) pour de faible valeurs de ε.

Dans la seconde partie nous avons proposé une méthode pour la résolution de problèmes impliquant une condition limite de géométrie complexe. Cette méthode est fondée sur l'utilisation d'une transformation conforme associée à une méthode multimodale. La transformation conforme permet de transformer la géométrie complexe en une géométrie simple. Le coût à payer pour cette simplification est l'apparition de coefficients variables dans les équations en volume du problème considéré. Cette méthode est particulièrement adaptée pour les problèmes faisant intervenir un opérateur Laplacien. En effet, le Laplacien est alors simplement transformé en un Laplacien multiplié par une fonction de l'espace. L'un des avantages de cette méthode réside dans le fait qu'une importante variété de géométries peut être considérée sans devoir faire d'hypothèse sur les ordres de grandeur des longueurs ou des courbures caractéristiques de ces géométries.

Cette méthode a été utilisée pour modéliser la réflection d'une onde par une surface de géométrie complexe. Le problème a été traité comme un guide d'onde. En outre, nous avons proposé une méthode permettant de trouver parmi une famille de géométries donnée, les géométries pouvant donner lieu à l'existence de modes quasi-piégés. La particularité de cette méthode est qu'elle permet de rechercher ces géométries en fonction de la fréquence, et non pas de rechercher pour une géométrie donnée les fréquences auxquelles existent des modes quasi-piégés. Nous avons aussi établi qu'il est plus probable de trouver de telles géométries pour des fréquences proches des fréquences de coupure du guide. De prochains travaux dans ce domaine pourront porter sur la recherche d'ondes de surface se propageant le long d'une surface géométriquement complexe, ou sur la prise en compte de conditions limites absorbantes dues à une impédance sur le mur. Dans ce travail, nous avons utilisé la transformation conforme pour modéliser la surface sur laquelle vient se réfléchir une onde incidente. Mais les transformations conformes pourraient tout aussi bien être utilisées pour modéliser par exemple les parois complexes d'un guide d'onde. Ces parois seraient alors transformées en parois droites. De tels travaux pourraient ainsi inclure le cas d'une guide de section variable, qui a déjà été traité par Pagneux *et al.* (1996). Remarquons que cette approche permettrait d'établir une équivalence entre un guide de section variable et un guide droit au sein duquel l'indice de réfraction varie.

Nous avons aussi appliqué la méthode que nous proposons à la modélisation de la couche limite visqueuse d'une fluide incompressible oscillant à proximité d'une surface de géométrie complexe périodique. Le problème est résolu sous la formulation vorticité–fonction de courant. Une solution analytique a été proposée pour un cas particulier. Les résultats obtenus par cette méthode analytique se montrent en parfait accord avec les résultats numériques. Notre méthode permet ainsi de mettre en évidence l'existence de zones de recirculation générées par le fluide oscillant à proximité de surfaces rugueuses. Notons que le problème que nous avons résolu ici est très proche de celui de la couche limite visqueuse que générerait une onde acoustique se propageant le long d'une paroi rugueuse. Il sera intéressant de poursuivre ce travail en utilisant une méthode d'homogénéisation afin de prendre en compte l'effet de la rugosité de la paroi sur l'atténuation d'une onde acoustique au sein d'un guide d'onde. Afin de modéliser à la fois les effets visqueux et thermiques, il conviendra de résoudre également de la même façon le problème

de la diffusion de la température le long d'un mur isotherme.

Enfin, l'utilisation conjointe d'une transformation conforme telle que celle proposée par Vandembroucq & Roux (1997), qui repose au final sur une série de Fourier, et d'une méthode de résolution multimodale, permet d'obtenir des équations différentielles ordinaires qui ouvrent la voix à des résolutions analytique. C'est ce que nous avons montré dans le chapitre 4, concernant la modélisation de la couche limite visqueuse, dans le cas où la série de Fourier de la transformation conforme est réduite à un seul terme (géométrie en forme de crête). Dans la perspective de la prise en compte de l'effet de la rugosité de la paroi sur l'atténuation d'une onde acoustique, mentionnée ci dessus, cela pourrait permettre de connaître l'ordre dominant de cet effet de façon analytique. La méthode perturbative que nous avons employée est généralisable au cas générale où cette série de Fourier contiendrait un nombre arbitraire de termes. L'obtention d'une telle expression aurait un intérêt remarquable dans la mesure où elle fournirait une solution analytique pour n'importe quelle géométrie pouvant être décrite au moyen de cette transformation conforme. Par ailleurs, une approche similaire pourrait être appliquée au problème de l'onde acoustique traité au chapitre 3. En effet l'équation (3.15) régissant l'évolution de la pression dans le problème de la réflection de l'onde acoustique du chapitre 3, est en de nombreux points similaire à l'équation (4.23a) régissant l'évolution de la vorticité dans le problème de la couche limite de Stokes du chapitre 4. Il est donc envisageable qu'une expression de l'évolution de la pression acoustique selon y puisse être obtenue par perturbations. Le seul obstacle théorique majeur à l'obtention d'une expression analytique complète du problème de la réflection d'une onde provient de la condition initiale du champ de pression réfléchi (équations (3.20) ou (3.37) selon que l'on considère le problème du guide d'onde ou de l'onde en espace libre). En effet ces équations font intervenir des intégrales dont la résolution peut poser des difficultés.

References

Berry, M. V. 1990 Histories of adiabatic quantum transitions. *Proc. R. Soc. Lond. A* **429**, 61–72.

Davis, J. P. & Pechukas, P. 1976 Nonadiabatic transitions induced by a time dependent hamiltonian in the semiclassical/adiabatic limit : The two state case. *J. Chem. Phys.* **64**, 3129–3137. (doi: 10.1063/1.432648)

Pagneux, V., Amir, N. & Kergomard, J. 1996 A study of wave propagation in varying cross-section waveguides by modal decomposition .1. theory and validation. *J. Acoust. Soc. Am.* **100**, 2034–2048. (doi: 10.1121/1.417913)

Vandembroucq, D. & Roux, S. 1997 Conformal mapping on rough boundaries. i. applications to harmonic problems. *Phys. Rev. E* **55**, 6171–6185. (doi: 10.1103/PhysRevE.55.6171)